FORMATION, PHOTOPHYSICS AND PHOTOCHEMISTRY OF WATER-SOLUBLE LANTHANIDE(III) PORPHYRINS

DOI:10.18136/PE.2016.612

PhD dissertation

written by

Muhammad Imran

Supervisors:
Dr. Ottó Horváth, DSc
Dr. Zsolt Valicsek, PhD

University of Pannonia
Doctoral School of Chemical and Environmental Sciences

Institute of Chemistry
Department of General and Inorganic Chemistry

Veszprém

2016

FORMATION, PHOTOPHYSICS AND PHOTOCHEMISTRY OF WATER-SOLUBLE LANTHANIDE(III) PORPHYRINS

Értekezés doktori (PhD) fokozat elnyerése érdekében

Írta:
Muhammad Imran

Készült a Pannon Egyetem Kémiai és Környezettudományi
Doktori Iskolája keretében.

Témavezetők:

Dr. Horváth Ottó
Elfogadásra javaslom (igen / nem) ……..
(aláírás)

Dr. Valicsek Zsolt
Elfogadásra javaslom (igen / nem) ……..
(aláírás)

A jelölt a doktori szigorlaton .....%-ot ért el,

Az értekezést bírálóként elfogadásra javaslom:

Bíráló neve: …..... …..... igen /nem

…….
(aláírás)

Bíráló neve: …..... …..... igen /nem

…….
(aláírás)

A jelölt az értekezés nyilvános vitáján ….....%-ot ért el.

Veszprém, …….
a Bíráló Bizottság elnöke

A doktori (PhD) oklevél minősítése….....

……
Az EDHT elnöke

Abstract

Porphyrins are the most widely studied macrocyclic compounds because of their several important roles in nature as well as their special coordinative, spectral and redox features. The cavity of the porphyrins containing four pyrrolic nitrogen is ideally suited for binding the vast majority of metal ions of the periodic table. If the metal ion is too big to fit co-planarly into the cavity of porphyrin, it is located out of the ligand plane and distorting it. This structure results in kinetic lability as well as peculiar photophysical and photochemical behavior. Lanthanide(III) ions, due to their large ionic radius and contraction upon increasing the atomic number, proved to be suitable for the fine tuning of the out-of-plane (OOP) distance of the metal center. In the presence of acetate ion as a potential axial ligand mainly the lanthanide(III) monoporphyrin species were formed, while, in the case of perchlorate ion, bisporphyrins (3:2 = metal ion : porphyrin) too. The stability constants increased with the atomic number in accordance with the stronger metal-ligand interaction due to the shorter OOP distance. The dome distortion of the macrocycle in these complexes manifested in the redshift of the visible absorption bands and the decrease of the S_1-fluorescence intensity compared to those of the free-base porphyrin. The moderate effect of dimerization on the absorption and emission properties indicated a weak interaction of the monomers in the bisporphyrins, which suggested a tail-to-tail structure connected through the peripheral sulfonate groups by a metal-ion bridge. Irradiation of the Ln(III) porphyrins at Soret- and Q-band maxima resulted in three types of photoinduced reactions, namely redox degradation, dissociation, and transformation between the Ln(III) mono- and bisporphyrins. Two types of photoproducts depending on the excitation wavelength were detected; Soret-band irradiation generated a short-lived intermediate, while Q-band excitation produced a stable end-product. The individual quantum yields of all the photochemical reactions were determined by the concentration distribution method for the lanthanide(III) porphyrins studied. For both the mono- and the bisporphyrins, the overall quantum yields, in which the efficiency of the redox degradation is predominant, display a decreasing trend (following a small increase) as a function of the atomic number of the metal center, as the consequence of the diminution of the out-of-plane distance and, thus, the chance for the charge separation following the photoinduced LMCT process.

Kivonat

A porfirinek a legszélesebb körben tanulmányozott makrociklusos vegyületek, mivel fontos szerepet játszanak a természetben, továbbá különleges koordinációs, spektrális és redoxi tulajdonságokkal rendelkeznek. A porfirinek négy pirrol-nitrogénnel rendelkező ürege ideális a fémionok többségének megkötésére. Ha a fémion mérete túl nagy ahhoz, hogy a porfirin koordinációs üregébe koplanárisan illeszkedjen, a ligandum síkja fölött helyezkedik el és azt torzítja. Ez a szerkezet kinetikai labilitást, valamint sajátos fotofizikai és fotokémiai viselkedést eredményez. A lantanoida(III)ionok – nagy ionsugaruk és a rendszám növekedésével járó méretcsökkenésük következtében – alkalmasnak bizonyultak a központi fémion síkon kívüli (OOP) távolságának finomhangolására. Acetátion mint potenciális axiális ligandum jelenlétében főként lantanoida(III)-monoporfirin képződött, míg perklorátionok mellett biszporfirin (3:2 = fémion:porfirin) is. A stabilitási állandók növekedtek a lantanoidák rendszámával – összhangban a rövidebb OOP távolságból adódó erősebb fém-ligandum kölcsönhatással. A ligandum dómos torzulása ezekben a komplexekben a látható tartományban a szabad porfirin elnyelési sávjainak vöröseltolódásában és az S_1-fluoreszcenciája intenzitásának csökkenésében nyilvánult meg. A dimerizáció csak mérsékelten befolyásolta az abszorpciós és emissziós tulajdonságokat, ami a monomerek gyenge kölcsönhatását jelezte a biszporfirinekben, "farok-farok" szerkezetet sugallva, melyben a kapcsolódás a szulfonát szubsztituensek közt valósul meg fémion-híd révén. A Ln(III)-porfirinek besugárzása a Soret- és Q-sávok maximumán háromféle fotoindukált reakciót idézett elő; redoxi lebomlást, disszociációt, valamint a mono- és a biszporfirinek közötti átalakulást. Emellett a besugárzási hullámhossztól függően kétféle, eddig nem észlelt fototerméket sikerült detektálni; a Soret-sávon a besugárzás egy rövid-élettartamú köztiterméket eredményezett, míg a Q-sávos gerjesztés egy stabil végterméket. A vizsgált lantanoida(III)-porfirinek valamennyi fotokémiai reakciójának egyedi kvantumhasznosítási tényezőjét meghatároztam a koncentráció-eloszlás módszerével. Mind a mono-, mind a biszporfirinekre vonatkozó bruttó érték, melyben a redoxi bomlás hatékonysága a meghatározó, a központi fémion rendszámának növekedtével – egy kis emelkedést követően – csökkenő tendenciát mutat, együtt a síkon kívüli távolsággal, s így a fotoindukált LMCT folyamatot követő töltésszétválás valószínűségével.

Zusammenfassung

Porphyrine sind die bestuntersuchten makrozyklischen Verbindungen, da sie in der Natur eine wichtige Rolle spielen und dafür spezielle Koordinations- und Redoxeigenschaften besitzen. Der Koordinationshohlraum der Porphyrine, die vier Pyrrol-Stickstoffmoleküle haben, ist ideal für die Bindung von vielen Metallionen. Wenn das Metallion zu groß ist, um sich in den Koordinationshohlraum des Porphyrins koplanar einzufügen, placiert es sich über der Ebene des Liganden und deformiert ihn dadurch. Diese Struktur verursacht kinetische Labilität, sowie besonderes photophysikalisches und photochemisches Verhalten. Lanthanoid(III)-Ionen, erwiesen sich, infolge ihrer großen Ionenradien und der Lanthaniodenkontraktion, als geeignet für die Feinabstimmung des "out-of-plane" (OOP) Abstandes. In Anwesenheit von Acetat-Ionen als potenzielle axiale Liganden bilden sich bevorzugt Lanthanoid(III)-Monoporphyrine, jedoch bei Anwesenheit von Perchlorat-Ionen werden auch Bisporphyrine (3:2 = Metallion : Porphyrin) gebildet. Die Stabilitätskonstanten nahmen mit der Ordnungszahl der Lanthanoiden zu – übereinstimmend mit der stärkeren Metall–Ligand-Wechselwirkung, die aus dem kürzerem OOP Abstand resultiert. Die kuppelförmige Deformation vom Ligand in diesen Komplexen äußerte sich als die Rotverschiebung in den Absorptionsbanden im sichtbaren Bereich und der Abnahme der Intensität der S_1-Fluoreszenz – im Vergleich mit den entsprechen Werten des freien Porphyrins. Die Dimerisierung beeinflusst die Absorptions- und Emissionseigenschaften nur mässig, was die schwache Wechselwirkung der Monomeren in den Bisporphyrinen zeigt, suggerierend eine "Schwanz-zu-Schwanz" Struktur, in der die Bindung zwischen den Sulfonat-Substituenten durch eine Metallion-Brücke gegeben ist. Die Bestrahlung der Ln(III)-Porphyrine in den Soret- und Q-Banden verursacht dreierlei photochemische Reaktionen; Redox-Zersetzung, Dissoziation, sowie Umwandlung zwischen Mono- und Bisporphyrinen. Daneben gelang es, zwei, bisher noch nicht beobachtete Photoprodukte zu bestimmen, die von der Anregungswellenlänge abhängen. Die Soret-Band-Bestrahlung ergab ein kurzlebiges Zwischenprodukt, während die Q-Band-Anregung zu einem stabilen Endprodukt führt. Die individuellen Quantenausbeuten für alle photochemischen Reaktionen der untersuchten Komplexe wurden durch die Methode der Konzentrationsverteilung bestimmt. Der Bruttowert, bei dem die Redox-Zersetzung maßgeblich ist, für Mono- als auch die Bisporphyrine zeigt – nach einer kleinen Zunahme – einen Abwärtstrend mit wachsender Ordnungszahl des Metallzentrums, infolge der Abnahme des OOP Abstands und somit der Möglichkeit der Ladungstrennung nach einem photo- induzierten LMCT Prozess.

Acknowledgments

Many thanks are extended to my supervisors, Prof. Ottó Horváth and Dr. Zsolt Valicsek for their continued guidance and advice throughout the research work in both practical and theoretical respects, and for the appropriate experimental conditions.

I am very grateful to the colleagues at the Department of General and Inorganic Chemistry of University of Pannonia for their help and competent assistance in any respects, and for their hospitality.

I am indebted to Prof. Günter Grampp and his colleagues at the Institute of Physical and Theoretical Chemistry at Graz University of Technology for their extensive help and assistance in the ESR measurements.

Many thanks are due to my family, first of all my parents and my wife, whose efforts, love, understanding and patience made my studies possible in a country far from our home.

I also appreciate the financial background of this work supported by the Hungarian Research Fund (NN107310), the Hungarian Government and the European Union, with the co-funding of the European Social Fund (TAMOP-4.2.2.A-11 /1/KONV-2012-0071) and the Austrian-Hungarian Action Foundation (86öu3).

Contents

Chapter 1: Introduction

1. Introduction of porphyrin chemistry

Porphyrins are the most plentiful chemical compounds found in nature which are biochemically important, medically useful, and synthetically fascinating compounds. Porphyrins that found in nature are playing a vibrant role on this planet to sustain life by assorted ways like oxygen transport (hemoglobin), its storage (myoglobin), chlorophyll for natural photosynthesis, enzymes like catalases, peroxidases, cytochromes and vitamins are of prime importance for living organisms [1]. Synthetic porphyrins and their metal complexes possess stimulating physical, chemical and biological properties and are significant candidates for utilization of solar energy, photodynamic therapy, electrooptics, mimicking of enzymes and as industrial catalysts. The electronic spectra of porphyrins have been extensively studied due to their important role in the natural biochemical processes and special absorption, emission, charge transfer, complexing properties [1]. The word porphyrin was coined first time by ancient Greeks, they used the word porphura for the intense purple color and have been used as a dye to color the cloths [2].

The structure of porphyrin (

Figure 1.1) is composed of four pyrrolic units that are linked by methine bridges at their α-positions. The four pyrrolic units after linking with each other give a planar structure to the porphyrin molecules with an extended conjugated 18 π-electron system being responsible for the aromatic behavior of porphyrins [3, 4, 5].

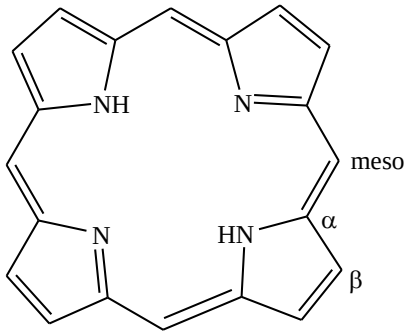

Figure 1.1. Structure of unsubstituted porphyrin [6,7]

Porphyrins being tetradentate ligand molecules can easily accommodate metal ions. In deprotonated form, they offer a square planar environment and a rigid cavity of a 0.6-0.7-Å

radius, which is ideally suited for metal incorporation [8, 9]. As in most of cases, the porphyrin dianion acts as a tetradentate ligand towards metal ions; the minimum coordination number of the metal is four.

The presence of highly conjugated π-electronic systems is responsible for the intense color and other distinctive electronic and redox properties of porphyrins. Compounds like chlorin and bacteriochlorin show resemblances in structure with porphyrin [10].

2. Nomenclature and isomerism of porphyrins

The first effort of giving names and directions for drawing the different isomers of porphyrins was made by Hans Fischer [11].

He numbered the eight outer carbon atoms belonging to the pyrrolic fragments from 1 to 8, while the four bridging C atoms as α, β, γ, and δ. The Fisher's nomenclature works only for simple porphyrins, but when the complexity of the substituents attached to the pyrrolic nitrogen increases, this system has limitation to assign them a systematic name [12]. To overcome the shortcomings in the Fischer's system, IUPAC gave a new organized and comprehensive system of naming for porphyrins and their derivatives, which was completed in 1987. In the IUPAC system all atoms in the porphyrinic macrocycle was numbered as shown in Figure **1.2**.

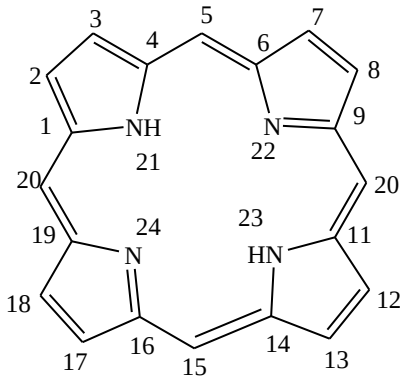

Figure 1.2. Numbering of atoms in porphyrin macrocycle according to IUPAC.

By given numbering to all the atoms was also useful because it helped give some structural information about the compound. In IUPAC system the positions of the principle groups determine the numbering of the substituted porphyrins and the name of the substituents (e.g. propionic and acetic acid) comes after the name of porphyrins, and an alphabetical ascending order was used for naming the substituents attached to the macrocycle periphery.

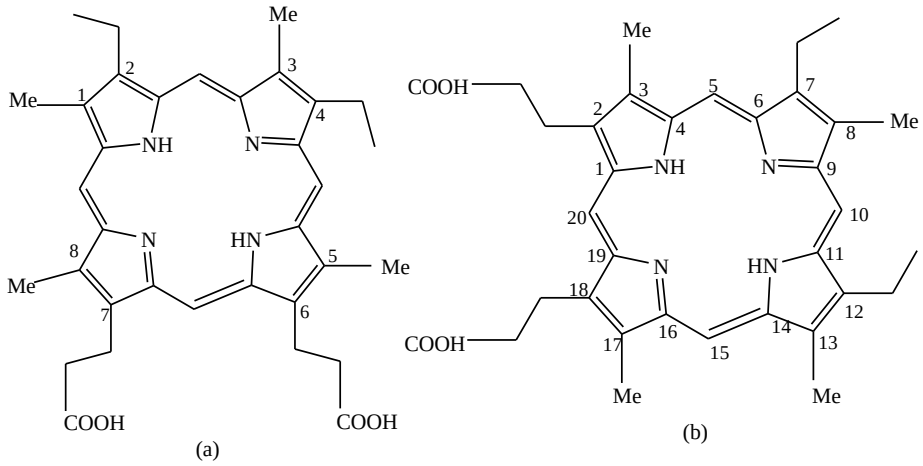

Figure 1.3 (a) 2, 4-diethyl-1, 4, 5, 8-tetramethylporphyrin-6, 7-dipropionic acid (mesoporphyrin) (b) 7, 12-diethyl-3, 8, 13, 17-tetramethylporphyrin-2, 18-dipropionic acid (mesoporphyrin) [4]

The name of mesoporphyrin according to the Fischer's nomenclature is 2,4-diethyl-1,4,5,8-tetramethylporphyrin-6,7-dipropionic acid and 7,12-diethyl-3,8, 13,17-tetramethylporphyrin-2,18-dipropionic acid is given to the same compound by the IUPAC system as shown in figure 1.3(a) and (b) respectively. In this work an anionic porphyrin was used, with four sulfonatophenyl groups which are attached at 5, 10, 15 and 20 position of the porphyrin macrocyclic ring and its name is 5,10,15,20-tetrakis(4-sulfonatophyenyl)porphyrin abbreviated as H_2TSPP^{4-} or simply H_2P.

3. Electronic properties of porphyrins

3.1. Light absorption

Porphyrins are the strongest light absorbing materials in nature and they are also called pigments of life. Hence the UV-Vis absorption spectroscopy is most fundamental and suitable analytical technique for the elucidation of electronic structure of porphyrins and their metal derivatives even at very low concentrations [13]. By monitoring the change in the intensity and wavelength of absorption spectra of porphyrins, a very substantial information on their excited states and a variation in the peripheral substituents of the porphyrin ring could be gained. The study of the photophysical properties, electronic structure, excited state and deactivation of porphyrins and their metal complexes is of prime importance to evaluate the possible applications. A brief explanation on the spectra of porphyrins is given in the following.

The extended conjugation of 18-π electrons on the frontier orbitals is responsible for their highly intense color. Porphyrins possess characteristic UV-visible spectra because of their fourfold symmetry and four nitrogen atoms directed towards the center of the electronic heart. The characteristic absorption spectra of porphyrins undergo perturbation by different factors like conjugation pathway, symmetry and other chemical variations [14]. They are helpful to distinguish between free-base porphyrins and their metal complexes. Upon the insertion of metal ion into the porphyrin cavity the D_{2h} symmetry changes to D_{4h}. [15]. Most of the porphyrins show two sets of distinct region or bands in their electronic absorption spectrum. The ranges of the first and second band sets are 350-500 nm and 500-750 nm, respectively. The first sets of band are called Soret- or B-bands with molar absorption coefficients of 10^5 $M^{-1}cm^{-1}$ and involve the electronic transition from the ground state to the second singlet exited state ($S_0 \rightarrow S_2$). The second set of band is called the Q-band with molar absorption coefficients of 10^4 M^{-1} cm^{-1} and involve the transition from the ground state to the first singlet exited state ($S_0 \rightarrow S_1$). The conjugation of 18-π-electrons gives advantageous spectroscopic features to porphyrins, which is supportive to monitoring the binding of diverse hosts to the porphyrin by using UV-visible spectroscopy [5, 16]. A UV-Vis spectrum within a wide range of Q-bands extended from 480 to 700 nm is shown in Figure 1.4 [17]. The electronic absorption spectra of porphyrins show different types of band. Depending on the type and intensity of the bands, a valued evidence could be obtained regarding the possible substitution or metalation, and classification of porphyrin spectra has also been made.

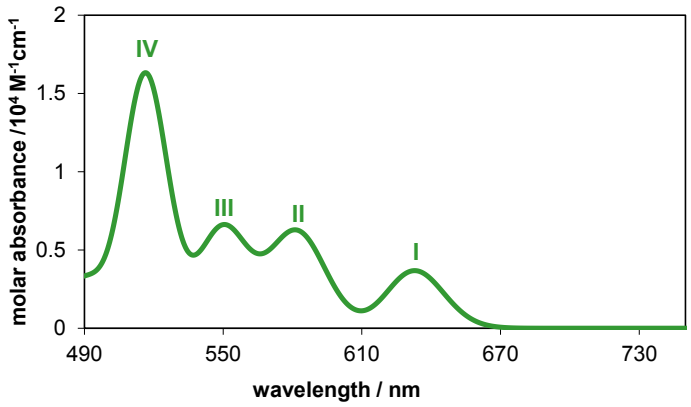

Figure 1.4 UV-Vis spectrum of porphyrin in the Q-region of 480-750 nm [17]

The four types of Q-bands could be seen in the absorption spectra of a free base porphyrin which are represented by roman numbers and are placed according to the increasing wavelength as IV, III, II and I. If the intensities of the Q bands are in order of IV > III >II > I

then the spectra will be of *etio-type*; and porphyrins will be called as etioporphyrins. This type of spectra is exhibited by all those porphyrins in which all the eight β-positions of macrocyle are substituted by the groups that do not possess π-electrons.

The relative intensities of the Q-bands show a slight modification when groups with π-electrons are attached at the β-positions (i.e., at the outer pyrrolic carbon atoms) of the macrocycle and the order of Q-bands are III > IV >II > I. The resulting spectra are called *rhodo-type* and the porphyrin will be rhodoporphyrin. In the third case, if the two groups with π-electrons are attached at the two pyrrol units that are opposite to each other, it gives rise to *oxo-rhodo-type* spectrum with an intensity diminution in the series of III > II >IV > I. At last, when the β-positions are unsubstituted, Q-band intensity series becomes IV > II >III > I, and the spectrum type is known as *phyllo-type* [4, 18]. Because of crucial significance of porphyrins and their derivatives in important life processes, many scientists have tried over the years to unveil more feature concerning the position and multiplicities of Q- and B-bands in the UV-Visible spectra of metal-free porphyrins.

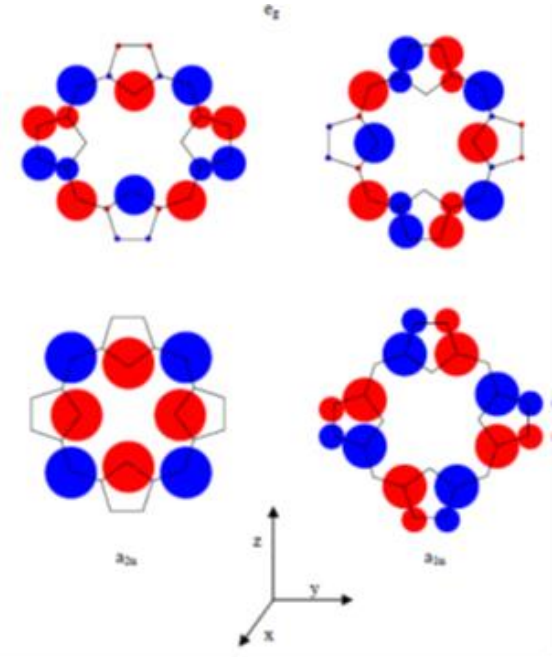

Figure 1.5 HOMOs (bottom) and LUMOs (top) [adapted from 19]

Notably, an American scientist, Martin Gouterman, developed a very well-known theory named as “four-orbital” model about the spectra of porphyrins [20]. The Gouterman’s model illustrated in

Figure **1.5**, helps us rationalize the electronic density in orbitals. According to Gouterman's four-orbital model, porphyrins have two highest occupied π orbitals titled as HOMOs and two lowest unoccupied π* orbitals termed as LUMOs. The transitions between these two sets of orbitals are responsible for the advent of the absorption bands of porphyrins [18]. HOMOs own a_{1u} and a_{2u} orbitals, while LUMOs are identified as a degenerate e_g set of orbitals, which are localized on the macrocycle ring. The HOMO a_{2u} orbital is localized on pyrrolic nitrogens and meso carbons, while $HOMO_{-1}$ a_{1u} is localized mainly on C_α and C_β atoms [21]. The Gouterman's four-orbital model pays a special attention to the electronic transition between filled bonding MO's levels a_{1u}, a_{2u} and antibonding MO's levels (e_g*). In porphyrin spectra HOMO to π* transition results in the appearance of four absorption peaks. Out of four absorption bands two are from x and two from y component of Q-bands. The Q_x and Q_y components are also composed of two types of vibrational excitations which are Q(0, 0) at lower energy and Q(1,0) at higher energy. Therefore, the four absorptions lines can be written as Q_x (0, 0), Q_x (1, 0), Q_y (0, 0) and Q_y (1, 0) in the increasing order of energy. Upon complexation porphyrins show the appearance of a very intense red-shifted absorption band in the Soret-region at 420-425 nm and two weak Q bands at 540-600 nm. These bands are assigned to intra ligand π-π* transitions of porphyrin [3, 16].

3.2. Light emission

Fluorescence and phosphorescence processes involves the relaxation of excited state molecules to ground state through photon emission which is just the opposite process to absorption. These photonic processes involve transition between electronic and vibrational states of molecules. Light emission is termed as fluorescence if no change of spin state accompanies the electronic transition [22, 23].

The Jablonski diagram (Figure 1.6) offers a good opportunity to explain the mechanism of the excitation and relaxation processes in molecules. The molecules are able to occupy higher energy singlet electronic states like S_1, S_2...S_n depending upon the energy of light absorbed [24]. According to the Kasha's rule, the relaxation process which takes place with emission of light principally starts from S_1, in solution, which is the lowest-energy excited electronic state, while in the case of higher-energy electronic excited state, like S_2 and S_3, there will be internal conversion prior to the emission [25]. The energy of emission is less than that of

absorption, thus, fluorescence occurs at longer wavelength as compared to the wavelength at which the molecule was excited. The difference between positions of the band maxima of the absorption and emission spectra of the same electronic transition is called Stokes-shift [26].

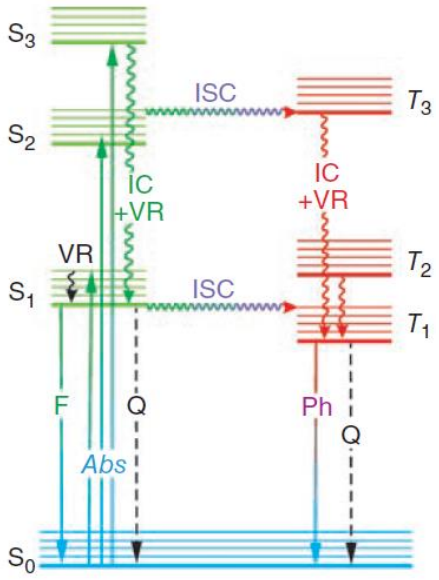

Figure 1.6 The Jablonski diagram: Abs, absorption; F, fluorescence; IC, interval conversion; ISC, intersystem crossing; Ph, phosphorescence; Q, quenching; VR, vibrational relaxing; S_0 is the ground singlet electronic state; S_1 and S_2 are higher-energy excited singlet electronic states; T_1 is the lowest-energy triplet state [27]

In most of the ground-state molecules with even number of electrons, the electrons occupy the low-energy-level orbitals with opposite spins and have zero for the sum of the spin quantum numbers; this state is called as singlet electronic state. When a molecule is excited, an electron moves from an occupied to an unoccupied orbital where it may keep its original spin state (singlet excited state) or changes it to the opposite orientation (triplet excited state). The return of this electron from a singlet excited state to the lower orbital takes place more than 100 ns. and this process is called fluorescence. If the electron returns from a triplet excited state to the singlet ground state, the electron undergoes a spin-reversal, which is a forbidden process and is the basis of phosphorescence, which is a less rapid process and may usually last from milliseconds to seconds [28].

The molecules in their singlet excited state may undergo a vibrational relaxation process to the lowest vibronic level of the corresponding excited state, and this process is completed by the releasing of the thermal energy to the surroundings. Beside the biological importance, porphyrins have interesting luminescence and non-radiative features [29]. The vibrational

relaxation of singlet-excited porphyrins is often relatively slow compared to their radiative and intersystem crossing processes. The overall quantum yield of fluorescence and intersystem crossing in formation of triplet states is over 95%. Due to this property, porphyrins are efficient in photosensitization [21]. Results from our research group on lanthanum(III) and mercury(II) porphyrin have shown that coordination of a metal ion into a porphyrin ligand results in a blueshift or hypsochromic effect on the emission bands and a significant decrease of fluorescence intensity and lifetime of monoporphyrins. Emission spectra of previously studied metalloporphyrins have indicated that the structure of the originally flat (free base) ligand is distorted in metalloporphyrins and the decrease in quantum yield is the consequence of distortion of ligand, which promotes other energy dissipation processes than light emission. Other out-of-plane metalloporphyrins, like Hg(II) $TSPP^{4-}$, Cd(II) $TSPP^{4-}$ and Bi(III)$TSPP^{3-}$, have shown the similar emission tendencies of the band-shift and quantum yield [30, 31].

4. Occurrence and preparation of porphyrins

Many types of metal-free porphyrins have been successfully isolated and modified from natural resources. A few examples of porphyrins obtained from natural resources and synthesis of metal-free porphyrins in laboratory are given below [32].

4.1. Natural porphyrins

Nature gives us a huge accumulation of porphyrins from which many other types of porphyrins can also be developed. Chlorophyll from plants and blood of animals are main sources to produce porphyrins [33].

Such a type is *protoporphyrin.* Scientists have developed numerous methods for the preparation of protoporphyrin from hemoglobin. In commonly adopted methods globin is first removed from hemoglobin to get hemin. [34, 35]. To obtain protoporphyrin, the solution of hemin or hematin is reduced in the presence of organic acid. According to Grinstein procedure as compared to protoporphyrin, protoporphyrin dimethyl ester can be easily obtained from hemin by simultaneous removal of iron and its esterification [36, 37].

Hematoporphyrin was prepared by treatment of blood with sulfuric acid [38]. It can also be isolated by treatment of hemin with hydrogen bromide in the presence of acetic acid [39].

Mesoporphyrin has been synthesized by the reduction of protohemin in the presence of hydrogen iodide [40, 41]. The most convenient way of obtaining large quantity of mesoporphyrin was developed by Caughey. In this method hydrogen was bubbled through the formic acid solution of hemin over PdO and no side product were obtained [42].

Harderoporphyrin is found in the harderian gland that is present in orbital cavity of Wister rats. It has the ability to synthesize harderoporphyrin. Various derivatives such as esters can be prepared from the harderian gland of rats [43].

Pemptoporphyrin was isolated in 1964, from feces of patients suffering from intestinal malabsorption [44, 45]. NMR studies were used to elucidate the structure of pemptoporphyrin as 4-vinyldeuteroporphyrin [45].

Uroporphyrin I and *coproporphyrin I* have been isolated from urine and feces of human and birds that have congenital erythropoietic porphyria disease [36, 46]. For isolation of uroporphyrin and coproporphyrin, urine sample is acidified with acetic acid and extracted with ether [47, 48].

Chlorophyll a and b is a rich source of different types of porphyrin. By following appropriate procedures and conditions a variety of porphyrins and chlorins could be obtain from chlorophyll as starting material [49, 50]. In 1907 Willstatter and Hocheder first time documented the sensitivity of chlorophyll a and b to change magnesium(II) ion to protons, forming *pheophytin* [51]. They treated chlorophyll obtained from spinach with acetic acid (Figure 1.7).

When chlorophylls are treated with strong acids then phytyl groups may be also hydrolyzed to pheophorbides with carbomethoxy groups [50]. Pheophytin has also been isolated from a neurodifferentiation compound that is present in marine brown alga known as Sargassum fulvellum [52].

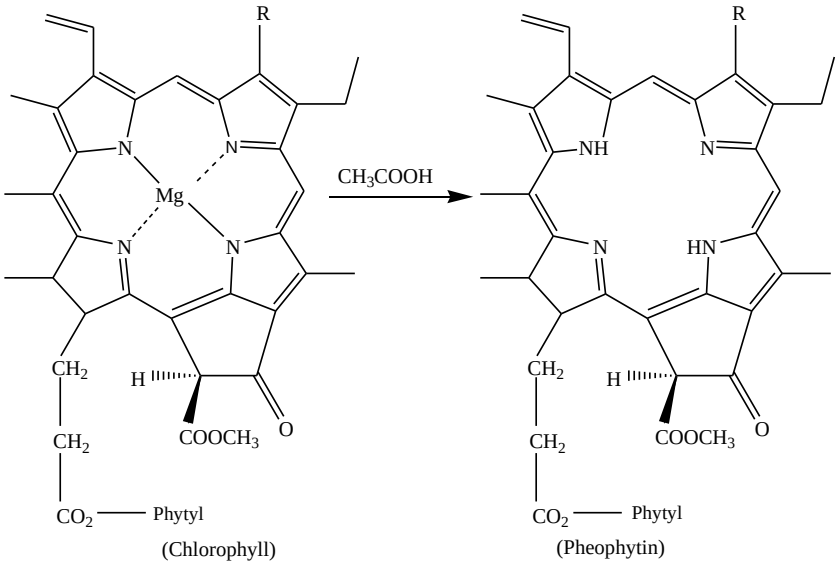

R= CH_3 pheophytin a, R= CHO pheophytin b

Phytyl: $-CH_2CH=C(CH_3)-(CH_2-CH_2-CH_2CH(CH_3))_3-CH_3$

Figure 1.7 Formation of pheophytin from chlorophyll [53]

4.2. Synthetic porphyrins

The synthetic history of porphyrins initiated from 1930. Until now, porphyrins of various types have been prepared and characterized by adopting diverse range of chemical strategies. The molecules like pyrrol, linear tetrapyrroles, tripyrranes, aldehydes and dipyrromethanes have been used as starting materials for the synthesis of porphyrins [18].

Fischer and Gleim in 1935 first time obtain 17 mg of porphyrin by reaction of pyrrole and aldehyde in the presence of formic acid under reflux condition [54]. In the same year Rothemund also reported the formation of porphyrin from pyrrol and aldehyde (formaldehyde and acetaldehyde) [55, 56]. His synthetic approach involves a one-step reaction between pyrrole and benzaldehyde (Figure 1.8).

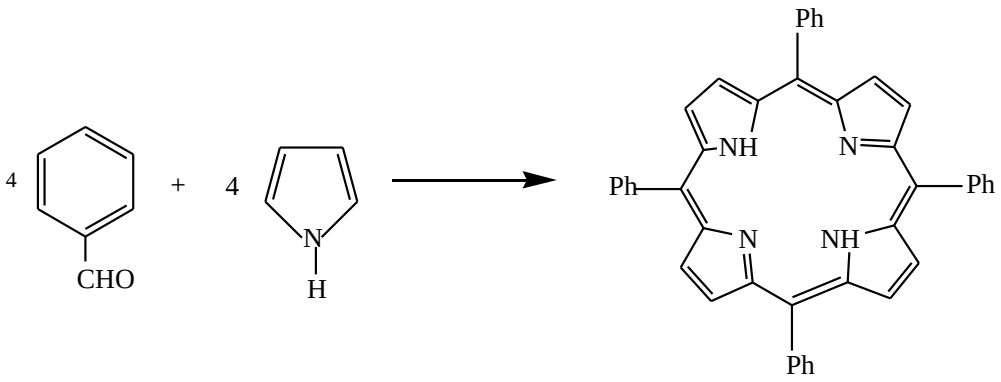

Figure 1.8 Rothemund synthesis of 5, 10, 15, 20-tetrapheny porphyrin

5. Metalloporphyrins

Metalloporphyrins are formed when one of the electron lone pairs existing on the central nitrogen atoms of the porphyrin ring is shared with the metal center acting like a Lewis acid [36, 57]. Because of their acidic character, the protons attached to the nitrogen atoms of the porphyrin can be easily deprotonated to produce tetradentate anionic porphyrinato ligand with superior coordinative properties. Thus, the dianion species having a planar framework with a cavity of specific size display an incredible property of bond formation with almost all metals and some metalloids, resulting in the formation of a wide variety of porphyrin derivatives [58]. Porphyrins behave as dibasic acids, the metal ion in porphyrin complexes exist in +2 oxidation state unless additional anionic ligands are attached at the axial location [59]. The metalloporphyrin formation process completes in different steps like protonation deprotonation equilibria of porphyrin, release of metal ion from metal salt, charge neutralization and completion of coordination sphere. Stability of metalloporphyrins depends upon the comparability of the size of the ionic radius of the metal ion and the cavity of the ligand; metalloporphyrins with comparable size of metal and ligand cavity are more stable and vice versa [59]. A generalized reaction for the formation of metalloporphyrins can be written as follows.

$$M^{2+} + H_2P \longrightarrow PM + 2H^+$$

In the above generalized reaction, H_2P represents the neutral porphyrin and PM is the resulting metalloporphyrin upon metal incorporation. The metal incorporation may adopt one of the following two possible routes given as A and B. In route A metal-porphyrin complex

forms before the loss of two protons while in route B in first step the porphyrin transforms into its monoanion or dianion form before reacting with the metal ion [60].

Route A

$$M^{2+} + H_2P \longrightarrow H_2PM^{2+} \longrightarrow PM + 2H^+$$

Route B

$$H_2P \longrightarrow HP^- + H^+ \longrightarrow P^{2-} + H^+$$

$$P^{2-} + M^{2+} \longrightarrow PM$$

Because of tetradentate nature of anionic porphyrinato ligand, in metalloporphyrins the minimum possible coordination number of metals is four, a divalent metal ion gives a neutral complex with square planar geometry. Porphyrins as ligands have the ability to stabilize different metal ions in their unusual oxidation states [10].

Porphyrins and their metal complexes are of prime importance in biological field (e.g. chlorophyll, heme, vitamin B12,) and are of equal importance in chemical and technological point of view [61, 62]. Silver porphyrin is the first metal porphyrin system that has documented in 1935 [63].

5.1. Natural metalloporphyrins

Chlorophylls are Mg(II) derivatives of tetrapyrroles; these molecules are present in the subcellular structure called chloroplast of all plant cells. They give green color to leaves and stems and their presence is essential for photosynthesis. Chlorophylls have the ability to absorb light at longer-wavelength range [64, 65]. A minor change in the porphyrin moiety of the basic magnesium(II) porphyrin system gives rise to different types of chlorophylls like chlorophyll a, b, c or bacteriochlorophyll (Figure 1.9), each of them possesses a different catalytic activity.

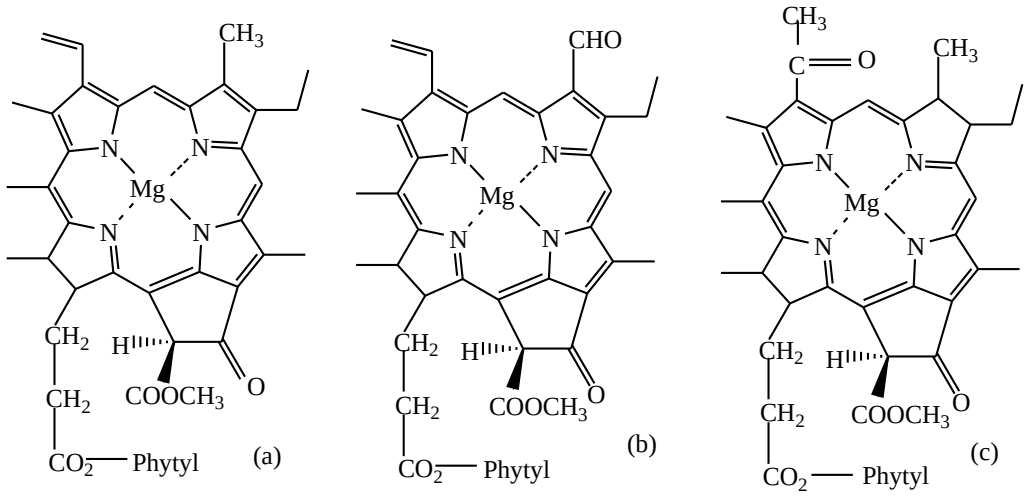

Figure 1.9 (a) Chlorophyll a, (b) Chlorophyll b (c) Bacteriochlorophyll a [33]

Chlorophyll a is present in algae and all other higher plants, hence this pigment is present in the largest amount on Earth. Some algae, mosses and other higher plants also have chlorophyll b. Bacteriochlorophyll a is present in a few photosynthetic bacteria [33]. Chlorophylls play significant roles in the light-driven reactions of photosynthesis. In this process chlorophylls harvest the light energy and utilize it in generation of reducing agents, ATP (adenosine triphosphate) as energy storing compound, and O_2 by oxidation of water. In the dark reactions reducing agents and ATP promote the formation of carbohydrates [4, 64, 66, 67].

5.1.1. Hemoglobin and myoglobin

In all higher animals the oxygen is transported and stored by hemoglobin and myoglobin. Hemoglobin transport oxygen from lungs to the cellular level of the organisms, where myoglobin stores it and facilitates oxygen for use in respiration process [68]. Hemoglobin and myoglobin are heme-containing proteins which are composed of two components; one is a metalloporphyrin (iron(II) porphyrin) known as heme prosthetic group and the second one is a polypeptide chain known as apoprotein [33]. The prosthetic group in hemoglobin and myoglobin is protoheme as shown in Figure 1.10.

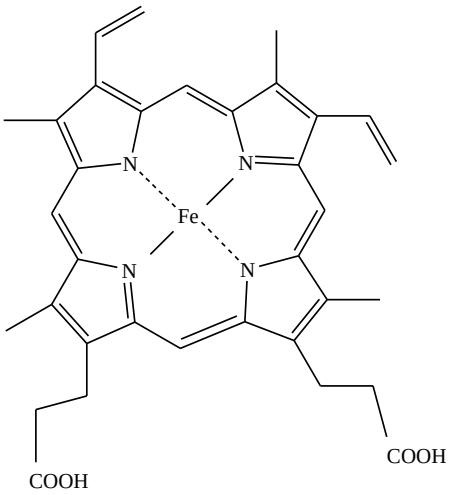

Figure 1.10 Structure of protoheme [33]

In the prosthetic group of hemoglobin and myoglobin, the iron coordinated to the pyrrolic nitrogen is in its + 2 oxidation state. When iron is in +3 state, the methemoglobin and metmyoglobin are formed which are unable to bind with dioxygen molecule. The protein portion of hemoglobin and myoglobin is helpful in stabilizing the Fe(II) by creating hydrophobic environment and by folded around the heme. These two factors only allow the coordination of dioxygen molecule and minimize the chance of water molecule to coordinate with heme [64, 68].

In myoglobin, the protein component is a single strand of 152 amino acids, while hemoglobin is composed of four globins; two of them contain 141 amino acids and called as α chains, the remaining two chains have 146 amino acids and represented as β chains [4]. Hemoglobin and myoglobin possess different helical regions; heme is squeezed between these regions, and oxygen binds on the distal side of porphyrin [69]. Myoglobin is easily converted to oxymyoglobin as compared to hemoglobin at lower oxygen concentration and affects the oxygen transport at cellular level [70]. At low oxygen pressure the detachment of oxygen molecules from hemoglobin which is fully saturated with O_2 occurs very easily [71].

After carrying oxygen in blood for a certain time period the red blood cells are transformed to liver where they are degraded into open chain tetrapyrroles known as bile pigments, accompanied by the release of iron. There are two common bile pigments named as biliverdin and bilirubin which are of greenish and yellowish color, respectively [12, 72].

In humans, the simultaneous breakdown and release of energy from heme results in the formation of bilirubin. To solubilize and make feasible for excretion into the intestine the body esterifies bilirubin with different kinds of sugar. Some of the bilirubins are also produced as a result of degradation of other hemoproteins like P450 [73, 74]. The structure of biliverdin and bilirubin are given in Figure 1.11.

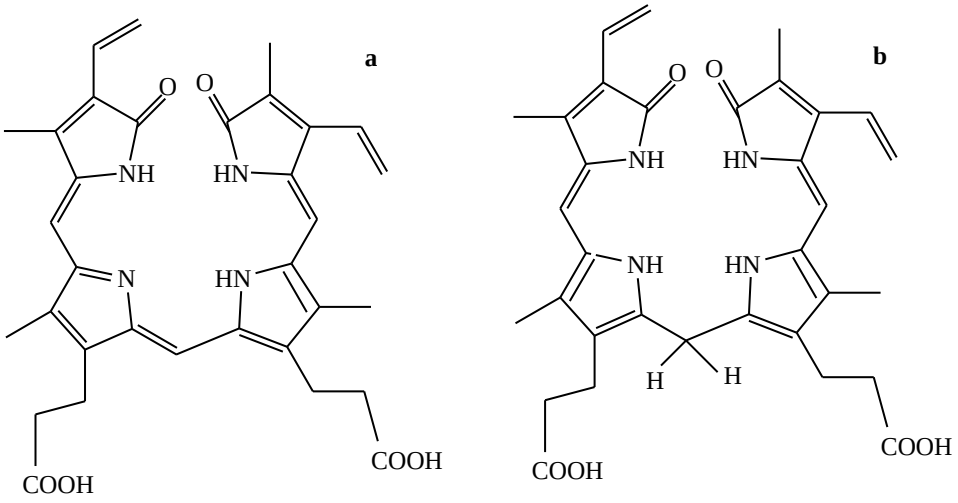

Figure 1.11 Structure of biliverdin (a) and bilirubin (b) [adopted from ref. 4]

5.1.2. Cytochromes

The cytochromes are iron containing metalloporphyrins which perform different functions in cells of animals and plants depending on the class of cytochromes. Some cytochromes transport electrons and are involved in cell respiration and photosynthesis, while others like cytochromes c and P450 are involved in oxidation-reduction reactions [8]. The cytochromes have the ability to make a reversible change between Fe (II) and Fe (III) oxidation states during a catalytic process [75]. Figure 1.12 shows that the iron porphyrin portion of cytochrome c is connected with amino acids of protein via cysteine and thio groups by covalent bonds, while in all other cytochromes have non covalent bonds [69].

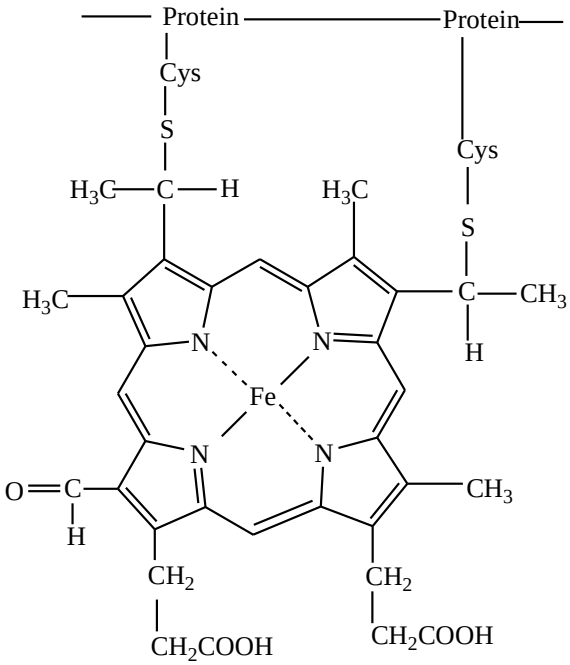

Figure 1.12 Structure of cytochrome c [adapted from 4]

5.1.3. Cofactor F_{430}

Cofactor F_{430} is a naturally occurring metalloporphyrin (Figure 1.13), which was first time obtained in 1978 from methyl-coenzyme M reductase (MCR) present in all methanogenic archaea. It is a nickel-containing tetrapyrrole and acts as a prosthetic group in methyl-coenzyme M reductase. This cofactor is of yellowish color with non-fluorescent behavior, and the name 430 was given because of its intense absorption band at 430 nm [69, 76, 77]. During the catalytic process of methane generation nickel ion acts as a catalytically active site and it changes its oxidation state while reaction is in progress [78]. This process results in a large, non-planarity change in the metal core size, which may affect its axial ligand affinity [79].

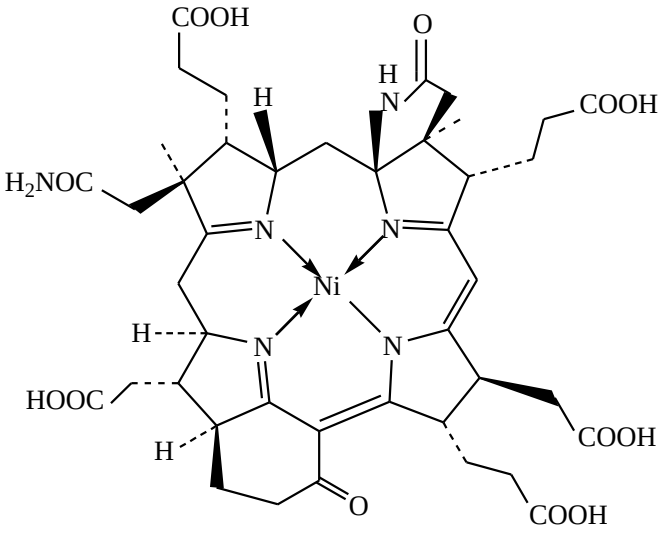

Figure 1.13 Structural representation of Cofactor F_{430} [adapted from ref 80]

5.1.4. Metalloporphyrins in petroleum

Metalloporphyrins found in petroleum are called petroporphyrins. Alfred Treibs was the first researcher who discovered the vanadyl deoxophylloerythroetionporphyrin (VODPEP) the major metalloporphyrins found in petroleum. His discovery suggested the biological origin of coal and oil. Beside vanadium in VODPEP nickel porphyrins are found in petroleum and oil shale. Nickel is present in its +2 oxidation state and bound in the plane of four pyrrole rings of the porphyrin macrocycle, while vanadium is in its +4 oxidation state and exists as vanadyl VO^{2+}. In vanadyl group the oxygen atom is situated perpendicularly to the plane of porphyrin macrocycle and vanadium atom lies about 0.48 Å overhead the plane of porphyrin in VODPEP as shown in Figure 1.14 [4, 81].

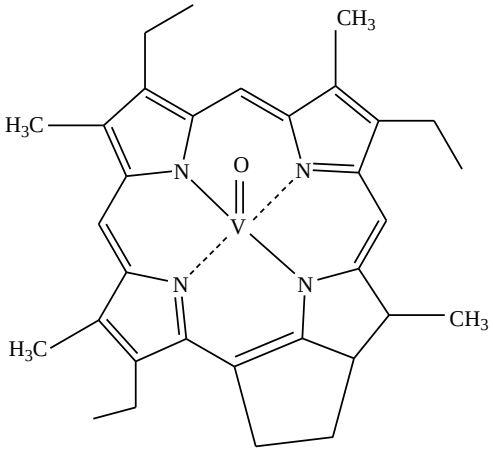

Figure 1.14 Structure of vanadyl DPEP [adapted from ref. 4]

Beside the above discussed, famous types of metalloporphyrins, there are many other naturally occurring metal porphyrin derivatives which includes vitamin B_{12} (cobalamins) and variety of other naturally occurring enzymes like oxygenases, peroxidases and catalase etc. [80].

5.2. Synthetic metalloporphyrins

The synthetic history of metalloporphyrins started in 1902. Owing to the diverse range of applications, especially in solar energy conversion, photocatalytic reactions and their understandable relevance as biological models metalloporphyrins have gained a significant importance. All the known metalloporphyrins are very stable and have been comprehensively investigated both theoretically and experimentally. Porphyrin complexes are recognized for most of the elements except for the rare gases, nitrogen and the halogens. In metalloporphyrins, the porphyrin macrocycle has the ability to act as bi-, tri-, tetra-, and hexadentate ligand, while the metal ions may possess 2-, 3-, 4-, 5-, 6- or 8-coordination. The square-planar coordination environment of the porphyrin ligand has the ability to leave vacant axial positions for the binding of further ligands which can assume cis or trans positions with respect to each other [82]. Trans ligation is preferred when the metal centre is situated in the porphyrin plane otherwise cis coordination has been observed. It has been noticed that two ligand at the trans position strive for the stronger bond formation to the metal centre. When the size of metal ions are large, then the another porphyrin molecule attaches its self as a second ligand and results in the development of double-decker complexes in which the metal ion is sandwich between two porphyrin molecules detail of such type of complexes will be discussed below. Metalation of porphyrin is also a vital biosynthetic reaction in which the insertion of the metal ions into the porphyrin cavity is assisted by enzymes [83, 84]. In metalloporphyrin synthesis generally, in first step, porphyrins are synthesized without metal ion and in the second step the metal ions are inserted into the cavity of porphyrins. Complexation of metal ion with porphyrin results in color change and alteration of the UV-Vis spectrum in the Soret- and Q-region. Synthetic metalloporphyrins can be classified into two types, depending upon the comparability of the ionic radius of the metal ions with the size of the π-macrocyclic hole of the porphyrin [36, 85, 86].

5.2.1. In-plane or coplanar metalloporphyrins

In addition to the versatile coordinative properties, the radius of the deprotonated porphyrinic macrocyle cavity is from 0.6 to 0.7 Å [9] created by four pyrrolic nitrogen atoms is ideally well-matched to bind nearly all metal ions. Because of these properties, a large variety of metalloporphyrins could be synthesized by the insertion of metals into the center of the macrocycles, which are of vital importance in many biochemical processes. The position of the metal center in the porphyrin cavity depends on its spin multiplicity, charge, and size. When the cationic radius of the coordinating metal is in the approximate range of 55-80 pm, the resulting metalloporphyrins is called in-plane/normal/regular or coplanar. In such type of metalloporphyrins the metal centers are situated within the plane of the porphyrin ring, and fit perfectly into the ligand cavity as represented in Figure 1.15 [18].

Figure 1.15 Representation of a regular metalloporphyrin [18]

Metal ions like Zn(II), Cu(II), Ni(II), Co(III) etc. are able to fit perfectly into the cavity of the porphyrin macrocycle and result in the formation of kinetically inert in-plane or coplanar metalloporphyrins. Most of the metalloporphyrins found in natural systems are of regular or co-planar type. The rate of formation of in-plane or normal metalloporphyrins is rather slow because of the rigidity of porphyrins. The symmetry of free-base porphyrins is D_{2h}, which is due to the presence of two protons attached to the diagonally located pyrrolic nitrogen atoms. Upon complexation the symmetry changes to D_{4h} [18]. Some examples of in-plane metalloporphyrins from literature are $Al^{III}TSPP^{3-}$ with ionic radius of 53.5 pm for Al(III) [87], $Fe^{III}TSPP^{3-}$ with ionic radius of 60 pm for Fe(III) [88, 89], and $Pd^{II}TSPP^{4-}$ with ionic radius of 86 pm for Pd(II) [87, 90] (H_2TSPP^{4-} = 5,10,15,20-tetrakis(4-sulfonatophenyl)porphyrin).

Porphyrins have the ability to form stable metal complexes without big structural change. The non-planarity of porphyrins play a crucial role in biological functions, for example hemoproteins such as peroxidases and cytochromes have distorted structures [80, 91]. Therefore, a considerable attention has been paid to the different types of porphyrin distortion on the property and reactivity of porphyrin complexes [92]. In biological systems, during the formation of metalloporphyrins, the amino acids of the metal ion inserting enzymes like

ferro-, nickel-, cobalt-chelatase distort the porphyrins to a saddle shape to enhance the metal incorporation. Distortions in porphyrin and their metal derivatives affect their catalytic activity, reactivity, and redox potentials. As a result of distortion, the symmetry decreases and changes in the various regions of the electromagnetic spectrum have been observed [80, 93].

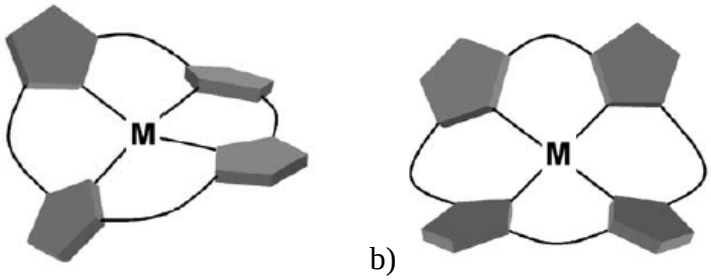

a) b)

Figure 1.16 Distortions of in-plane metalloporphyrins a) saddle and b) ruffled type [92]

In-plane or coplanar metalloporphyrins may exhibit ruffled or saddle types of distortion as shown in Figure 1.16. These types of distortion arise from the congested substitution on the periphery of the porphyrin macrocyle, the protonation of alkylation of the pyrrolic nitrogens, and too short metal nitrogen bonds (shorter than 2Å) which results in the contraction of the coordination cavity. The examples of these types of metalloporphyrins are low-spin nickel(II) [94, 95], chromium(III), titanium(IV), and manganese(III) porphyrins [96, 97]. Ruffled and saddle distortions result in a stronger deviation from the plane, which can be confirmed by the N-C_{α}-C_{meso}-$C_{\tilde{\alpha}}$ dihedral angles [17] Distortion in the planar geometry of porphyrins may tune the chemical and photochemical characteristics of metalloporphyrins. In natural biochemical processes the distortion in the porphyrin ring realizes in different ways for example by axial ligation. The effect of distortion in metalloporphyrins on their chemical reactivity can be explained by an enzymatic reaction in methanogenic bacteria, which requires a highly reduced nickel tetrapyrrole cofactor F_{430} for the production of methane by reducing methyl sulfide. The highly distorted F_{430} controls the reactivity of this enzymatic reaction since nickel protoporphyrin IX which is a planar type are ineffective for this reaction. Drain et al. has explained their findings on nickel porphyrin, their results demonstrated that how intensely electronic properties and excited state dynamics are regulated by distortions in metalloporphyrins [98, 99]. Jentzen et al. and other researches confirm the presence of ruffled and saddle type of distortion in zinc and nickel metalloporphyrin. They also explained that the nonplanar distortions have the ability to modify the photophysical and photochemical properties of metalloporphyrins. The nonplanar

distortion in porphyrins has spectroscopic consequences which have been observed as a red shift in the absorption band in UV-visible spectrum. The size of red shift depends on the magnitude of distortion [80, 100, 101]. Researchers have developed numerous in-plane metal porphyrin complexes for variety of applications [102, 103, 104].

5.2.2. Out-of-plane or SAT metalloporphyrins

Out-of-plane (OOP) metalloporphyrins are formed when the metal centers are unable to fit into the porphyrin cavity. Metal ions of ionic radius greater than 80-90 pm are too large to fit into the porphyrin hole and they are located out of the porphyrin macrocycle plane, distorting it and results in the formation of sitting-atop (SAT) or out-of-plane complexes. Different names like allo, exoplanar, dome metalloporphyrins, roof, sitting above the plane of ligand have been used by researchers for the SAT or OOP complexes. [105, 106, 107, 108]. But the SAT term has been used for out-of-plane products of complexation. [109] In order to avoid misunderstanding, I shall use the out-of-plane (OOP) or sitting-atop (SAT) term in my dissertation. These metal porphyrin complexes exhibit special properties originating from the non-planar structure caused by the size of the metallic cation. A simple representation of out-of-plane metalloporphyrins is shown in Figure 1.17 [18].

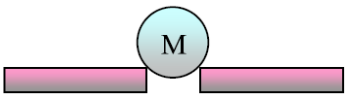

Figure 1.17 Representation of SAT complexes [18]

The out-of-plane metalloporphyrins are kinetically labile, thermodynamically less stable compounds and possess distinguishing structural and photoinduced features which are different from those of the normal or in-plane metalloporphyrins. The OOP complexes formed at faster rate and are more reactive [110]. The out-of-plane position of the metal in SAT complexes induces superior photochemical and photophysical features to all of this class of compounds. The symmetry of SAT complexes is C_{4v} to C_1, which is lower than those of the free-base porphyrins (D_{2h}) and in-plane metalloporphyrins complexes (D_{4h}), in which the metal ion fits into the porphyrin cavity. Because of the inflexibility of porphyrins, the rate of the formation of sitting-atop metalloporphyrins is much faster as compared to the in-plane or

normal metalloporphyrins. In SAT complexes, the distortion in the porphyrin macrocycle produced by the out-of-plane locality of the metal center makes the two diagonal pyrrolic nitrogens more accessible on the other side of the ligand due to the sp^3 hybridization. Structural representations of the out-of-plane metallo-TSPP are shown in Figure 1.18, clearly indicating that the metal ion lies in an out-of-plane position of the porphyrin cavity [18, 30].

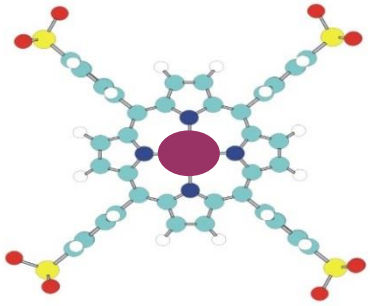

Figure 1.18 Structural model of out-of-plane metallo-TSPP {TSPP=5, 10, 15, 20-tetrakis (4-sulfonatophenyl) porphyrin} [87]

In out-of-plane metalloporphyrins, due to the large radius of the metal center or its coordination ability not preferring square planar arrangement and may result in a distortion known as dome distortion as shown in Figure 1.19. This type of distortion can be observed when the M-N bonds are much longer than half of the diagonal N-N bond distance in the free-base porphyrin. In some special case small metal ions may have out-of-plane position which cause dome distortion; this happens if it coordinates a ligand in axial position [87, 90].

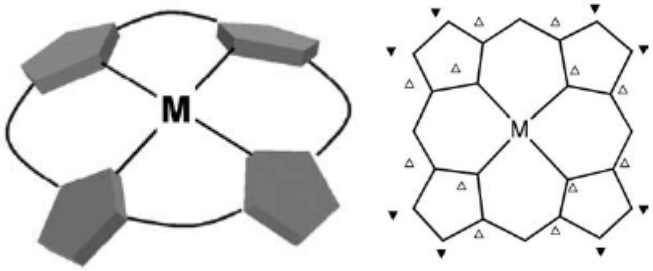

Figure 1.19 Dome distortion in SAT complexes (left) the deviation of atom from the mean plane of the 24-atom porphyrin core: above (Δ) and below (▼) (right) [92]

This dome distorted structure in SAT metalloporphyrins imparts peculiar photochemical characteristics. They can undergo photoinduced charge transfer from the porphyrin macrocyclic ligand towards the metal center. The emission and absorption features of SAT complexes are dissimilar from the in-plane metalloporphyrins [30]. Some out-of-plane

metalloporphyrins of heavy metal ions, like Hg^{2+}, Cd^{2+}, and Pb^{2+}, have the ability to catalyze the synthesis of in-plane complexes via exchangeability through the formation of SAT complexes as intermediates as shown in Figure 1.20 [87, 111]. A small amount of a larger-sized metal ion can accelerate the insertion of smaller metal ions into the ligand cavity.

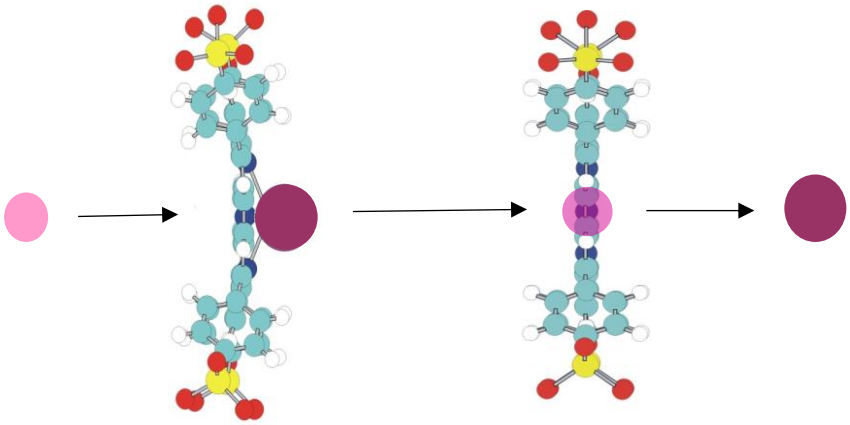

Figure 1.20 Synthesis of in-plane metalloporphyrins [87]

J. H. Wang et al. have also reported the formation of sitting atop the flat porphyrin molecule complexes as a reaction intermediate during the generation of normal or in-plane metalloporphyrin [82]. According to the published literature, photolysis of normal or in-plane metalloporphyrins does not lead to photooxidation of the porphyrin macrocycle for example in palladium(II) [112] and aluminium(III) porphyrins [113]. The reason for this type of behavior is their planar structure and kinetic stability (inertness), which hinder an efficient ligand-to-metal charge-transfer (LMCT) reactions. Contrary to in-plane complexes, out-of-plane metalloporphyrins like tin(II) [114] and (di)(thallium (I) [115] and some border-line complexes [110], for example magnesium(II) and zinc(II) complexes, display a characteristic photoredox chemistry due to the irreversible photodegradation of the porphyrin ligand [31, 87, 116]. This photochemical behavior is caused by an efficient separation of the reduced metal center and the oxidized macrocyle, following the LMCT reaction, which leads to irreversible ring-cleavage giving open-chain dioxo-tetrapyrrol bilindions [118, 119]. The free-base ligand may undergo a photoinduced ring-oxidation but with very low quantum yields and metallation can increase the efficiency of this process [14, 120].

Scientists have successfully carried out the experiments for the insertion of metal ions into the porphyrin cavity. The out-of-plane or sitting-atop position of different metals in porphyrin plane has been fully elucidated on the basis of X-ray structural analysis data, characteristics

absorption bands and proton NMR data [108, 121, 122]. Water-soluble sitting-atop (SAT) ferrous porphyrin ($Fe^{II}TPPS$) has been reported [88]. Some more examples of water-soluble SAT metalloporphyrins are $Ag^{II}TSPP^{4-}$ with ionic radius of 94 pm [63], $Hg^{II}TSPP^{4-}$ with ionic radius of 102 pm [31, 123], and Bi^{III} $TSPP^{3-}$ with 103-pm ionic radius [124].There are different types of out-of-plane complexes, depending on the number of porphyrin or phthalocyanine ligands and metal ions involved in a species. The first type contains mononuclear monoporphyrin complexes. The examples of this type of OOP complexes are zirconium(IV) and hafnium(IV) porphyrins also having two acetate ligands in axial position. The second type of complex in this category is mononuclear bisporphyrins or phthalocyanines. Tin(IV) phthalocyanines are typical examples of such a structure, X-ray analysis has elucidated that tin(IV) is out of both phthalocyanine planes on S_2 axis [125, 126].

Porphyrins have the ability to coordinate two metal centers, forming dinuclear monoporphyrins. Tsutsui has prepared such kind of dirhenium and ditechnetium complexes [127, 128].

In sitting-atop complexes, the out-of-plane position of metal in the porphyrin plane is vulnerable for the probability of aggregation by different bonding modes. These complexes can interconnect by head-to-tail interaction through peripheral substituents on the porphyrin molecule. Moreover, one out-of-plane metal ion may coordinate simultaneously to the cavities of two porphyrin macrocycles, resulting the formation of sandwich shaped structure. Researchers have reported the different possible modes of bonding in out-of-plane complexes and the formation of sandwich type structures [129-132]. Examples of sandwiched or stacked polymer type metalloporphyrins are trinuclear bisporphyrin mercury complexes in which three metal ions are bonded with two macrocycles, representing the third class of out-of-plane complexes. In these sandwich complexes the π-π interactions between porphyrin macrocycles can result in interesting electronic, steric, as well as photophysical and photochemical consequences [125, 129].

In the literature several lanthanide monoporphyrinates and sandwich complexes have been reported. In sandwich type complexes two or three macrocycles are linked with one or two lanthanide ions; in these type of complexes strong electronic interactions between the porphyrin macrocycles impart unique properties to these systems. Because of too large size of lanthanides to fit into the porphyrin cavity, a considerable out-of-plane displacement of the

metal in lanthanide porphyrins has been noticed [133-136]. The upcoming subchapter will further discuss exclusively lanthanide porphyrins.

5.2.2.1. Lanthanide porphyrins

Porphyrin complexes of lanthanide(III) ions have prominent place among a widespread variety of metalloporphyrins. The triplet state of porphyrin has the ability to sensitize the emission of lanthanides. Porphyrins can adopt different structural modifications, which is useful for tuning the photophysical properties. Upon complexation of a lanthanide ion, four coordinating atoms are provided in their deprotonated form. In lanthanide porphyrin systems the metal centre is in +3 oxidation state, thus a secondary anion is necessary for charge balancing, which may be a tri- or bidentate ligand [137].

Lanthanide(III) ion can form stable complexes with porphyrins and related macrocycles. In these complexes due to large ionic radius values the metal ions are positioned above the porphyrin plane and form sitting-atop (SAT) or out-of-plane (OOP) metalloporphyrins. These complexes suggest worthy prospect to scrutinize the distinctive photochemical and photophysical features by exploiting the famous lanthanide contraction [30, 133]. This can be useful for fine-tuning of the sitting-atop position of the metal centre in out-of-plane Ln(III) porphyrin complexes, which may distort the ligand plane and influence photoinduced properties [138].

Lanthanide(III) porphyrin complexes were first time described in 1974 [139]. In start, they were tried in development of an innovative dipolar NMR probe for the applications in biological system [140]. This invention started a new area of research on lanthanide(III) porphyrin chemistry. They have also been tried for the production of singlet oxygen that is used in photodynamic therapy [141]. Horrocks et al. have reported their study on lanthanide water-soluble porphyrin complexes as proton resonance shift reagents toward water, anionic, neutral and cationic substrates [142].

The photophysical properties of porphyrin complexes with trivalent lanthanide ions Ln^{3+} have been subject of many papers [143-146]. Researchers have studied the spectroscopic properties of porphyrins soluble in aqueous and organic solvent. It has been reported that addition of lanthanide(III) ions decrease the emission efficiency of porphyrin. Only unpredicted behavior has been observed in case of low concentration of Pr(III), which

increased the porphyrin emission intensity. Lanthanide ions influence the absorption as well as emission spectra of porphyrins [147].

G. E. Khalil et al. has recorded emission and excitation spectra, lifetime and relative quantum yield measurements for Gd, Yb, Nd and Er porphyrins in different solvents. His study provide results on stable NIR porphyrin based emitters and reported complete emission spectra of gadolinium porphyrins [148]. The fluorescence, phosphorescence and quantum yield of the emission of Gd(III) and Lu(III) porphyrin complexes have been determined in solution at different temperatures. The photophysical results on Gd(III) and Lu(III) porphyrins have suggested the possibility of utilization of lanthanide porphyrins complexes in the intraratiometric luminescence intensity-based oxygen sensing [149]. Lanthanide porphyrins offer prodigious advantages over the conventional visible-light emitters in sensing and bio-imaging because of their deep penetration, sensitization of the near-infrared (NIR, 700-16 nm) emission of lanthanide(III) centre due to their long-lived triplet exited state. Luminescent properties of lanthanide porphyrin complexes has also been studied is detail [134, 150]. H. He has published his results on different Ln(III) porphyrin complexes due to their unique emission in near-infrared (NIR) and potential applications in biomedical diagnosis. In addition, he studied impact of structural change on the NIR emission efficiency [137]. V. Bulach has also presented his review article on the synthesis and photophysical properties of near-infrared emitting lanthanide porphyrin complexes. He has explained in detail about the sensitization mechanism and different factors effecting the overall quantum yield of the NIR emission process of lanthanide porphyrin complexes [132]. The interaction of lanthanide(III) ions with porphyrins results in the formation of different types of complexes, depending on the modes of coordination and number of porphyrin molecules involved. Lanthanide(III) ion can form monoporphyrins, LnPor, in which one metal centre coordinates one porphyrin along with an axial ligand. In lanthanide sandwich complexes also known as bis- (oligo-) porphyrins ($Ln(Por)_2$), one out-of-plane metal ion can simultaneously connect to two macrocycles. In these sandwich complexes the π-π interactions can result in interesting electronic, steric, as well as photophysical and photochemical features [133]. W. K. Wong has synthesised and studied the photophysical properties of lanthanide(III) monoporphyrinate complexes. He showed that the porphyrinato dianion acted as an antenna sensitizing the Ln^{3+} ion emission in the NIR region [134]. J. Jiang et al have reported the formation of the cerium porphyrin double-decker and have confirmed the constitution of their double-decker property by UV-visible and IR spectra [151]. Wittmer and

Holten have made comparison of the photophysics monomer, double- and triple-decker complexes of lanthanide porphyrins. The results obtained from steady-state and time-resolved optical spectra for the double-decker porphyrin sandwiched complexes were similar to those of the triple-decker but was different in the case of monomeric metalloporphyrins. These results can be interpreted by the presence of strong π-π interactions between the macrocycles of the sandwich complexes [152]. Moreover, with lanthanide contraction, the absorption band may be blue- or red-shifted, depending on the nature of electronic transition. Lanthanide ions facilitate the deactivation process of photo-excited complexes by heavy-atom enhancement of intersystem crossing rate [136]. Lanthanide bisporphyrins are advantageous as structural models of the photosynthetic reaction centre in bacteria. Lanthanide(III) trisporphyrin (triple-decker) complexes could be prepared in organic solvents [30, 133].

In oligoporphyrins there are many possibilities regarding the coordination of the Ln(III) ions; instead of coordination in the porphyrin cavity, Ln(III) may be coordinated through the peripheral substituents attached to the macrocyle. This type of coordination is designated as tail-to-tail. The second possibility is head-to-tail coordination, in which one Ln(III) ion is simultaneously coordinated through four pyrrolic nitrogens and peripheral substituents [17]. In 2007 Lipstman and co-workers reported the synthesis and possible bonding modes of coordination polymers by the reaction of lanthanide metal ions with *meso*-tetra(4-carboxyphenyl)porphyrin (TCPP). In these coordination polymers every lanthanide ion binds to the lateral carboxylate functions of five neighbouring TCPP units as shown in Figure 1.21. The coordination sphere includes six carboxylate O-atom (three carboxylate group) and two water molecules at each metal nodes [153].

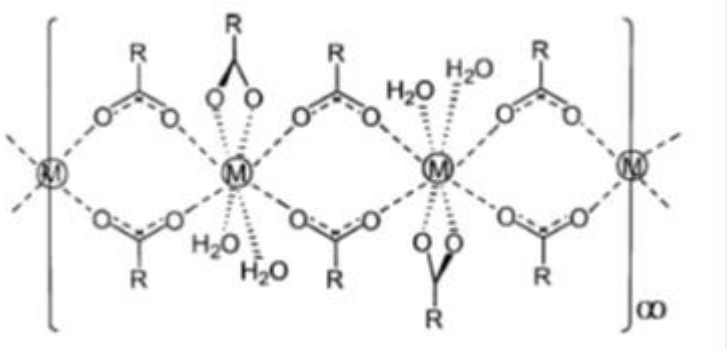

Figure 1.21 Schematic illustration of the coordination polymerization mode in M (TCPP) $(H_2O)_2$. M= Dy, Sm, Pr, Gd or Er, and R represents the porphyrin framework associated with the carboxylate group [153]

The out-op-plane position of the metal in lanthanide porphyrins is suitable for photoredox reactions. Upon irradiation with visible light, lanthanide porphyrin complexes have the ability to undergo photochemical oxidation and reduction reactions. S. Radzki has reported his photolysis experiments on Ce(IV) porphyrin sandwich complexes in the presence of carbon tetrachloride as an electron acceptor which led to the generation of π cation radical. The photolysis process was monitored by using electron absorption and circular dichroism spectroscopy [154].

5.2.2.2 Lanthanide chemistry

Lanthanides (abbreviated as Ln) are a series of elements that starts from lanthanum (La) with atomic number 57 to lutetium (Lu) with atomic number 71, which are located in the first row of *f*-block in the periodic table. With the addition of scandium and yttrium, which are in the same sub-group the overall 17 elements are also collectively known as rare-earth metals (REE) [155]. From historical point of view, the discovery of lanthanides or rare-earth metals started in 1794 when Johan Gadolin discovered yttrium in Scandinavia. During investigations on yttrium, he discovered additional elements like gadolinium, dysprosium, terbium and ytterbium etc. Later on, in the year 1803 other scientists' isolated and discovered further lanthanides like cerium, neodymium and europium etc. Henry Moseley also verified lanthanides by the use of X-ray spectroscopy [156-157].

The lanthanide chemistry is different from that of the *d*-block elements in various aspects. Lanthanides usually form cation with +3 oxidation state and their *f*-orbitals are at higher energy as compared to 5*s* and 5*p* orbitals but are also shielded by these orbitals. According to the low energy principle, there are two kinds of electronic configurations for Ln elements which are [Xe]$4f^n6s^2$ and [Xe]$4f^{n-1}5d^16s^2$, where *n* ranges from 1 to 14. La, Ce, and Gd fit in the first scheme, while the others follow the second scheme [155]. This special type of electronic configuration gives very exceptional photophysical properties to the lanthanides [158]. Another distinguished feature is the well-known lanthanide contraction, according to which the size of the Ln^{3+} ions decreases from left to right in the periodic table. The decrease in ionic radius of Ln^{3+} in coordination number eight and other selected properties of lanthanides ions is given in Table 1.1. The penetration of 4*f* electrons into the 5*s* and 5*p* orbitals results in insufficient shielding of 5*s* and 5*p* electrons from the increasing nuclear

charge. Due to this inadequate shielding, the electron cloud contraction and decrease in ionic radius by increase in effective nuclear charge could be observed [159].

Table 1.1 Selected properties of lanthanides [159, 160, 161]

Atomic Number	Name	Symbol	Neutral Valence Electron	$M3^+$ Valence Electrons	Ionic Radius (M^{3+} pm) in Coordination Number 8
57	Lanthanum	La	$5d^1\ 6s^2$	-	116
58	Cerium	Ce	$4f^1 5d^1 6s^2$	$4f^1$	114.3
59	Praseodymium	Pr	$4f^3 6s^2$	4f2	112.6
60	Neodymium	Nd	$4f^4 6s^2$	$4f^3$	110.9
61	Promethium	Pm	$4f^5 6s^2$	$4f^4$	109.3
62	Samarium	Sm	$4f^6 6s^2$	$4f^5$	107.9
63	Europium	Eu	$4f^7 6s^2$	$4f^6$	106.6
64	Gadolinium	Gd	$4f^7 5d^1 6s^2$	$4f^7$	105.3
65	Terbium	Tb	$4f^9 6s^2$	$4f^8$	104.0
66	Dysprosium	Dy	$4f106s2$	4f9	102.7
67	Holmium	Ho	$4f^{11} 6s^2$	$4f^{10}$	101.5
68	Erbium	Er	$4f^{12} 6s^2$	$4f^{11}$	100.4
69	Thulium	Tm	$4f^{13} 6s^2$	$4f^{12}$	99.4
70	Ytterbium	Yb	$4f^{13} 6s^2$	$4f^{13}$	98.5
71	Lutetium	Lu	$4f^{14} 5d^1 6s^2$	$4f^{14}$	97.7

The lanthanides have typical magnetic and absorption properties that are different from *d*-block elements. Ln^{3+} ions show transitions in the near UV range and no absorption in the visible range [162], and the transitions with *f*-orbital manifold are parity forbidden, which gives rise to low molar absorption, long lifetime (in milliseconds) of their excited state and luminescence [163]. The absorption spectra of lanthanides are line-like and originate from *f-f* transitions [164]. The 4*f* orbitals are scarcely affected by adjoining environment which make the transitions at fixed wavelength (line-like) or having close resemblance of free metal ions.

The lanthanide ions, except for Lu^{3+} and Gd^{3+} show luminescence in the UV and NIR region. Lu^{3+} being completely filled and Gd^{3+} being half-filled are not luminescent. Gd^{3+} is also not luminescent because of highly excited states. The magnetic moments of lanthanide(III) ions can be determined with equations using *J* state [163, 165].

As discussed above, lanthanide ions have low molar absorption coefficients. Due to this feature, the excitation of their electronic states is not effective. It has been reported that lanthanide emissions can be sensitized by absorption of organic ligands which transfer energy to the metal center [166, 167]. Numerous visible emitting lanthanide complexes have been prepared that are of immense importance in time-resolved immunoassays and diagnostic imaging etc. [163, 168, 169].

Another feature of lanthanides is the tendency of bond formation with non-metals. According to Pearson's classification, lanthanides are hard Lewis acids and prefer to bind hard bases like nitrogen and oxygen atoms [159, 170]. The coordination number of lanthanides is between 3 to 12, but 8 and 9 are most common and the crystal field stabilization energy is 4.18 kJ/mole [171]. These coordination numbers are advantageous for the formation of sandwich type complexes with cubic or square antiprism polyhedron. Their typical *f-f* absorption and emission bands are favorable for deeper investigation of ligand-to-metal charge transfer (LMCT) processes. The lanthanide contraction is beneficial to the study of the fine tuning of the out-of-plane distance in lanthanide(III) complexes especially with porphyrin type ligands, due to their planar structure. The low redox potential values of lanthanides are very useful in photoinduced cleavage of water [170].

5.3. Applications of metalloporphyrins

The chemistry of metalloporphyrins has become a wide-ranging research area, which is very attention-grabbing and worthwhile for researchers not only in the field of chemistry but also in medicines, biochemistry, industrial catalysis and in many photochemical processes. Porphyrin complexes with metals like nickel, magnesium, iron and cobalt are primary metabolites and without these it would be difficult to sustain life on this planet [172].

Metalloporphyrins offer a versatile synthetic base for a variety of applications. Their assemblies have been increasingly explored as building blocks for tailored material properties on the area of sensors, field-responsive materials, optical communication, and data storage.

Besides, mono- and di-cation porphyrin π-radicals are stable and are applicable in photoionization processes [173].

Metalloporphyrins are also widely used in fields like gas storage, photonic devices, separation, molecular sensing, magnets, and heterogeneous catalysis. They have the ability to selectively catalyze the oxidation of cyclohexane to the corresponding alcohol or ketone under mild conditions without producing any other byproducts. They can easily be immobilized on inorganic supports and tailored the selectivity of the resulting catalyst [174]. Complexes of porphyrin with zinc, cobalt and rhodium have the ability to initiate free radical type of polymerization [175, 176].

Currently, there is a great interest in the near infrared luminescence (NIR) and energy transfer mechanism of lanthanide porphyrin complexes because of their possible application in biological imaging, fluoro-immuno-assays, and photodynamic therapy (PDT). Due to the f-f forbidden transitions, lanthanides need to be sensitized by a chromophore (antenna) [134, 150]. PDT is a developing technique for the treatment of cancerous tumors. In this method a photosensitizer is activated by light in the presence of oxygen, after light irradiation of the photosensitizer, the energy from the excited matter is transferred to the surrounding molecule, i.e. dissolved oxygen [177].

Metalloporphyrins are also promising for solar energy utilization. They have potential for photochemical splitting of water into hydrogen and oxygen by utilizing solar energy. The generated molecular hydrogen could be separated and used for clean burning as inexhaustible and environmentally friendly energy source. In photochemical reduction of water a photosensitizer collects light energy and converts it into excited electrons; this step is the same as in chlorophyll during photosynthesis. In the second step the electrons are collected by a metal catalyst which uses them to reduce water to hydrogen and there is a sacrificial electron donor, whose job is to replenish the electron lost by photosensitizer [4, 178]. In this contest, the light-absorbing power of porphyrin-related compounds should be used in the near future for many other applications and much more can still be studied in the future.

6. Water-soluble porphyrins

Porphyrins and their metal derivatives have played a significant role in modeling the natural photosynthetic process and development of photochemical systems for solar energy conversion. All these advantageous properties of porphyrins are due to their promising redox properties, long life time of their triplet electronic states and great light absorbing properties [179]. There is an increasing interest in carrying out photophysical, photochemical processes and photo dissociation of water into hydrogen and oxygen experiments that involve porphyrin and their metal derivatives in aqueous solutions as a water-soluble photosensitizer [180].

Depending on the solubility, there are two categories of porphyrins. The first type are natural porphyrins which have one or more carboxylic substituents attached to the pyrrolic groups of the porphyrin macrocycle. These are soluble in aqueous alkaline solution, but only few natural porphyrins are water-soluble. The second type of porphyrins belongs to the synthetic ones which are not sufficiently soluble at or close to neutral pH either. For an extensive investigation of physiochemical characteristics of porphyrins and their derivatives, it is required to make them water-soluble [180, 181]. Tetrapyridylporphyrins (TPyP) and tetraphenylporphyrin (TPP) are meso-substituted synthetic porphyrins, which are used to study photochemical reaction. Different types of water-soluble porphyrins were made by introducing of some moieties like COO^{-}, NMe_3^{+}, SO_3^{-}, $-O^{-}$ etc. on the phenyl group of TPP and in the case of TPyP by quaternization of the pyridyl N center. The structural formulas of some common water-soluble porphyrins like sulfonatophenyl (TPPS), carboxyphenyl (TPPC) and N-methylpyridyl (TMPyP) derivatives are shown in

Figure **1.22** [182, 183].

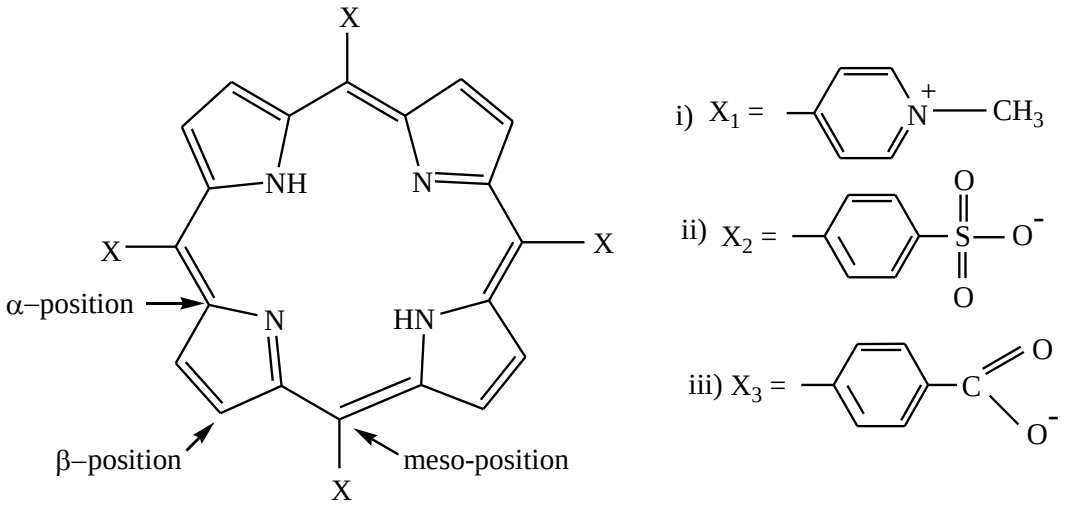

Figure 1.22 Synthetic water-soluble porphyrins i) X=X_1, H_2TMPyP^{4+}= 5,10,15,20-tetrakis(4-*N*-methylpiridinium) porphyrin ii) X=X_2, H_2TSPP^{4-} = 5,10,15,20-tetrakis(4-sulfonatophyenyl)porphyrin iii) X=X_3, H_2TCPP^{4-} = 5,10,15,20-tetrakis(4-carboxyphenyl)-porphyrin

From acid-base equilibrium point of view, porphyrins and their derivatives are of amphoteric nature, i.e., they can behave as both bacids and bases. The presence of nitrogen atoms in porphyrin cavity gives rise to this stimulating feature. In acidic medium two-imine nitrogen atoms can be protonated to form mono- or di-cation and can be represented as PH_3^+ and PH_4^{2+} respectively. While the removal of protons attached to the nitrogens by addition of base leads to mono- or dianions (PH^- and P^{2-}). A change in absorption spectra is helpful to determine the equilibria. Upon metalation, the porphyrin are no more amphoteric due to the bond formation with metals. The knowledge of pK values is very helpful to explain the acid-base behaviour of porphyrins. The pK_3 values of free base porphyrin (PH_2/PH_3^+) depends on the nature of side chains attached to the pyrrole ring. The normal range of pK_3 is from 2.5 to 5.5. The order of some pKa values of some common free base porphyrin is $TMPyP^{4+}$ < $TAPP^{4+}$< $TPPS^{4+}$ < MesoP < EtioP. In the oxidation reduction potential values follow the basicity of the ligand. It is difficult to reduce basic porphyrins [21].

The basicity of porphyrin macrocyle depend on the nature of peripheral substituents. The most commonly studied porphyrin in literature are those with charged substituents at para position. In addition to the basicity, the presence of charged substituents at the periphery of porphyrin macrocycle influences the chemical, photochemical and redox properties of porphyrins. The electron donating groups increase the basicity of porphyrins. The presence of carboxylate and sulfonate as peripheral substituents either at meso or β-pyrrole position

further increase the basicity of porphyrin. The electron donating groups as peripheral substituents affect the kinetic and redox behavior of the porphyrins. Studies have shown that there is a marked difference between the photophysical and redox properties of tetrapyridyl and tetrapheny porphyrins. TPyPs are more acidic than TPPs [180, 182].

Water-soluble porphyrins and their metal derivatives have the ability to exist as monomer, dimer or as aggregates in aqueous medium W. I. White has studied this phenomenon [184]. Aggregation of porphyrins causes a perturbation in absorption and emission which can be monitored spectroscopically. Aggregation largely depends on the type of porphyrin and the polarity of the medium. The aggregates are stabilized by weak interactions and by π-π interactions of the porphyrin macrocycle [21].

Aggregation of meso-substituted porphyrins depends on the charge and nature of peripheral substituent, concentration, metal ions and porphyrins type. The geometry of porphyrin aggregates is dictated by porphyrin unit [185, 186]. Porphyrins having negative substituents at the periphery are more basic and have greater tendency to form aggregates as compared to the porphyrins with positively charged substituents at periphery. Studies have shown that some meso-substituted porphyrins dimerize in aqueous solution [182]. Pasternack et al found no aggregation at 0.1 M concentration and 298 K in the case of NiTMPyP, CuTMPyP, ZnTMPyP and ZnTCPP but NiTCPP and CuTCPP dimerize at this concentration [187].

Tetraphenylporphyrin tetrasulfonate $TPPS^{4-}$ is soluble in water and up to a millimolar level it does not aggregate but $TPPS^{3-}$ has limited water solubility and shows extensive aggregation. The solution properties of $TPPS^{4-}$ were studied by Fleisher et al and dimerization was found in neutral solution but in acidic solutions it showed a complicated behavior. At pH less than 2 an extensive aggregation could be seen but above the pH 3 it did not aggregate [21, 188].

Metal complexes of water-soluble porphyrins like Mn(III) meso-tetra (4-sulfonatophenyl) porphyrin (Mn^{III}TPPS) haven been reported as a possible MRI contrast agent in magnetic resonance imaging (MRI). Complexes of Gd(III) and Fe(III) porphyrins have also been reported and studied in this field. Complexes of porphyrins like [Mn^{III} (TPPIS) Cl] and [Mn^{III} (TPPAS) Cl] are now patented as MRI contrast agents [189, 190]. From past few years several admirable reviews have been published on lanthanide porphyrin water soluble systems and their possible applications in many fields for example in biomedical, NMR and development of luminescent lanthanide complexes operating in aqueous media [191, 192].

Chapter 2: Objectives

The main goals of my PhD research work were the investigation of the formation and elucidation of the mechanism of the photoredox reactions of water-soluble lanthanide(III) porphyrin out-of-plane complexes. For tuning the photoredox activity of SAT metalloporphyrins, preparation of out-of-plane complexes of a series of lanthanides ions (La, Ce, Nd, Sm, Eu, Gd, Dy, Er, Yb, and Lu) with wide range of ionic radii was planned with the anionic porphyrin 5,10,15,20-tetrakis (4-sulfonatophenyl) porphyrin (H_2TSPP^{4-}) as a ligand. Lanthanide ions as metal centers offer good possibility of fine tuning, due to the well-known lanthanide contraction at constant oxidation state +3 resulting in different out-of-plane positions and, thus, different distortions of the ligand plane.

Regarding the complex formation, the investigation of the effect of potential axial ligands was targeted. Hence, the influence of the very weakly coordinating perchlorate ion compared to that of the acetate ion, which is a hard and efficiently binding ligand, was planned for realization of different complex equilibrium systems. Also determination of the formation constants of these metalloporphyrins was aimed in order to reveal how the size of the metal center, i.e., the lanthanide contraction, affects the stability of these species.

Within the photophysical studies, the measurements of both the absorption and emission properties were planned to gather useful pieces of information how the structure and the metal influence the transitions between the various electronic states of these complexes. Besides, reversely, the results of such spectroscopic (both steady-state and time-resolved) experiments could efficiently contribute to the determination of the structure of the lanthanide(III) porphyrin complexes formed in these systems.

The photochemical investigations targeted to reveal the various photoinduced reactions taking place upon excitation of these complexes at both the Soret- and the Q-bands. Comparisons of the efficiencies and the partial contributions of the individual photoreactions for each complexes could provide relevant data for recognition and interpretation of trends in the functions of the ionic radius of the metal center. These experimental results gained under various conditions would enable us to choose the most promising systems and complexes for long-term photocatalytic purposes.

Chapter 3: Experimental

1. Materials

In the experimental work, the lanthanide metals including cerium, neodymium, samarium, europium, gadolinium, dysprosium, erbium and ytterbium were used in the form of chloride salts with 6 H_2O. Tetrasodium salt of 5,10,15,20-tetrakis(4-sulphonatophenyl)porphyrin (H_2TSPP^{4-}) with molecular formula $C_{44}H_{26}N_4O_{12}S_4Na_4.12H_2O$ was applied as water soluble ligand. Sodium hydroxide (NaOH), acetic acid (CH_3COOH), and sodium perchlorate ($NaClO_4^-$) were used for making buffer solution and as ionic strength adjustor, while for making actinometry 1,10-phenanthrolein and potassium trisoxalatoferrate (III) $K_3[Fe(C_2O_4)_3]$ were applied. All the chemicals purchased from Sigma-Aldrich (Germany) were of high purity and were used without any further purification. Argon gas was used for bubbling and removing oxygen from the samples . Water served as solvent after doubly-distillation and purification with Millipore Milli-Q system manufactured by Millipore, France. All experiments were carried out at room temperature (295 K), in open air and atmospheric conditions. Oxygen was removed by bubbling argon using Schlenk system where needed. Properly washed and dried glass ware and magnetic stirrer to homogenize the reaction mixture were used. For accurate and precise results, mechanical micropipettes ranging from 1-5000 µl along with pipette tips for perfect fitting made by Biohit Company were used. For absorption and emission measurements quartz cuvettes of various optical pathlengths manufactured by Hellma Analytics Company were applied. The cuvettes are cleaned and stored with care to avoid the build-up of porphyrin or any other impurity on the walls. Because of very sensitive nature of porphyrin toward the reaction with metals, even at very low concentrations, dilute HCl solution followed by the washing with distilled water was used for cleaning of cuvettes to eliminate the possibility of any sort of contamination. These cuvettes were also used as reaction vessels for photolysis of water soluble metal porphyrins systems.

2. Preparation of Ln(III) porphyrin complexes

Water-soluble lanthanide(III) porphyrin complexes were prepared by the interaction of selected lanthanide(III) chloride salts (of La, Ce, Nd, Sm, Eu, Gd, Dy, Er and Yb) with 510,15,20-tetrakis (4-sulphonatophenyl) porphyrin (H_2TSPP^{4-}) also abbreviated as H_2P^{4-} in the presence of 2.5M sodium acetate buffer of pH 6.0 or 1.51M sodium perchlorate as an ionic strength adjustor. The concentration range of the metal ions was from 1×10^{-4} to 1×10^{-3} M while for H_2TSPP^{4-} from 1×10^{-7} to 1×10^{-6} M. The general reaction scheme between metal ion and ligand is given below in Equation 2.1

$$y\ H_2P^{4-} + x\ M^{z+} \longleftrightarrow M_x P_y^{(xz-6y)} + 2y\ H^+$$

Equation 2.1 General reaction between Ln(III) and H_2TSPP^{4-}

The metal and ligand salts were dissolved in properly purified water for preparation of stock solutions. By using micropipettes, the appropriate volume from the stock solutions of metal, ligand and ionic strength adjustors was added in volumetric flasks. Metal ions were in excess compared to the porphyrin ligand, in order to shift the equilibrium toward the complex formation. To ensure the onset of complex equilibrium the solutions containing metalloporphyrins and buffer or ionic strength adjustor were put in oven at 333 K for about one day (in the case of some reactions the heating time was more than one day). For each selected lanthanide(III) member different series of solutions containing metal porphyrins were prepared by varying the concentration of metal ion, porphyrin, buffer and ionic strength adjustor.

3. Instrumentation and methods

3.1. UV-Visible absorption spectrophotometry

The basic principal of spectroscopy is the interaction of electromagnetic radiations with matter that results in the absorption of ultraviolet and visible light by molecules. Ultraviolet and visible absorption spectroscopy (UV-Vis) involves the measurement of light intensity after passing through a sample. After the absorption of electromagnetic radiations by molecules, the most probable transition is the moving of electrons from the highest occupied molecular orbital (HOMO) to lowest unoccupied molecular orbital (LUMO). The molecular

orbitals at the lower energy level are occupied σ and π orbitals, while π* and σ* are at higher energy level. The amount of light absorbed is proportional to the concentration of the absorbing molecule and is described by the Beer-Lambert law. Thus it can also be used to calculate the concentration of sample, according to the following equation,

$$A = \log_{10} I_o/I = \varepsilon\, c\, l$$

where A is absorbance, I_o and I are the intensities of the incoming and transmitted light, respectively, ε (L mol^{-1} cm^{-1}) is the molar absorption coefficient, c (mol dm^{-3}) is the concentration of the sample and l (cm) is the pathlength [193].

The highly delocalized 18 π-electrons of a porphyrin ring offer an easy and precise monitoring opportunity for the ligand-metal binding process by UV-Visible absorption spectrophotometry. The UV-Visible spectral measurements represented in this dissertation were performed predominantly on a Specord S-600 diode-array spectrophotometer made by Analytik Jena in Germany.

In the solutions of H_2TSPP^{4-} the ionic strength and pH need special attention because at pH≤5 protonation and aggregation of the porphyrin may occur due to the corresponding equilibrium constants (pK_3 = 4.99 and pK_4 = 4.76) regarding the protonation of the two diagonally situated pyrrolic nitrogen atoms of this free base [31]. The actual concentration of H_2TSPP^{4-} can be estimated spectrophotometrically by using its Soret-band at 413 nm. According to the literature, its molar absorption coefficient at this wavelength is ε_{max} = 4.66× 10^5 M^{-1} cm^{-1} [194]. In the solutions containing Ln(III) porphyrins a pH value of 6.0 was adjusted by the addition of buffer and ionic strength adjustor. The absorption spectra of Ln(III) porphyrin complexes were analyzed by spectral deconvolution. This kind of evaluation was carried out in MS Excel. The formula for Gaussian and Lorenz curves are given as Equation 2.2 a and b [195],

Equation 2.2 a) the Gaussian curve, b) the Lorenz curve

a) $$A(\bar{\nu}) = \frac{A_{max}(\bar{\nu}_0)}{\exp\frac{(\bar{\nu}-\bar{\nu}_0)^2}{2\sigma^2}}$$ b) $$A(\bar{\nu}) = \frac{A_{max}(\bar{\nu}_0)}{(\bar{\nu}-\bar{\nu}_0)^2 + \frac{\Delta^2}{4}}$$

where A is absorbance, $\bar{\nu}$ is wavenumber, $\bar{\nu}_0$ is the wavenumber of the absorption maximum, $\omega_{1/2}=\Delta=2\sqrt{2ln2}\,\sigma$ the halfwidth (cm^{-1}).

The electronic states in a molecule strongly depend on the symmetry, thus the electronic spectra are helpful in structural determination. The molecular eigenfunctions of the ground states and different excited states determine the possibility, thus the intensities of electronic transitions, taking the selection rules into consideration. The correlation between theory and experiment is expressed by the *oscillator strength "f"*n (Equation 2.3), from which the Einstein transitions probability can be determined. The oscillator strength is a number ranging from one to zero. Forbidden transitions have oscillator strength close to zero, while electronically allowed transitions show values of close to one [196, 197, 198].

Equation 2.3 The oscillator strength

$$f = \frac{8\pi^2 cm_e \omega_{1/2}}{3he^2} g_{12}[M]^2 = \left(4{,}32 * 10^{-9}\,Mcm^2\right) F \int \varepsilon(\omega) d\omega \approx \left(4{,}6 * 10^{-9}\,Mcm^2\right) F \varepsilon_{max} \Delta\nu_{1/2}$$

In equation 2.3 c is the speed of light (299792458 ms^{-1}), m_e is the mass of electron (9.109×10^{-31} kg), $\omega_{1/2}$ the transition wavenumber (cm^{-1}), h is Planck's constant (6.626×10^{-34} J s), g is the degree of degeneracy, *[M]* is Einstein's transition moment, $F=9n/(n^2+2)^2$ is the refraction factor, $\varepsilon(\omega)$ is the molar absorption coefficient ($M^{-1}cm^{-1}$) at the wavenumber ω), $\Delta\nu_{1/2}$ is the Gaussian width at half maximum (cm^{-1}).

For evaluation of the experimental results in this work, the spectral data of spectrophotometric titrations were used to calculate the molar absorption coefficient at a given wavelength and stability constants of Ln(III) water-soluble anionic porphyrin complexes.by using Equation 2.4 and Equation 2.5. For fitting the calculated absorption spectra to the measured ones MS excel procedures were applied.

Equation 2.4 For calculation of absorbance

$$A_\lambda = l \sum_{j=1}^{n} \varepsilon_{j\lambda} \beta_j \prod_{i=1}^{k} [c_i]^{\alpha_{ji}}$$

where A_λ and λ are absorbance and wavelength, l is pathlength (cm), $\varepsilon_{j\lambda}$ is the molar absorption coefficient (M^{-1} cm^{-1}) of the j^{th} species, β_j is its stability constant (M^m), $[c_i]$ is the equilibrium concentration of the free analyte, α_{ji} component particles in stoichiometric index

The anionic Ln(III) porphyrins studied in this work are kinetically labile sitting-atop (SAT) metalloporphyrins. As seen later, the presence and absence of acetate ion as a bidentate O-donor ligand proved to be the key factor from the viewpoint of the metal-porphyrin interaction, i.e. regarding the formation of bisporphyrin complexes.

Equation 2.5 The generalized (equilibrium) reaction equation for the formation of metalloporphyrins

$$y\,H_2P^{4-} + x\,M^{z+} \Leftrightarrow M_xP_y^{(xz-6y)} + 2y\,H^+$$

$$\beta_i = \frac{\beta_i'}{[H^+]^{2y}} = \frac{[M_xP_y^{(xz-6y)}]}{[H_2P^{4-}]^y[M^{z+}]^x}$$

3.2. Fluorescence spectroscopy and lifetime measurements

Fluorescence spectroscopy is a technique which is used to study the emission and excitation processes in various materials. Molecules have the ability to go into their electronically excited state when they absorb light of wavelength covering the energy gap between the ground and excited state. This phenomenon is termed as molecular light absorption. The absorption depends on concentration and other factors as described by the Beer-Lambert's law. In the absorption of molecules we were interested only in the transitions from ground to excited states. Fluorescence is a photon emission process that completes by molecular relaxation from the excited electronic states.

In this research work all the fluorescence measurements were recorded by using a Fluoromax-4 (Horiba Jobin Yvon) spectrofluorometer supplemented with a time-correlated single-photon counting accessory for the determination of the fluorescence lifetimes. For this purpose a nanoLED of 393 nm was the excitation sources. The Equation 2.6 gives the relationship between the radiation quantum efficiency and lifetime for S_1 state. For estimation of the quantum yield for S_1 fluorescence Equation 2.7 was used.

Equation 2.6 For S_1 lifetime calculation.

$$\varphi_r = \frac{k_r}{k_r + k_{nr}} = k_r\tau$$

In equation 2.6 k_r and k_{nr} are radiative and non-radiative rate constants, τ is lifetime, while in equation 2.7 A_r and A_{ref} are the area under the emission intensity curve for the sample and the reference. $\Phi_{S1\text{-}B}$ is the quantum yield of S_1-fluorescence using the Soret- or B-band for excitation, IC is internal conversion.

Equation 2.7 For determination of S_1-fluorescence quantum yield.

$$\Phi_s = \Phi_{ref} \frac{A_s}{A_{ref}} \qquad \Phi_{S1\text{-}B} = \varphi_{S1} \times \varphi_{IC}$$

3.3. Photolysis instrumentation and procedures

For the investigation of photochemical reactions under continuous irradiations, an AMKO LTI photolysis equipment containing a 200-W Xe-Hg lamp and a manually operating monochromator was used. The light intensity of the monochromator was measured by ferrioxalate actinometry for given geometries at different wavelengths [199, 200, 201]. Before and after every photolysis experiment, the relative light intensity was measured with a thermopile. The simplified scheme of the photolysis instrument is shown in Figure 3.1.

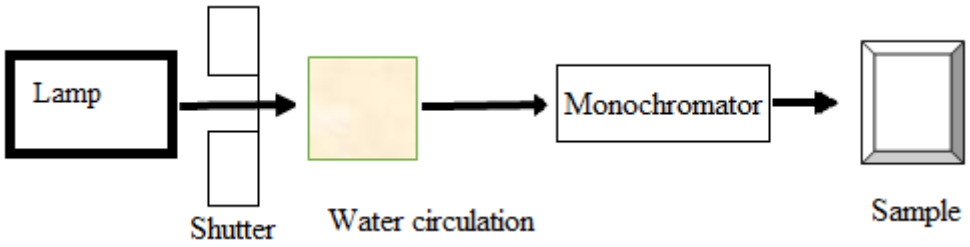

Figure 3.1 Components of photolysis set-up

Photolysis experiments were normally carried out to study photoredox chemistry, photo oxidation of the porphyrin macrocycle and to estimate the photochemical quantum yield.

All the prepared Ln(III) porphyrin systems were irradiated at both the Soret-band (421 nm) in a cuvette of 1cm and at the Q-band of 555nm in 5cm cuvettes. The samples were irradiated until the absorbance diminishes to approximately half as compared to its start value at the selected wavelength. The sampling time was 1, 2, 4, 8, 16 minutes and so on. To reveal the effect of O_2 on photoxidation and quantum yield of the photochemical process, all the prepared complex solutions were photolyzed not only in open air (air saturated) atmosphere, but also in deoxygenation form. To get rid of oxygen from the solutions of metal porphyrin, they were purged with argon. All the irradiated solutions were saved to measure the absorbance after one day in dark to check the stability of the photo-products.

For the accurate determination of photochemical quantum yield, initial slope, integral fitting and concentration distribution methods could be used. In simple case, the initial slop method can be used which is based on the Equation 2.8 (a). This method is based on the change in the concentration of the absorbing species during the photolysis, resulting in a monotonous change of light absorption.

Equation 2.8 For initial slope method

$$I_0\Phi(1-10^{-A}) = \frac{dc}{dt} = -\frac{dA}{\varepsilon l dt} \quad .....(a)$$

$$I_0\Phi\varepsilon l(1-10^{-A_0})t = A_0 - A \quad .....(b)$$

In Equation 2.8 a and b I_0 is the concentration of the incident photons in cuvette per second (mol dm^{-3} s^{-1} , Φ is the overall photochemical quantum yield, A is the absorbance at the wavelength of irradiation, $\Delta c/\Delta t$ is the reaction rate, which is the change in concentration over time, ε is the molar absorption of the complex at the wavelength of irradiation (dm^3 $mol^{-1}cm^{-1}$), l is optical pathlength of the cuvette in centimeters and $\Delta A/\Delta t$ is the change of absorbance over time. The initial-slop method is unable to take the degradation of the photoactive complex over the whole irradiation time into consideration. Instead, it uses the first measurement points for the calculation. A modified form of the initial-slop method is Equation 2.8 b, in which A_0 is the initial absorbance of the irradiated solution at the given wavelength. A second method for the calculation of quantum yield is integral fitting (Equation 2.9) [30].

Equation 2.9 For integral fitting method

$$\Phi\int_0^t dt = -\frac{1}{I_0\varepsilon l}\int_{A_0}^{A}\frac{1}{1-10^{-A}}dA$$

$$\Phi t = \frac{A_0 - A + \lg\frac{1-10^{-A_0}}{1-10^{-A}}}{I_0\varepsilon l}$$

Integral fitting method is useful in the case of one absorbing species and if the photochemical process is only dependent on the concentration of the complex. The third method for calculation of photochemical quantum yield is the concentration distribution method (Equation 2.10), which is helpful for calculating the concentration of all the species in all

moments during the photolysis (c_i) and determination of the absorbed photons by all species (I_i) together with the photochemical quantum yield of various photochemical reactions.

Equation 2.10 For concentration distribution method

$$A_{obs.}(\lambda, t) = \sum A_i(\lambda, t) = \sum \varepsilon_i(\lambda) \times c_i(t) \times \ell$$

$$I_i = I_0 \times \left(1 - 10^{-A_{total}}\right) \times \frac{1 - 10^{-A_i}}{n - \sum_{j=1}^{n} 10^{-A_j}}$$

Individual quantum yields can be determined for the photoinduced reactions of the particular species [30].

3.4. ESR measurements

Numerous experiments were carried out to follow the formation or disappearance of paramagnetic species in the aqueous solutions of the lanthanide(III) porphyrins investigated. Unfortunately, none of the complexes studied proved to be suitable for this technique because in the case of the starting paramagnetic lanthanide(III) porphyrins and the corresponding lanthanide(III) ions as well, the ESR signal was so wide (and, thus, flat) that it could not be used for any kind of analysis. Hence, no change could be observed after irradiation either.

Chapter 4: Results and discussion

1. Formation, structure and absorption spectra of Ln(III) porphyrins

Porphyrins and their metal complexes are the strongest light-absorbing compounds in nature, therefore ultraviolet-visible spectroscopy is the most feasible spectroscopic method to study these systems. For the determination of formation, structure, composition and stability constant values for water-soluble lanthanide(III) porphyrins the absorption spectra of formed complexes were recorded at various concentrations of porphyrins and metal ions in the presence of different ionic strength adjustors. Lanthanide(III) ions offer good opportunities for fine tuning of the out-of-plane distance, utilizing the monotonous decrease of their ionic radii from lanthanum (116 pm) to lutetium (98 pm) in their +3 oxidation state and at coordination number 8 upon increasing atomic number [161]. Additionally, they are prone to form bis- or oligoporphyrins.[135, 130, 202] All the Ln(III) ions are able to forms typical out-of-plane (-OOP or sitting-atop = SAT) complexes with dome-distorted structure.[17] Deviating from the coplanar or in-plane metalloporphyrins, the out-of-plane (-OOP) complexes are distinct from the view point of their thermodynamic instability, kinetic liability, typical photophysical and photochemical features [90]. These complexes display special photoinduced charge transfer characteristics from the porphyrin ligand to the metal center. The photoinduced properties of –OOP complexes are strongly depends upon the π-π interactions between the macrocycles.

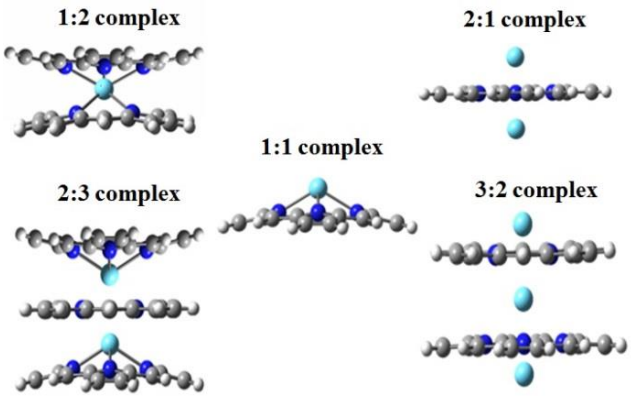

Figure 4.1. Structure of the out-of-plane complexes with different metal porphyrin compositions

Structural models of possible out-of-plane (-OOP) complexes formed by lanthanide(III) with various metal porphyrin compositions are shown in Figure 4.1. Notably, the porphyrins are

able to efficiently sensitize the near-infrared luminescence of lanthanide(III) ions, which can be widely applied from telecommunication to biomedical optical imaging.[137, 150] Besides these applicabilities, lanthanide(III) porphyrins may be applied for photocatalytic hydrogen production from water because their reduced metal centers (Ln(II) formed in photoinduced LMCT processes (typical for OOP complexes have highly negative redox potentials (except for europium) the trends in lanthanide(III) contraction and their redox potential in periodic table are presented in Figure 4.2 [141, 170, 203].

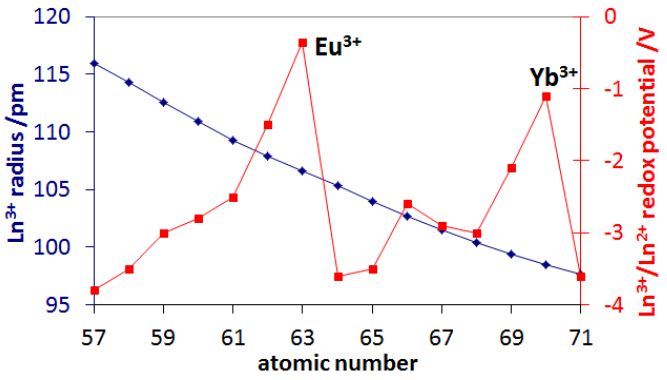

Figure 4.2. Contraction and redox potentials of lanthanide(III) ions [170]

As I discussed in previous chapters, in lanthanide porphyrin complexes due the large ionic radius of Ln(III) they are not able to fit into the cavity of porphyrin molecule, hence it is located above the porphyrin plane and cause distortion of macrocycle. The symmetry of this structure is lower from $C_{4v} \rightarrow C_1$ which is lower than that of both the free-base porphyrin (D_{2h}) and co-planar or in-plane metalloporphyrins (D_{4h}). Formation of in-plane metalloporphyrins is slow as compared to that of out-of-plane metalloporphyrins because of the inflexibility of the ligands . In out-of-plane complexes the distortion of the porphyrin ligand initiated by the out-of-plane locality of the metal center makes two diagonal pyrrolic nitrogens more accessible on the other side of the ligand because of the strengthening of sp^3 hybridization [30, 204]. Lanthanide(III) ions are hard Lewis acids according to the classification of Pearson, therefore their insertion into the coordination cavity of the tetradentate, N-donor porphyrin ligand is a very slow process in aqueous solution. It is partly the consequence of the strong Ln(III)-H_2O coordinative bond. This kinetic barrier is vanquishable by heating in my case at ~ 333 K. The out-of-plane position of Ln(III) ions in the porphyrin cavity and the susceptibility of higher coordination number promote the formation of bis- or oligoporphyrins, which are also called sandwich complexes [205]. As a consequence of the strong susceptibility of lanthanides for the formation of such

oligoporphyrins, the investigation of their monoporphyrin complexes is complicated. I applied acetate ion as a bidentate O-donor ligand, which may enhance the coordination of first porphyrin ligand, due to its trans effect, but it can hinder the connection of further porphyrin i.e. the formation of -oligo or bisporphyrins, because it remains on the lanthanide(III) ions in axial position as shown in Figure 4.3.. Beside acetate the reactions were also carried out in the presence of perchlorate to study the oligo or bisporphyrins. Kinetically labile complexes are examined mostly in the excess of ligand but, in the case of my experiments, metal ion was applied in excess because of spectrophotometric measurements and extremely high molar absorbances mainly at the Soret-band of porphyrins [30, 170].

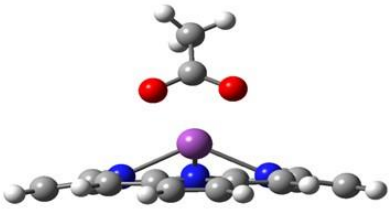

Figure 4.3. Coordination of acetate as axial ligand to a metalloporphyrin

Formation of kinetically labile –OOP complexes deviating from that of coplanar metalloporphyrins is an equilibrium process and results in red-shifts and the hyperchromicity of the UV-Vis absorption bands assigned mainly to intraligand ππ* electron transitions. All the selected lanthanides(III) were similarly reacted with H_2TSPP^{4-} both in the presence of acetate and perchlorate ions; as well. The formed complexes display common OOP absorption properties [17, 170].. Therefore, the results of Ce(III) with H_2TSPP^{4-} are given as representative samples. The interaction of cerium(III) with the anionic porphyrin in the presence of acetate ion results in a red-shift of the Soret-band of H_2TSPP^{4-} from 413 nm to 421 nm, which latter one is characteristic for the typical OOP metallo-monoporphyrins (CeP^{3-}), e.g. Hg(II), Hg(I), Tl(I), Fe(II), Cd(II) ions [123, 124, 206]; suggesting that monoporphyrin complex was formed in my case, too. In the presence of perchlorate, bisporphyrin ($Ce_3P_2^{3-}$) can be formed, which has slightly redshifted and broadened absorption bands compared to that of monoporphyrin. Oligo- or bisporphyrins (sandwich mode of bonding in metalloporphyrins) have been found in the case of mercury(II) with ionic radius 102 pm [161], which forms typical OOP complexes with different compositions: HgP (1 metal ion: 1 porphyrin molecule), Hg_2P_2 (2:2) and Hg_3P_2 (3:2) [31]. Structure of bisporphyrins may be parallel head-to-tail, e.g. the dimer of protonated porphyrin (H_4TSPP^{2-}

$)_2$ [132] or the 2:2 bisporphyrin of mercury(II) $Hg^{II}{}_2(TSPP)_2{}^{8-}$, and head-to-head, as $Hg^{II}{}_3(TSPP)_2{}^{6-}$ [17, 31]. An exclusive explanation about the structural information of Ce(III) mono- and bisporphyrin will be discussed in next chapters. The spectral changes for the complexation of cerium(III) in the presence of acetate and perchlorate are shown in Figure 4.4 a and b respectively; however, similar spectra were measured for the other investigated lanthanides.

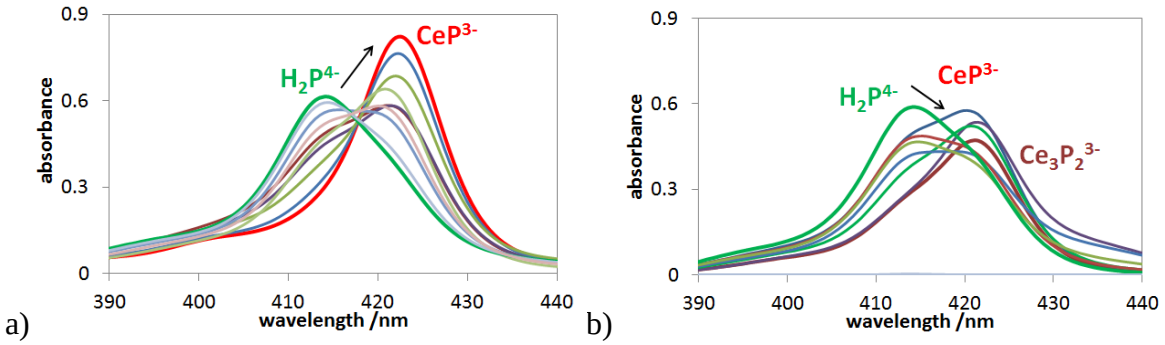

Figure 4.4. Spectrophotometric titration: a) 1.3×10^{-6} M H_2P^{4-} and 0- 9.2×10^{-4}M Ce (III), 0.01 M acetate and b) 1.0×10^{-6} M $H_2P^{4-}$and 0-1×10^{-3}M Ce(III), 0.01M perchlorate

Evaluation of spectrophotometric titrations by the application of Equation 2.4 and 2.5 result in the determination of the individual molar absorption spectra and the stability constants of mono- and bisporphyrin complexes, in the Soret- and Q range in Figure 4.5 a and b. In the presence of acetate buffer the stability constant for the Ce(III) monoporphyrin complex is lgβ1:1 = 4.0. Ce^{3+}, being a hard Lewis acid according to the classification of Pearson, forms a relatively strong coordination bond with the similarly hard bidentate O-donor acetate ion, which can strengthen the bonds between the metal ion and pyrrolic nitrogens as the consequence of its trans effect. Moreover, it may hinder the formation of bisporphyrin complexes.

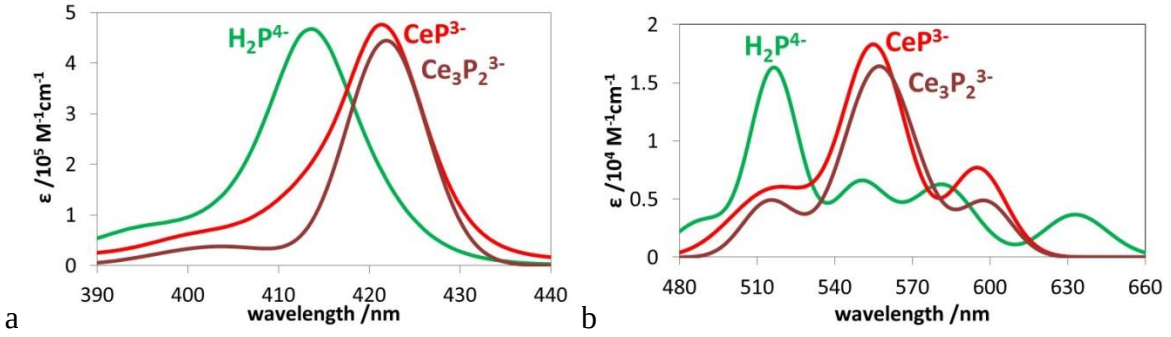

Figure 4.5. Molar absorption spectra of CeP^{3-} $Ce_3P_2{}^{3-}$ compared to free-base porphyrin, a) in Soret-range, b) Q-range

In the presence of perchlorate, the coordination of metal ion is weaker and results in the formation of bisporphyrin complexes. The stability constants for the mono and bisporphyrin complex are lgβ1:1 = 3.6 and lgβ3:2 = 16.3, respectively; which are very close to those of lanthanum(III) porphyrin (Table 4.3) [30] Spectrum analyses of Soret- and Q-band absorption data for free-base, cerium mono- and bisporphyrin were carried out by fitting Gaussian and Lorentzian curves with the application of Equation 2.2. Data for Soret- and Q-bands are given in Table 4.1 and Table 4.2.

Table 4.1. Soret-band absorption data of free-base and cerium(III) porphyrins

species	**H_2P^{4-}**	**CeP^{3-}**	**$Ce_3P_2^{3-}$**
λ {B(1,0)} /nm	395	405	404
ε_{max} {B(1,0)} /10^4 $M^{-1}cm^{-1}$	8.09	8.06	3.80
λ_{Gauss} {B(1,0)} /nm	396	405	404
ε_{Gauss} {B(1,0)} /10^4 $M^{-1}cm^{-1}$	8.13	8.11	3.80
$\omega_{1/2}$ {B(1,0)} /cm^{-1}	1149	1365	1048
f {B(1,0)}	0.361	0.428	0.154
ν {B(1,0)} /cm^{-1}	1090	953	1073
λ {B(0,0)} /nm	413	421	422
ε_{max} {B(0,0)} /10^5 $M^{-1}cm^{-1}$	4.66	4.76	4.52
λ_{Gauss} {B(0,0)} /nm	414	421	422
ε_{Gauss} {B(0,0)} /10^5 $M^{-1}cm^{-1}$	4.45	4.40	4.43
$\omega_{1/2}$ {B(0,0)} /cm^{-1}	785	704	586
f {B(0,0)}	1.35	1.20	1.00
B-shift /cm^{-1}	-	-429	-460

Table 4.2. Q-band absorption data of free-base and cerium(III) porphyrins

species	H_2P^{4-} y	H_2P^{4-} x	CeP^{3-}	$Ce_3P_2^{3-}$
λ {Q(2,0)} /nm	490		516	518
ε_{max} {Q(2,0)} /$M^{-1}cm^{-1}$	3347		5576	4866
λ_{Gauss} {Q(2,0)} /nm	489		518	515
ε_{Gauss} {Q(2,0)} /$M^{-1}cm^{-1}$	3167		5997	4866
$\omega_{1/2}$ {Q(2,0)} /cm^{-1}	1121		1558	944
f {Q(2,0)}	0.0137		0.0255	0.0255
ν {Q(2,0)} /cm^{-1}	1080		1311	1471
λ{Q(1,0)} /nm	516	579	556	556
ε_{max} {Q(1,0)} /$M^{-1}cm^{-1}$	16657	6669	18669	16426
λ_{Gauss} {Q(1,0)} /nm	517	582	556	557
ε_{Gauss} {Q(1,0)} /$M^{-1}cm^{-1}$	16062	6155	17453	16426
$\omega_{1/2}$ {Q(1,0)} /cm^{-1}	827	846	917	1048
f {Q(1,0)}	0.0513	0.0201	0.0619	0.0666
ν {Q(1,0)} /cm^{-1}	1180	1385	1209	1247
λ{Q(0,0)} /nm	553	633	596	595
ε_{max} {Q(0,0)} /$M^{-1}cm^{-1}$	6985	3980	7745	4796
λ_{Gauss} {Q(0,0)} /nm	550	633	595	599
ε_{Gauss} {Q(0,0)} /$M^{-1}cm^{-1}$	6433	3676	7564	4540
$\omega_{1/2}$ {Q(0,0)} /cm^{-1}	830	727	708	640
f {Q(0,0)}	0.0206	0.0103	0.0207	0.0112
B-Q energy gap /cm^{-1}	7174		6941	7003
Q-shift /cm^{-1}	-	-	-195	-288
$\varepsilon(B_{max})/ \varepsilon(Q_{max})$	28.0		25.5	27.5
f(B)/f(Q)	14.7		15.0	11.2

λ is measured wavelength; λ_{Gauss} is wavelength from spectrum analysis; $\omega_{1/2}$ is halfwidth; *f* is oscillator strength; ν is wavenumber of vibronic overtones. Q-shifts were determined to the average of the free-base's Q_y (0, 0) and Q_x(0, 0) bands.

From the absorption spectra, the Soret- or B-bands assigned to the $S_0 \rightarrow S_2$ (b_{1g} LUMO+1) transitions in the 350-500-nm range and the Q-bands assigned to the $S_0 \rightarrow S_1$ (e_g LUMO) transitions are in the 450-750-nm range. The molar absorption spectra of free-base, cerium(III) mono- and bisporphyrin complexes in the range of Soret- and Q-bands are presented in Figure 4.5 a and b, and show that the cerium(III) porphyrins are typical out-of-plane complexes confirmed by redshift. The magnitude of these shifts increases with the complexity of the molecule in both the Soret- and the Q-band of the visible spectra. The same bathochromic effect has been obtained for other typical sitting-atop metalloporphyrins, like Hg(II)$TPPS^{4-}$. On the contrary, the position of the Soret- and Q-bands of the typical regular or in-plane metalloporphyrins (e.g. Al(III)$TPPS^{3-}$) is blueshifted compared to the free-base

porphyrin. To determine the shift of Q-bands is difficult because the protons in the free-base porphyrin lower the symmetry and split the Q-band into Q_x+Q_y; hence, there are five bands in free-base and three in metalloporphyrins [15, 207].

In regular or coplanar metalloporphyrins, the energy difference between the HOMO a_{2u} and the LUMO+1 b_{1g} molecular orbital of the ligand (Soret-absorption, S_2-excitation) is larger than in the free-base porphyrin, while this difference in the sitting-atop complex is smaller. [87]. The out-of-plane coordination of metal ion in the cavity of porphyrin ligand results in the dome distortion and Q-band degeneracy is restored by the dissociation of the pyrrolic protons. Acetate ion as axial ligand has insignificant effect on the absorption bands. In the Soret- or B(0, 0) and Q(0, 0) electronic transitions the first number in parentheses represents the vibrational quantum number of the excited state and the second one designates that of the ground state [112].

I observed that the molar absorption coefficients and oscillator strengths of CeP^{3-} in Soret-absorption are somewhat higher than those for $Ce_3P_2^{3-}$; while the energies of the vibronic overtones show the opposite trend as listed in Table 4.1. The Q-band absorption data for the free-base, cerium mono- and bisporphyrins are listed in Table 4.2 and show the same trend as in the case of Soret-absorption, only the energy of vibronic overtones is lower for CeP^{3-} than for $Ce_3P_2^{3-}$. The results of cerium porphyrins are in agreement with other out-of-plane complexes formed by e.g. the lanthanum(III) and mercury(II) porphyrins, which have the ability to absorb light more strongly than the free-base porphyrin ligand or co-planar metalloporphyrins. Due to these characteristics, they could be more efficiently used for light harvesting, artificial photosynthesis and other photocatalytic procedures [30, 31].

1.1. Trend in stability constants

The stability constant values for mono- and bisporphyrins show an increasing trend with a decrease in the ionic radii of lanthanide(III) metal ions. Due to the lanthanide contraction, the out-of-plane distance and domedness decrease resulting in the strengthening of coordinative bonds. The stability constant values are determined on the basis of Equation 2.4 For calculation of absorbances. The stability constants for other members of lanthanide series are given in Table 4.3.

In the second half of the lanthanide series, the stability constants of bisporphyrins start to slightly decrease, and neither those of the monoporphyrins increase as strongly as in the first half. The required periods of time to reach the equilibrium are longer, too. Both phenomena may originate from the harder type of late lanthanides, what can cause the higher stability of the aqua complexes, together with the hindrance of the coordination to the cavity, but mainly to the peripheral sulfonato groups of the porphyrin.

Table 4.3 Stability constants of the investigated lanthanide(III) mono- and bisporphyrin complexes

Lanthanide ions	La^{3+}	Ce^{3+}	Nd^{3+}	Sm^{3+}	Eu^{3+}	Gd^{3+}	Dy^{3+}	Er^{3+}	Yb^{3+}
+3 Ionic radius /pm*	116	114.3	110.9	107.9	106.6	105.3	102.7	100.4	98.5
estimated out-of-plane distance /pm	112	108	101	94	90	87	80	73	67
lgβ1:1 in the presence of CH_3COO^-	3.80	4.00	4.55	4.89	5.01	5.11	5.29	5.43	5.52
lgβ1:1	3.30	3.60	4.20	4.64	4.80	4.94	5.19	5.38	5.52
lgβ3:2	15.90	16.30	17.10	17.47	17.51	17.53	17.48	17.39	17.30

*=at coordination number 8.

The equilibrial trend for all the investigated lanthanide(III) porphyrins are shown in Figure 4.6. The stability constants increase about 2 orders of magnitude in the whole lanthanide series, which may seem to be too high compared to the only 16 % decrease of the ionic radii. However, the volume along with the charge density, the latter one isproportioniato the hardness, change about 40 %. Furthermore, we tried to estimate the out-of-plane distances of the central atom, on the basis of the size of the cavity ($d_{N\text{-}N}$≈420 pm is the distance between two diagonally located pyrrolic nitrogens) and the covalent radius of the pyrrolic nitrogens (r_N≈122 pm) (both data originate from earlier DFT calculations of our research group for the

structure of post-transition metal ions' typical out-of-plane complexes [85]), and using the Pythagorean theorem:

$$d_{OOP}^2 + \left(\frac{d_{N-N}}{2}\right)^2 = (r_{Ln^{3+}} + r_N)^2$$

The total decrease of OOP distance for the whole series is again about 40 %; moreover, the electrostatic forces increase with its second power, which means a three-times growths. The remaining part of the increasing trend among the stability constants may derive from the much stronger covalent character of the metal-nitrogen bonds.

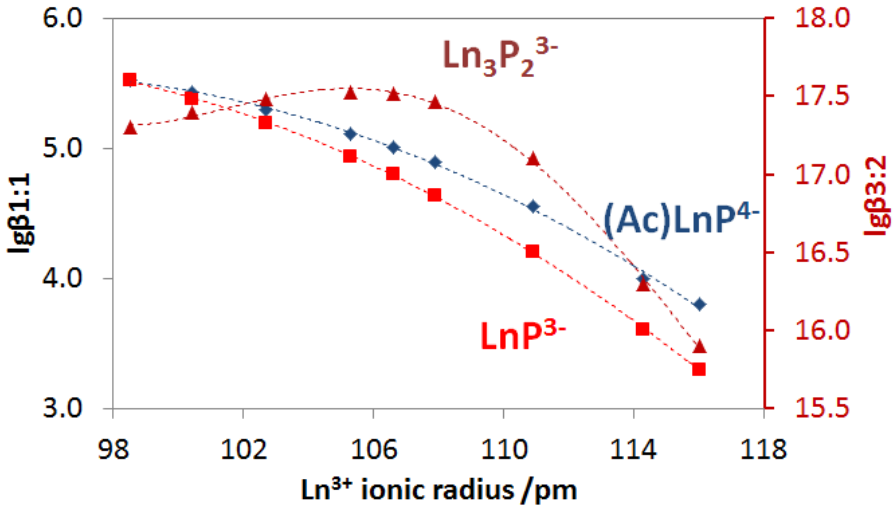

Figure 4.6. Equilibrial trends for lanthanide(III) porphyrins

2. Photophysics of lanthanide(III) mono- and bisporphyrins

The emission properties of porphyrins are determined by the 18 π-electrons of the 16-membered porphyrin macrocyclic ring. Nevertheless, an alteration in the central metal atom and effects of changing the conjugation path way as well as the peripheral substituents lead to change in the luminescence. However, the coordinated metal ions usually have smaller effects on the photophysical properties of macrocycle as the consequence of the weaker interactions between them. The description of emission spectra based on substitution patterns and different central substituents has been well studied in the literature. Porphyrins possess energetically low-lying, electronic excited singlet states. Substituents can strongly affect the fluorescence: the electron-donating substituents have the ability to increase the fluorescence quantum yield because they increase the probability of radiative transitions between the

lowest singlet excited state and the ground state, while electron-withdrawing groups, such as Br, can decrease or quench the fluorescence completely, also owing to their heavy-atom effects. The substitution with bulky groups may cause the deformation of planar structure as well as the decrease of fluorescence quantum yield. The excitation and relaxation processes of ground and various excited states of porphyrins have been discussed by using Jablonski diagram in the Chapter 3.2. Light emission [206, 208].

Beside the biological significance of porphyrins, they are interesting class of compounds from the viewpoint of fluorescence, phosphorescence and non-radiative decay properties. Only a small portion of their excitation energy is lost through the heat dissipation from their singlet states because the overall quantum yield of fluorescence and intersystem crossing resulting in formation of triplet states is over 95 %. Due to this property, porphyrins are efficient in optical sensitization and photosensitization [21]. Due to the rigidity and the presence of aromatic electronic system, the porphyrins possess two types of fluorescence: the S_2-fluorescence is very rare and weak, while the S_1-fluorescence is widely studied and strong. The latter one in arylated porphyrins display an impartially unusual uniqueness, its spectrum is antisymmetric to its absorption spectrum. In the free-base porphyrins, the emission originates from the energetically lower S_{1x}-state populated by the $Q_x(0, 0)$ absorption, consequently these bands must be compared. The extension of delocalization in the S_1-excited state by the twisting of aryl substituents from nearly perpendicular position into the direction of porphyrin plane, causing an alternating excited states, which may be the possible reason for the antisymmetricity. The energy difference between $Q_x(0, 0)$ absorption and $S_1(0, 0)$ emission band, is called Stokes shift, which is a very significant photophysical parameter about the structural change during the excitation.

The photophysical properties of porphyrin are affected by the coordination of metal ions. The energy of absorption and emission bands in metalloporphyrins depends strongly on the electronic structure of the coordinated metal ion. Transition metal ions without *d*-electrons, such as Sc^{III}, Ti^{IV}, and post-transition metal ions with fulfilled d-subshell, e.g. Cu^{I}, Zn^{II} weakly perturb the π-system of porphyrins; namely they have small influence on the emission and absorption spectra of the macrocycle, therefore, such metalloporphyrins are called *regular* type complexes with normal emission and absorption properties. In contrast, the metal ions like $Mn^{III, IV}$, Fe^{II}, $Co^{II, III}$ and Ni^{II} possessing partially filled *d*-orbital and in-plane coordination position significantly affect the absorption and emission spectra of porphyrin ring through the appearance of low-energy charge transfers; these metalloporphyrins are

called as *irregular* ones. They are further classified in two types on the basis of the shift of Q bands compared to those of free-base ligand. Hypso metalloporphyrins exhibit Q band that are blueshifted relative to the corresponding normal spectra of regular metalloporphyrins. Second type of *irregular* metalloporphyrins are hyper ones, which are characterized by redshifted absorption bands and the disappearance of fluorescence [209]. However, in these cases, the photophysical changes may originate mainly from steric effects, .i.e. from the strong distortions of the macrocycle [17].

The insertion of metal ions into the porphyrin cavity usually causes the decrease of fluorescence quantum yield and increase in the efficiency of intersystem crossing. Fluorescence and phosphorescence quantum yields of metalloporphyrins are in the range 10^{-3} - 0.2 and 10^{-4} - 0.2, respectively [208].

Photophysics of trivalent lanthanide (Ln^{3+}) porphyrin complexes has been subject of many papers [210]. Their distinctive and fascinating photophysical properties make these systems supreme for the development of luminescent metal porphyrin derivatives [211]. The f-f transitions, which result in the emission of light from lanthanide ions in the visible and near-infrared (NIR) regions of the spectrum, are spin and parity forbidden, therefore absorption in lanthanide complexes originates from the capturing of photon by a chromophoric ligand, called antenna, and subsequent intramolecular energy transfer from its excited states to the metal ion. Due to the forbidden 4f-4f transitions, lanthanides are unable to catch photons and show enormously low molar absorptivities, shielding of 4f-orbitals of the lanthanides by the 5s and 5p subshells results in narrow line-like emissions and long radiative lifetimes [211].

To elucidate the structure and mode of coordination in cerium mono- and bisporphyrins as well as to make comparison with the already reported out-of-plane metalloporphyrins, the S_1-fluorescence properties were studied, too. First only the results of cerium(III) mono- and bisporphyrins are discussed in details. Same procedure was used for the other investigated lanthanide(III) mono- and bisporphyrins. For determination of S_1-fluorescence for cerium mono- and bisporphyrin, the sample solution was excited at 417 nm, which was a quasi-isosbestic point obtained in the absorption spectral series during the titration of porphyrin with cerium in the presence of acetate buffer as shown in Figure 4.4.a.

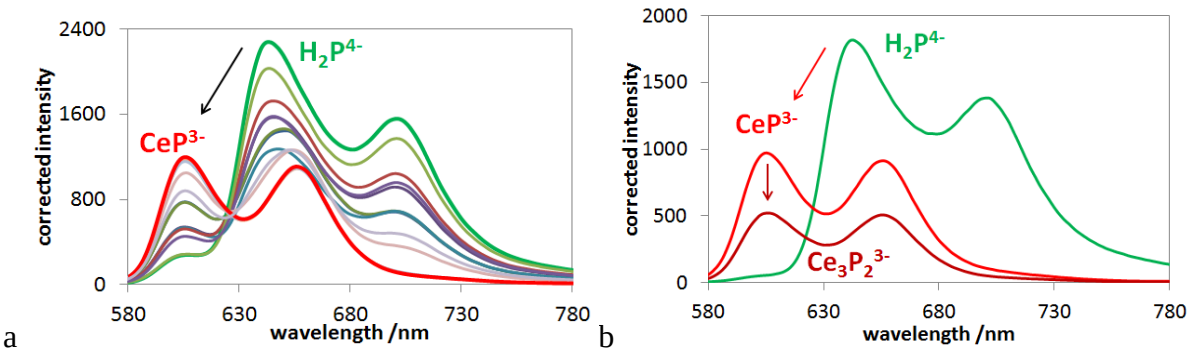

Figure 4.7. a) Spectrofluorimetric titration series (excitation wavelength was the quasi isosbestic point of Figure 4.4.a) possesses a quasi-isostilbic point. b) Individual tS_1 fluorescence spectra of cerium(III) mono- and bisporphyrin,as well as the corresponding free base

S_1-fluorescence spectra of free-base, cerium(III) mono- and bisporphyrin are compared in Figure 4.7. It can be seen from fluorescence spectra, when cerium(III) ion is coordinated to the porphyrin ligand, that the emission bands became strongly blueshifted and less intense compared to those of free-base porphyrin. The characteristic data for S_1-fluorescence of free-base, cerium mono- and bisporphyrins are summarized in Table 4.4.

Table 4.4 Characteristic S_1-fluorescence date of the cerium(III) mono- and bisporphyrins as compared to that of the corresponding free base H_2P^{4-}

species	**H_2P^{4-}**			**CeP^{3-}**			**$Ce_3P_2^{3-}$**		
transition	**$S_1(0,0)$**	**$S_1(0,1)$**	**$S_1(0,2)$**	**$S_1(0,0)$**	**$S_1(0,1)$**	**$S_1(0,2)$**	**$S_1(0,0)$**	**$S_1(0,1)$**	**$S_1(0,2)$**
$\lambda\{S_1(0,i)\}$ /nm	647	705	780	607	654	708	607	655	708
$I_{max}(0,i)/I_{max}(0,0)$	-	0.712	0.0527	-	0.917	0.0792	-	0.944	0.0703
$\omega_{1/2}$ $\{S_1(0,i)\}$ /cm^{-1}	828	1065	1005	801	927	897	813	907	972
$\phi\{S_1(0,i)\}$ /10^{-2}	3.81	3.49	0.243	1.44	1.53	0.128	0.666	0.702	0.056
$\nu\{S_1(0,i)\}$ /cm^{-1}	-	1197	1342	-	1198	1161	-	1190	1147
S_1-Stokes/cm^{-1}	360			316			234		
S_1-shift /cm^{-1}	-			1036			1024		
$\phi(S_1)$ /10^{-2}	7.53 (6.24 Q_y)			3.10			1.42		
$\Phi(S_1\text{-}B)$ /10^{-2}	5.62			2.06			0.948		
ϕ(IC)	0.746 (0.828 Q_y)			0.664			0.666		
$\tau(S_1)$ /ns	10.03			1.97			2.00		
$k_r(S_1)$ /$10^6 s^{-1}$	7.51			15.7			7.12		
$k_{nr}(S_1)$ /$10^7 s^{-1}$	9.22			49.2			49.3		

The position of cerium(III) out of the porphyrin plane causes a dome distortion in the structure, consequently the fluorescence quantum yield of monoporphyrin decreases compared to the free-base porphyrin. The formation of bisporphyrin results in a further diminution because of the more complicated structure. After the coordination of cerium(III) ion into the porphyrin cavity, the fluorescence spectrum shows a hypsochromic effect compared to the redshift of absorption band. This irregularity between blue- and redshift is apparent because the shift in absorption must be calculated from the average of the splitted $Q_x(0, 0)$ and $Q_y(0, 0)$ bands of the free-base porphyrin; however, the emission originates from the energetically lower S_{1x}-state. It can be assumed from both of above mentioned phenomena, that the structure of H_2TSPP^{4-} is planar and that of cerium(III) porphyrin is distorted. The coordination of metal with porphyrin considerably reduces the quantum yield of S_1-fluorescence from 7.53 % of free-base porphyrin to 3.10 and 1.42 % for cerium(III)

mono- and bisporphyrins, respectively. The reason behind the decrease in quantum yield would be the dome distortion caused by the out-of-plane coordination of cerium, which may also stimulate other, non-radiative energy dissipation processes. Same tendencies in the band shift and fluorescence quantum yield have been observed in out-of-plane porphyrin complexes of post-transition metal ions {e.g. Hg(II)TSPP^{4-}, $(Hg(I)_2)_2$TSPP^{2-}, Cd(II)TSPP^{4-}, as well as high-spin Fe(II)TSPP^{4-}}; hence, these evidences, together with the characteristics of absorption spectra, confirm the out-of-plane position of metal ion [31, 89, 116, 212, 213]. Excitation of cerium(III) porphyrin at Soret-band results in the S_1-fluoresence after the efficient internal conversion from the second singlet excited state to the first one. From the fluorescence quantum yields at different excitations (on B- or Q-bands) the efficiency of internal conversion (IC) is determinable (Eq. 2.7.b). The internal conversion value for free base is 0.746, upon coordination of cerium ion, it decreases to 0.664 as a consequence of the potential intersystem crossing from singlet-2 to triplet-2 excited state. Contrary to sandwich-type (head-to-head) out-of-plane metallo-oligoporphyrins, for example trimercury(II) bisporphyrin, cerium(III) bisporphyrin shows S_1-fluorescence. The formation of complicated structure promoting more vibronic decays may be one of the possible reasons for the weakening of emission; moreover, the ring-to-ring or ring-to-metal charge transfers may also cause the quenching of the fluorescence [214]. The magnitude of the structural change during the excitation can be characterized by the Stokes-shift, which is the difference (in energy) between the Q(0, 0) transitions in the absorption and the emission. The Stokes-shift of free base porphyrin is about 360 cm^{-1}. Normal or in-plane metalloporphyrins usually have lower and out-of-plane metalloporphyrin have higher values [17]. Stokes-shifts for the CeP^{-3} and $Ce_3P_2^{3-}$ are in agreement with other out-of-plane metalloporphyrins (Table 4.4). The higher value of CeP^{3-} than H_2P^{4-} confirms that the cerium porphyrin complex is non-planar, while the free base is planar in the ground state; from this knowledge some evidence about the excited state geometry can be attained. Also the vibronic overtone (ν_1) of many metal porphyrins complexes have the similar value about 1200 cm^{-1}, in the S_1-exicited state generally all the metalloporphyrins have the same degree of deformation [31].

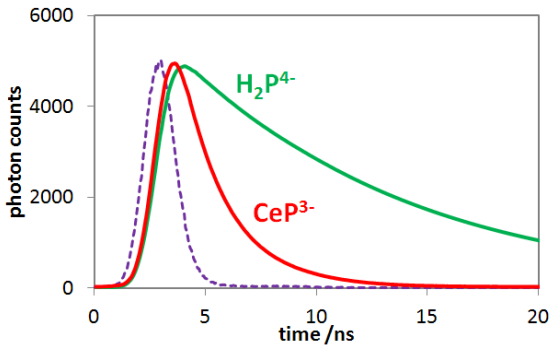

Figure 4.8. Lifetime of S_1-fluorescence of monoporphyrins

According to my measurements, the lifetime for S_1-fluorescence of free-base porphyrin is 10.0 ns which shows a close resemblance with that of already published values of in literature τ_{S1} = 10.4 and 12.4 ns [112,29, 215, 216]. However, no reported values were available for cerium(III) mono- and bisporphyrins. Upon metalation, the S_1-fluorescence lifetime values of free-base porphyrin decreases to 1.97 and 2.00 ns for cerium(III) mono- and bisporphyrins, respectively. These values are close enough and show agreements with other out-of-plane complexes, like HgP^{4-} 2.7 ns. It has been reported: when the symmetry of a molecular structure is reduced, the fluorescence yield also decreases. Besides, in the case of out-of-plane complexes, the non-radiative decays show an accelerating trend with the increase of structural distortions [13, 217]. The rate constants for radiative (k_r) and non-radiative (k_{nr}) processes for H_2P^{4-}, CeP^{3-} and $Ce_3P_2^{3-}$ also show the same trend. The radiative rate of H_2P^{4-} decreases slightly upon complexation with cerium(III), and the non-radiative values increases 5 times. From this phenomenon, it can be concluded that the significant increase in the non-radiative decay rate is the determining factor in the reduction of fluorescence lifetimes and not the deceleration of the radiative process as supposed in the published results [21, 29]. The possible explanation for S_1-fluorescence from cerium(III) bisporphyrins are discussed on the basis of Figure 4.9 a and b. For the determination of S_1-fluorescence quantum yield of bisporphyrins, it was necessary to extract the fluorescence signal of cerium monoporphyrin, which remains in a significant amount in the equilibrium. The S_1-fluorescence quantum yield of bisporphyrin complex is about ~54 % lower compared to that of monoporphyrin. Their S_1-lifetimes are very similar; hence, the formation of bisporphyrin only results in the decrease of the radiative rate constant.

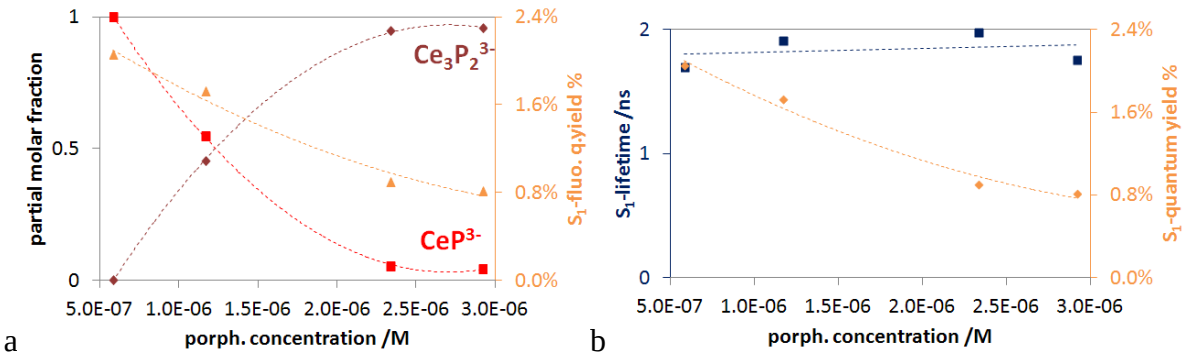

Figure 4.9. a) Effect of porphyrin concentration on partial molar fraction of Ce(III) mono- and bisporphyrins b) on S_1-fluorescence lifetimes and quantum yields

With an increasing porphyrin concentration and at constant cerium(III) concentration, the partial molar fraction of CeP^{3-} decreases, while that of $Ce_3P_2^{3-}$ increases as depicted in the Figure 4.9 a.; on this way, the individual fluorescence spectra and quantum yields for the mono- and bisporphyrin complexes are separately determinable.

The unexpected fluorescence of cerium bisporphyrin may be explained from the comparison of molar absorption spectra of cerium and mercury bisporphyrins, mainly in the Q-range (Figure 4.10 a and b).

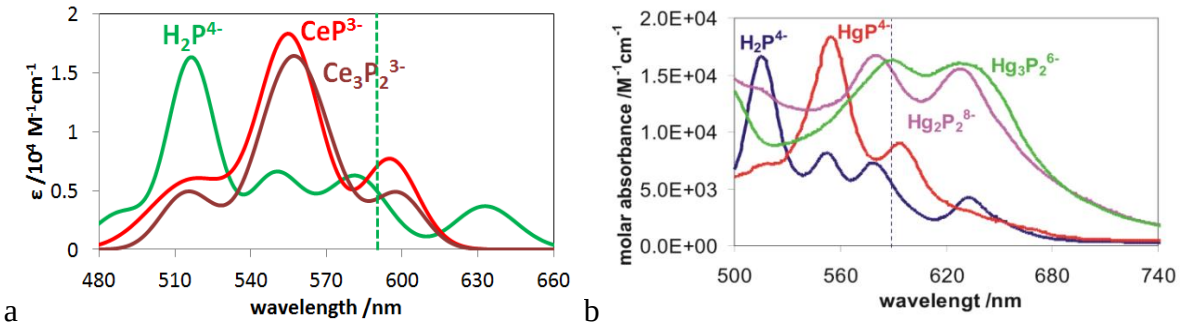

Figure 4.10. a) Molar absorption spectra of cerium and b) mercury bisporphyrins compared to the free-base porphyrin in the Q-range.

The molar absorption spectrum of cerium(III) bisporphyrin is very similar to that of the monoporphyrin, only its intensity is somewhat higher due to the weak π-π interactions between the two macrocycles. This is a clear indication of the tail-to-tail dimerization through a metal bridge between the peripheral sulfonato substituents (Figure 4.11).

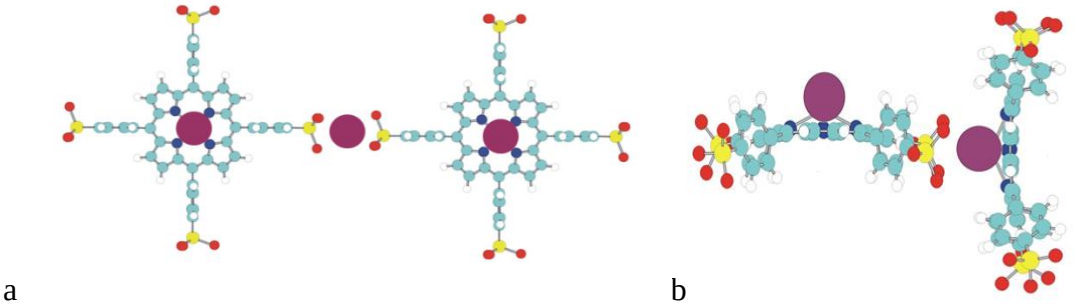

a b

Figure 4.11. a) Representation of tail-to-tail dimerization and b) perpendicular head-to-tail.

This type of bonding mode shows deviation from the head-to-head connection or also called as sandwich type complexes as shown in Figure 4.12. In this case the absorption band would show much larger redshifts, as well as hyperchromicities and the fluorescence would be much weaker and may disappear during the formation of bisporphyrin as with the parallel head-to-tail dimerization of protonated porphyrin $(H_4TSPP^{2-})_2$ and the typical OOP, sandwich-type bisporphyrins of mercury(II) ion: (parallel) head-to-tail $Hg^{II}{}_2(TSPP)_2^{8-}$ and typical head-to-head $Hg^{II}{}_3(TSPP)_2^{6-}$.

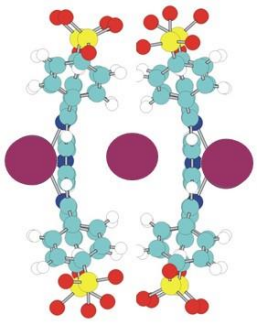

Figure 4.12. Head-to-head or sandwich type connection

A more well-defined (DFT-calculated) structures for mercury porphyrins 2:2 and 3:2 complex is depicted in Figure 4.13. In the 3:2 type structure, two porphyrin rings are connected by a central mercury ion, and two outer ones are also coordinated, and all the three mercury ions are located alongside D_4 symmetry axis of the complex [31].

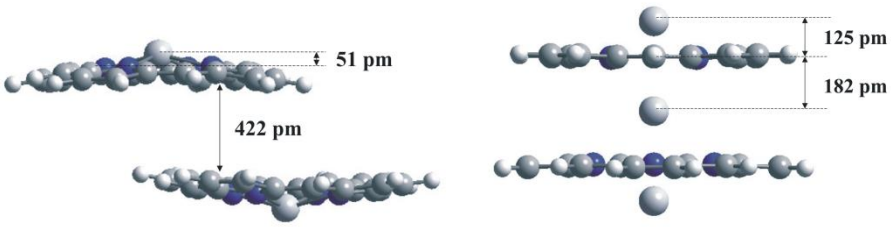

Figure 4.13. Structure of the 2:2 and 3:2 complex between Hg(II) and porphin [31]

As compared to cerium(III) complex, the mercury(II) bisporphyrins, as the consequences of strong π-π interactions in head-to-head or parallel head-to-tail structures, show significant broadening, large redshift of the absorption bands (Figure 4.10), as well as the disappearance of fluorescence. .

2.1. Trends in photophysical properties

I investigated the photophysical properties of cerium(III) mono- and bisporphyrins; moreover, and same procedure was adopted for the other studied lanthanide(III) TSPP complexes, which are summarized in Table 4.5.

Table 4.5 Photophysical parameters of lanthanide(III) porphyrins

Ln^{3+}	H_2TSPP^{4-}	La	Ce	Nd	Sm	Eu	Gd	Dy	Er	Yb
ionic radius +3 /(8)pm		116	114.3	110.9	107.9	106.6	105.3	102.7	100.4	98.5
LnP^{3-} (Ac)										
$\phi(S_1)$ /10^{-2}	7.53 (6.24 Qy)	2.74	3.1	3.93	4.39	4.47	4.15	3.43	3.51	3.60
$\phi(S_1$-B) /10^{-2}	5.62	1.62	2.06	3.05	3.03	2.86	2.91	2.33	2.51	2.73
ϕ(IC)	0.746 (0.828 Qy)	0.591	0.664	0.776	0.689	0.640	0.702	0.681	0.714	0.758
τ(S1) /ns	10.03	2	1.97	1.94	1.93	1.94	1.93	2.01	1.96	1.97
$k_r(S_1)$ /10^6 s^{-1}	7.51	14	15.7	20.2	22.8	23.1	21.5	17.0	17.9	18.3
$k_{nr}(S_1)$ /10^7 s^{-1}	9.22	48	49.2	49.4	49.6	49.2	49.7	48.0	49.3	49.0
$Ln_3P_2^{3-}$										
$\phi(S_1)$ /10^{-2}		1.03	1.42	2.59	3.09	2.88	2.37	2.08	2.26	2.39
$\phi(S_1$-B) /10^{-2}		0.671	0.948	1.71	2.20	1.92	1.73	1.56	1.78	1.99
ϕ(IC)		0.65	0.666	0.662	0.713	0.667	0.727	0.747	0.790	0.833
τ(S1) /ns		2	2.00	1.99	1.94	1.95	1.94	2.02	1.96	1.96
$k_r(S_1)$ /10^6 s^{-1}		5	7.12	13.0	16.0	14.8	12.3	10.3	14.6	12.2
$k_{nr}(S_1)$ /10^7 s^{-1}		49	49.3	48.8	50.0	49.8	50.4	48.4	49.7	49.8

The trends in fluorescence quantum yield of lanthanide(III) porphyrins are explicated on the basis of electronic and steric factors (Figure 4.14). The electronic factor is the increasing number of unpaired electrons together with the atomic number up to the half-filled subshell (Gd^{3+}), what enhances the strong interaction with π-electron system, may strengthen the spin-forbidden decays and cause a decrease in the fluorescence quantum yield. The steric factor is the lanthanide contraction, namely: the radii of 3+ lanthanide ions decrease with the increasing atomic number, what reduces the out-of-pane (OOP) distance as well as the dome distortion of their porphyrin complexes, consequently the fluorescence quantum yields may increase.

S_1-fluorescence lifetimes of all studied lanthanide mono- and bisporphyrin complexes are near constant (~2 ns) as the consequence of the similar non-radiative decays ($k_{nr} \approx 5 \times 10^8$ s^{-1}). Hence, the quantum yields change totally parallel with the radiative rate constants (k_r).

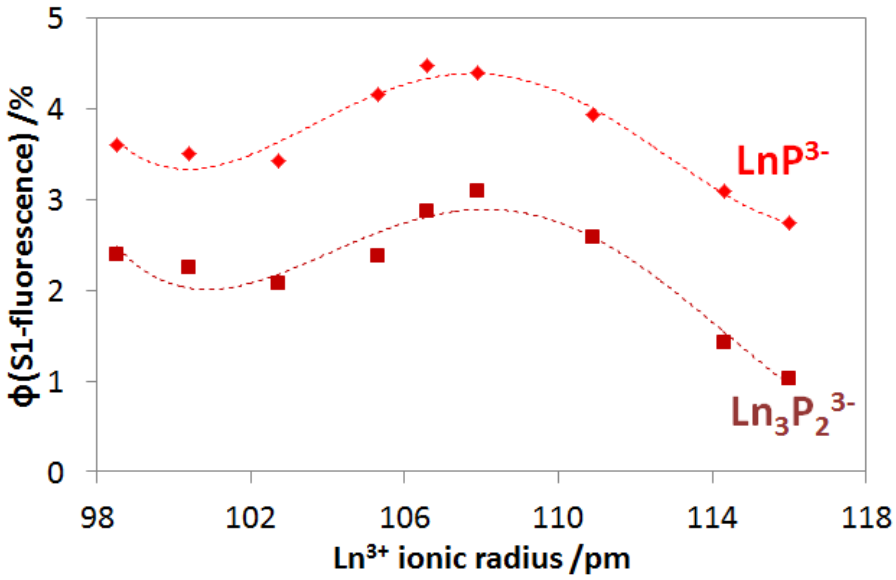

Figure 4.14. Trends for fluorescence quantum yield of lanthanide(III) porphyrins

3. Photochemistry of lanthanide(III) mono- and bisporphyrins

The photochemistry of porphyrin derivatives has attracted significant consideration since the relation between the pigments of plants and animals became recognized [218]. The reason for interest in porphyrins and their metal complexes is because they display excellent light-harvesting efficiency as the consequence of their charge-separated states as models of the photosynthetic reaction centers and photovoltaic cells for energy conversion [219, 220, 221].

They comprise extensively conjugated 16 or 18 π-electron system, which permit effective electron-transfer because the acceptance or release of electrons commonly results in insignificant structural change [222]. Their derivatives have been employed as electron donors in electron donor-acceptor systems [223]. The photochemical reactions of metalloporphyrins and related compounds have received very considerable interest in a wide variety of areas approaching the subject [224].

The porphyrins have shown good results in artificial photosynthesis and photosensitization processes [21, 215]. The role of metal center in porphyrin macrocycle for photochemical process needs to pay special attention. As a consequence of kinetic stability and planar structure the normal or in-plane metalloporphyrins do not undergo effective photoinduced ligand-to-metal charge transfer reactions. The sitting-atop (SAT) complexes show a typical photoredox chemistry, which can be characterized by irreversible photodegradation of the porphyrin ligand [206]. The special photochemical characteristics are produced in out-of-plane metalloporphyrins due to the efficient separation of the reduced metal center and the oxidized macrocycle following the ligand-to-metal charge transfer reactions. This LMCT reaction finally leads to irreversible ring opening and give rise to open-chain dioxo-tetrapyrrol derivatives like bilindions. The same type of reactions and end products have been found for the photo-oxygenation of Tl(I) and Mg(II) meso-tetraphenylporphyrin [225, 226]. Beside the formation of bilindions as an end product, other kinds of oxidized derivatives of porphyrins may also form, but the extended conjugation of double bonds in the end product is ceased, which has indicated from the extreme spectral change. Among the lanthanide(III) porphyrins, excluding La(III) porphyrin, no studies have been made regarding their primary photochemistry.

The out-of-plane position of the metal center in porphyrin complexes can generally cause two types of photochemical reactions. First is the photoinduced dissociation of the metal ion from the cavity of the ligand without the charge transfer process as a consequence of the lability of the complex and the second is the photoredox degradation of the macrocycle initialized by an irreversible ligand to metal charge transfer reaction resulting in oxidation of the ligand and reduction of the metal center [170]. The suggested steps for the photodegradation of OOP metalloporphyrins are presented in Scheme 4.1.

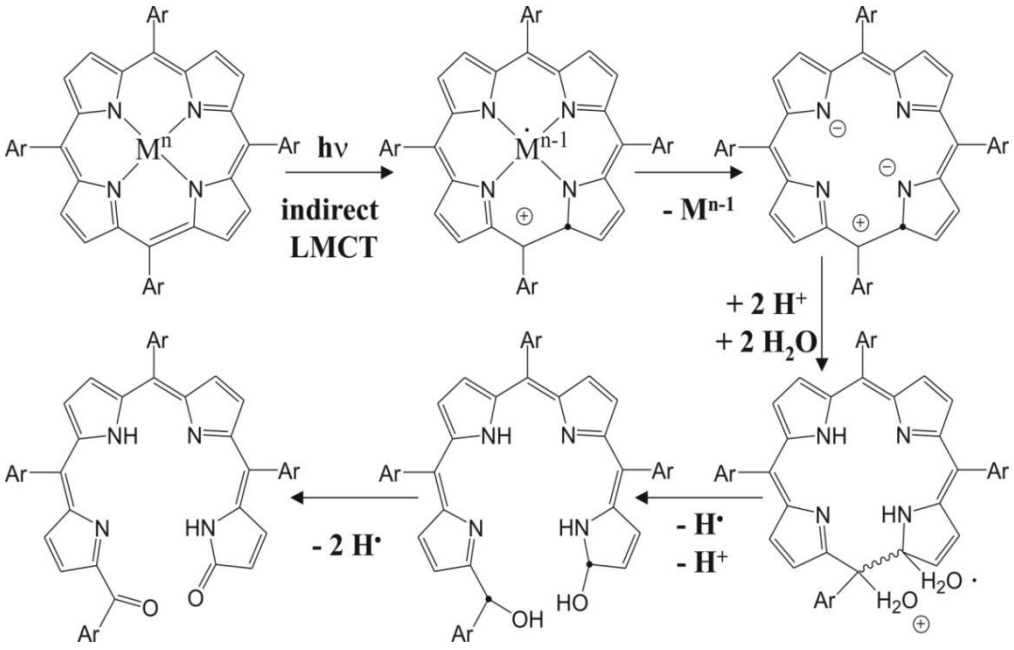

Scheme 4.1. Suggested steps for the photodegradation of -OOP metalloporphyrins [90]

The charge of the metal center decreases and its size increases, which results in the reduction of charge density and the coordinative bonds can easily split. The reduced metal ion can step out from the cavity, mainly in polar solvent, and can induce further redox reactions depending on the stability in the given medium. The oxidized and metal-free porphyrin cationic radical acts as a strong base and get protons immediately from the free-base radical, which is long-lived and a relatively strong oxidizer mainly in oxygen-free solution. But it would oxidize water to oxygen only at higher pH. Therefore a slightly stronger reducer, for example water soluble alcohols or aldehydes, is required, from which useful byproducts can be formed in catalytic hydrogen production. In the absence of reducer, the primary photochemical processes take place in an overall four-electron oxidation and open-chain dioxo-tetrapyrrol derivative (bilindions) can form. This ring-opening process can be spectrophotometrically followed due to the disappearance of the Soret-band [87, 90, 227].

During the photolysis experiments, I carried out the irradiation of cerium(III) porphyrins at the Soret-band (421 nm) and Q-band (555 nm) in aerated systems as well as with oxygen free samples. According to already published results, free-base porphyrins show very minor degradation at the Soret-band excitation and do not show any calculable change upon irradiation at the Q-band in air-saturated and deaerated solutions [31, 87, 123, 206, 213].

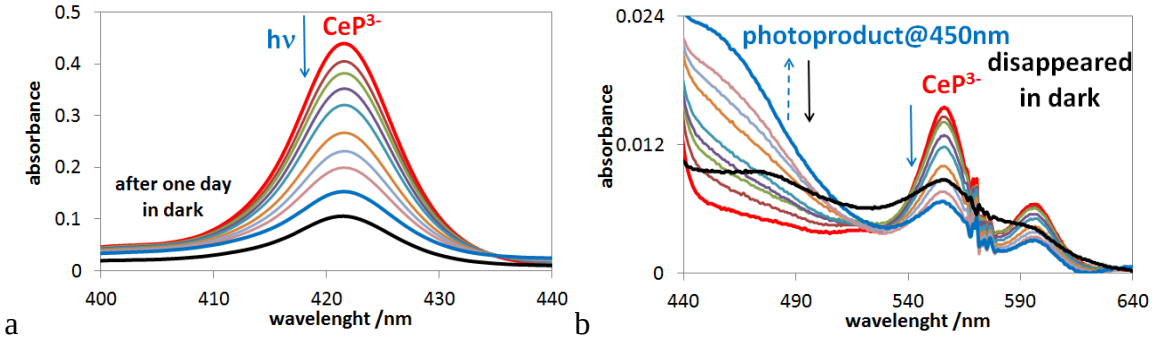

a b

Figure 4.15. a) Soret- b) Q-band spectral change during the Soret-band irradiation of cerium(III) porphyrin in the presence of 0.01M NaAc, 9.2×10^{-7} M H_2TSPP^{4-}, 1.0×10^{-3} M Ce^{3+}, pH ≈ 6, I_0 (421 nm) = 1.2×10^{-5} M photons/s, ℓ = 1cm

I carried out the photolysis of CeP^{3-} at 421 nm in aerated systems, which results in the decrease of the absorption as shown in Figure 4.15. a) at the characteristic bands, which indicates the irreversible photoredox degradation of the ligand is accompanied by less efficient dissociation to the free base and the cerium(III) ion. This behavior is due to the lability of the out-of-plane complexes, which also have been shown by other OOP porphyrin complexes of Bi(III) [124], Hg(II) [31], and Cd(II) [206]. After irradiation of the sample for 14 minutes it was placed in dark and the absorbance was measured after one day. The spectral analysis in the Q-band region shows the formation of a short-lived intermediate at 450 nm as shown in Figure 4.15. b), which disappears in dark.

For the estimation of the lifetime of this intermediate photoproduct, I carried out a longer (3 h) irradiation at the Soret-band maximum. In the Figure 4.16 it is observable, that it starts to disappear after 50 minutes; hence, its lifetime is not longer, than several ten minutes.

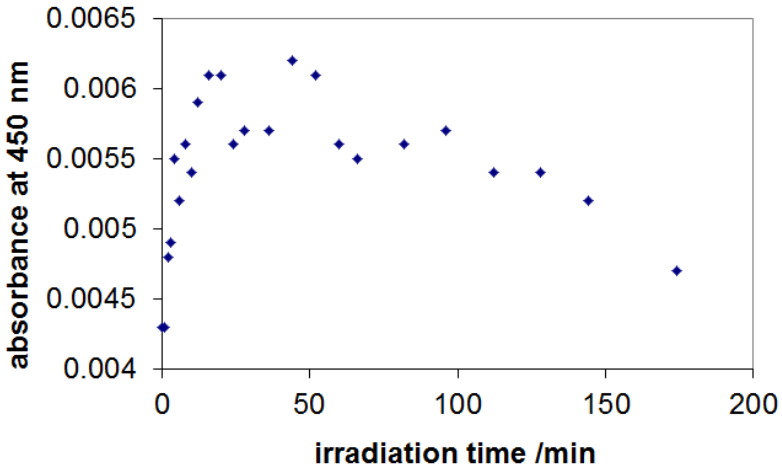

Figure 4.16. Formation and disappearance of the intermediate photoproduct during the Soret-band irradiation.

However, during the photolysis of cerium(III) porphyrins at the maximum of the Q-band (~555 nm) for about 62 minutes, a new type of photoproduct appears, which is stable in dark as shown in Figure 4.17 and this type of photoproduct is undetectable in the case of post-transition metal ions which also form typical out-of-plane complexes [87, 90, 170].

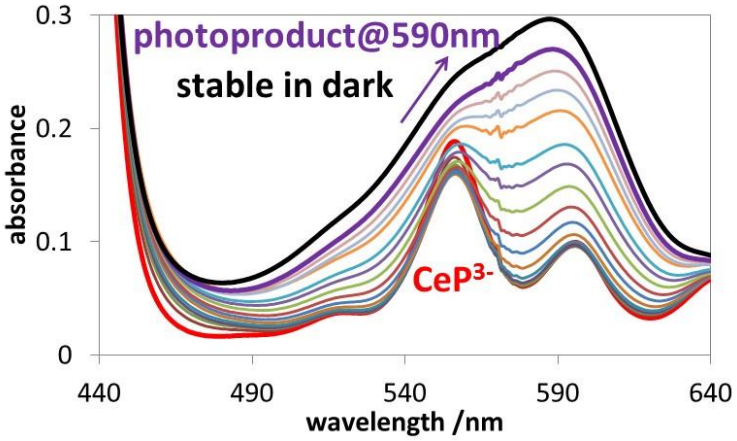

Figure 4.17. Spectral changes during the photolysis at the Q-maximum (555 nm)

The Soret-band disappeared as a consequence of the ring-opening reaction; hence the absorption band at 590 nm may be assigned to a complex between cerium(III) and the open-chain dioxo-tetrapyrrol derivatives as shown in scheme 3.1, owing to the high affinity of cerium ion to the oxo-groups.

In the absence of acetate, the cerium(III) mono- and bisporphyrins are in equilibrium, more over free-base ligands may also remain; hence during the photolysis they are simultaneously excited. Owing to deeper evaluation of spectral change, also photoinduced transformation between the mono- and bisporphyrin complexes can be identified, beside the photoredox degradation to the above mentioned open-chain photoproducts and dissociation to the free-base porphyrin. The equilibria between the complexes are varied by excitation, that is the significant part of the overall photochemical quantum yields originate from these photoinduced transformations of complexes to each other in this photostationary state [30]. Light accelerates these reactions by order of magnitude compared to their very low rate in dark at room temperature [205].

The free-base ligand may also undergo the photoinduced ring-oxidation with very low quantum yield value [123, 179, 228]. Upon metalation an increase in quantum yield may be observed due to an indirect photoinduced ligand to metal charge transfer. The increase in the rate of photooxidation is more expressed if the chance of backward metal-to-ligand charge

transfer is enormously decreased, which is observable in the out-of-plane complexes, as a consequence of the metal ion's location away from the porphyrin cavity. The possibility of electron ejection can basically be omitted and the only process is LMCT that can cause the metal induced increase of the photoxidation quantum yield [31]. The efficiency of photoinduced ligand to metal charge transfer depends on the redox potential value of the metal center bonded with porphyrin ligand. The already published results from our group have indicated that the out-of-plane position and size of the metal are responsible for the dissociation of the metal center [87]. As discussed in chapter 3.3 Photolysis instrumentation and procedures, different methods are used for the evaluation of quantum yield of a photochemical reaction. In a simple case, the initial slope method is used, which is based on equation 2.8, expressing the change in the concentration of the absorbing species during the photolysis, resulting in a change of light absorption as shown in Figure 4.18.

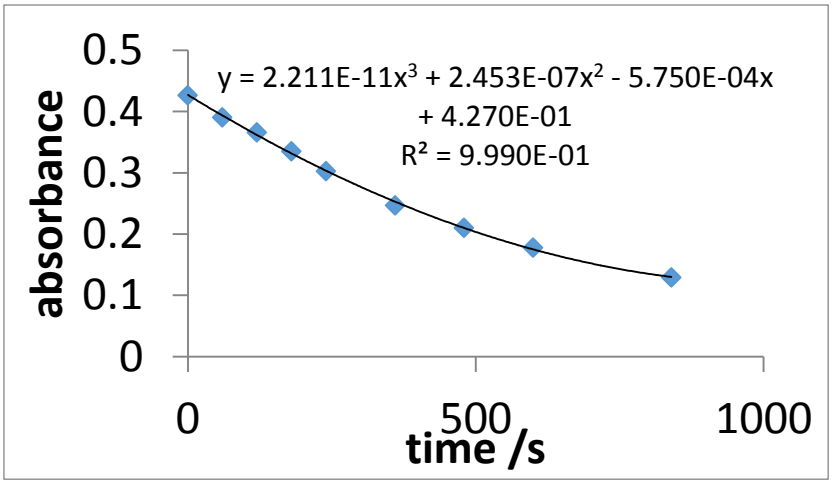

Figure 4.18. Initial slope method

The initial slope method does not take the degradation of the complex over the whole irradiation time into account. Instead, it uses predominantly the first measurement points in the calculation. As depicted in Figure 3.17, absorbance decreases exponentially with time and excel is usually unable to precisely fit exponential curve for the measured points; moreover this method does not calculate with the decrease of absorbed light intensity Thus, to overcome this drawback, a second method, named as integral fitting method was applied for the determination of photochemical quantum yield (Equation 2.9). This method is helpful, if there is only one absorbing species and the photochemical process is only dependent on the concentration of this species. Plot of time versus integral fitting values is given in Figure 4.19.

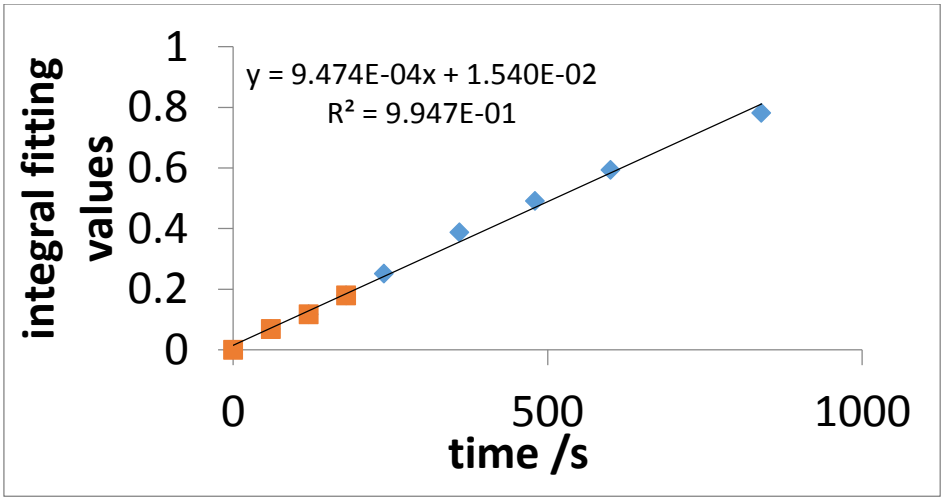

Figure 4.19. The integral fitting method applied to the spectral changes in Figure 4.15. The values of the y coordinate are calculated by Equation 2.9

Because of appearance of different species as a result of photoinduced reactions, the absorbance of these species becomes considerable at irradiation wavelength and initial slope and integral fitting methods are not effective. To determine the concentration and absorbance of all the species in all the time along with the quantum yield of the various photochemical reactions a third method, known as concentration distribution method was applied (Equation 2.10). The molar absorption spectra in Soret- and Q-bands of all the possible species formed during the photoinduced reactions are depicted in Figure 4.20 a and b, respectively.

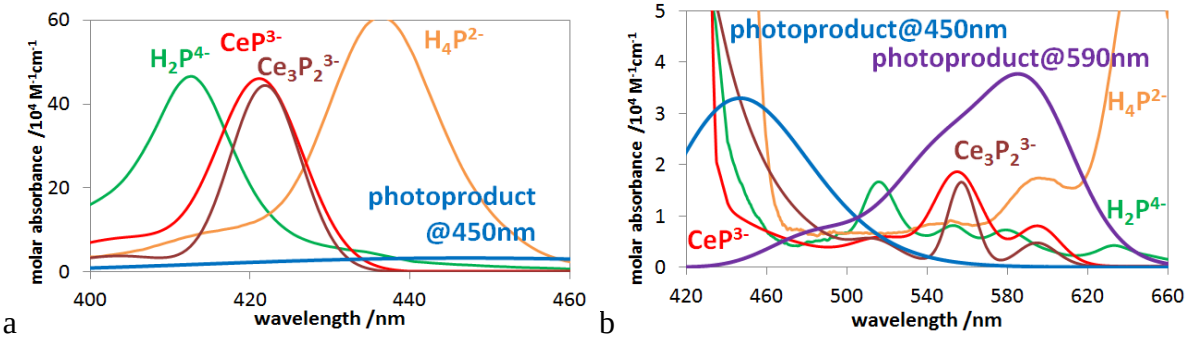

Figure 4.20. Molar absorption spectra of all the species a) in Soret- b) Q-range.

From the molar absorption spectra it can be seen that the photoproducts formed at 450 and 590 nm do not have absorption bands in the Soret-range, while in the Q-range they have. The irradiation of the cerium(III) porphyrins at the Soret- and Q-bands causes different type photoinduced reactions, which are redox, dissociation and transformation. Redox reaction gives rise to degradation and ring opening process, while the dissociation leads to the formation of free-base porphyrin, and in transformation mono- and bisporphyrins are formed.

The equation for the rate of different possible photoinduced reactions are summarized as follows.

$$d\{CeP\}/dt = v(CeP\ redox) + v(CeP \rightarrow H_2P) + v(CeP \rightarrow Ce_3P_2) - v(Ce_3P_2 \rightarrow CeP) - v(H_2P \rightarrow CeP)$$
$$d\{Ce_3P_2\}/dt = v(Ce_3P_2\ redox) + v(Ce_3P_2 \rightarrow CeP) + v(Ce_3P_2 \rightarrow H_2P) - v(CeP \rightarrow Ce_3P_2)$$
$$d\{H_2P\}/dt = v(H_2P\ redox) + v(H_2P \rightarrow Ce_xP_y) + v(H_2P \rightarrow H_4P) - v(Ce_xP_y \rightarrow H_2P) - v(H_4P \rightarrow H_2P)$$
$$d\{H_4P\}/dt = v(H_4P\ redox) + v(H_4P \rightarrow H_2P) - v(H_2P \rightarrow H_4P)$$
$$d\{total\,porph.\}/dt = v(CeP\ redox) + v(Ce_3P_2\ redox) + v(H_2P\ redox) + v(H_4P\ redox)$$

The change in concentration distribution of all the species formed as a result of photoinduced reactions with respect to time is presented in Figure 4.21 a and b. During the photolysis at Soret- and Q-band maxima, the concentration of cerium(III) mono- and bisporphyrins decreases, while the concentration of photoproducts increases.

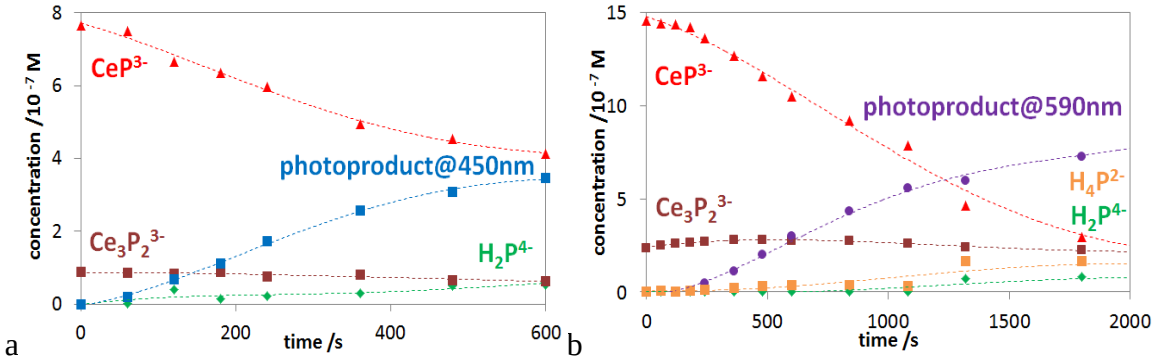

Figure 4.21. Concentration distribution of all species and a) photoproduct at 450 b) at 590 nm

3.1. Mechanistic investigations of the photochemical reactions

I tried to investigate the mechanism of possible photochemical reactions of cerium(III) porphyrins in different aspects and determined the photochemical quantum yield for the individual photoinduced reactions of the particular species. First, the concentration of anionic porphyrin ligand was changed in the presence of constant concentration of cerium(III) and perchlorate as ionic strength adjustor. The photochemical quantum yield determined by the different evaluation methods are given in Table 4.6.

Table 4.6 Photochemical quantum yields for the Ce(III) porphyrin system containing perchlorate (0.01 M)

c(porph)/ 10^{-6}M	Φ(initial slope)/ 10^{-4}	Φ(integral fitting)/ 10^{-4}	Φ (CeP)/ 10^{-4}	redox %	diss. %	transf. %	Φ (Ce_3P_2)/ 10^{-4}	redox %	diss. %	transf. %
1.8	3.2	3.1	4.4	87	13	0	6.0	79	16	5
2.8	2.9	2.6	1.4	93	7	0	6.6	74	16	11
3.7	2.4	2.4	2.5	80	16	4	5.7	87	13	0

Φ is the overall photochemical quantum yield observed in Soret-band photolysis and % redox, diss. and transf. denotes the fraction of the photoinduced redox, dissociation and transformation reactions in the overall quantum yield.

By changing the porphyrin concentration, I observed the decrease of the overall photochemical quantum yield. There is a possibility that the excited complex can react with another one in excited state, or rather in ground-state. I carried out similar photolysis experiments in deoxygenated solutions and determined the individual quantum yields for different porphyrin forms by the use of concentration distribution method. Total photochemical quantum yield of bisporphyrin complexes increased, while it decreased in the presence of oxygen. It indicates that for the above-mentioned bimolecular reaction of bisporphyrin complex is responsible the triplet excited state, which can be quenched by triplet oxygen (forming singlet oxygen), while in the absence of oxygen, the different types of primary photochemical reactions, but mainly the redox degradation took place. The effect of changing porphyrin concentration on the overall photochemical quantum yield and individual quantum yield of cerium(III) mono- and bisporphyrin is depicted in Figure 4.22 a and b respectively, which clearly demonstrates that upon increasing porphyrin concentration the overall quantum yield (calculated by initial slope and integral fitting methods) decreases. Because of the perchlorate ions the formation of cerium monoporphyrins in hindered and its quantum is also lower as compared to the bisporphyrins as presented in Figure 4.22 b.

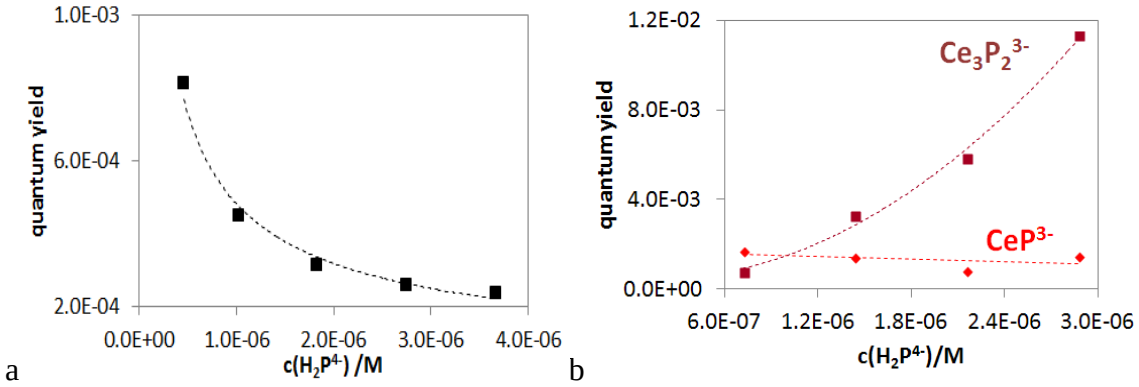

Figure 4.22. Effect of H_2P^{4-}concentration on a) over all and b) individual quantum yields of mono- and bisporphyrins c (Ce^{3+}) = 1.0×10^{-3} M and c ($NaClO_4$) =0.01 M

The photolysis experiments are carried out under same conditions, only the ionic strength adjustor was exchanged to sodium acetate in Table 4.7.

Table 4.7 The quantum yields of Ce(III) porphyrin system with changing porphyrin concentration containing acetate (0.01M)

c(porph)/ 10^{-6}M	Φ(initial slope)/ 10^{-4}	Φ(integral fitting)/ 10^{-4}	Φ (CeP)/ 10^{-4}	redox %	diss. %	transf. %	Φ (Ce_3P_2)/ 10^{-4}	redox %	diss. %	transf. %
1.8	1.6	2.3	5.2	84	16	0	5.6	77	15	8
2.8	1.9	2.4	4.8	77	19	4	5.6	83	17	0
4.6	2.3	3.0	4.1	79	19	2	7.6	85	15	0

Secondly, I investigated the effect of different ionic strength adjustors for different photoinduced reactions. To check the effect of ionic strength adjustors reaction mixture are made with varying concentration of perchlorate and acetate by keeping a constant concentration of cerium(III) metal ion and porphyrin. The reaction mixture containing cerium(III) porphyrin complex are photolyzed in Soret- and Q- band maximum in aerated as well as in deoxygenated form (Table 4.8).

Table 4.8 The quantum yields of Ce(III) porphyrin system with changing perchlorate concentration

c($NaClO_4$) /M	Φ(initial slope)/ 10^{-4}	Φ(integral fitting)/ 10^{-4}	Φ (CeP)/ 10^{-4}	redox %	diss. %	transf. %	Φ (Ce_3P_2)/ 10^{-4}	redox %	diss. %	transf. %
0.0	15	14	13	82	0	18	11	100	0	0
0.1	8.6	7.2	7.5	78	18	4	47	85	15	0
0.3	8.3	8.3	8.0	96	3	1	28	98	2	0
0.5	13	9.8	13	85	15	0	66	83	13	3
0.8	9.8	12	28	94	6	0	26	82	11	7
1.0	12	16	18	90	10	0	50	77	14	9

The overall photochemical quantum yields show an increasing trend with increasing ionic strength as a consequence of enhanced possibility of the photoinduced charge separation after the ligand-to-metal charge-transfer process. However, this statement is valid only in the case of monoporphyrins because on increasing the concentration of acetate, the equilibrial bisporphyrin concentration decreasew together with the possibility for the photoinduced bimolecular reaction of bisporphyrin. The effect of ionic strength adjustors on photochemical quantum yields are depicted in Figure 4.23 a and b.

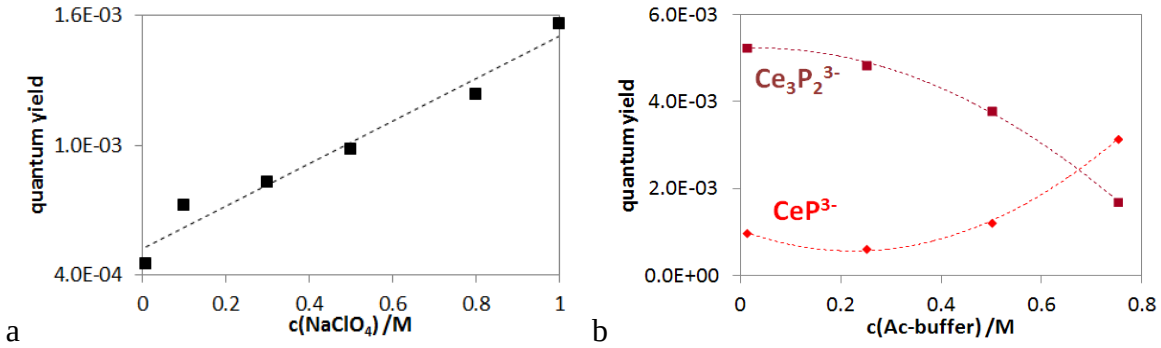

Figure 4.23. Effect of a) perchlorate b) acetate concentration on quantum yield of mono- and bisporphyrins c (Ce^{3+}) = 1.0×10^{-3} M and c (H_2P^{4-}) = 1.0×10^{-6} M

Table 4.9 The quantum yields for Ce(III) porphyrin system with changing acetate concentration

c(acetate) /M	Φ(initial slope)/ 10^{-4}	Φ(integral fitting)/ 10^{-4}	Φ (CeP)/ 10^{-4}	redox %	diss. %	transf. %	Φ (Ce_3P_2)/ 10^{-4}	redox %	diss. %	transf. %
0.01	11	9.5	9.8	80	14	6	52	90	10	0
0.1	9.5	6.7	3.3	100	0	0	0	63	9	28
0.3	10	8.9	6.1	100	0	0	48	74	8	18
0.5	9.9	8.9	12	100	0	0	38	68	10	22
0.8	8.4	7.8	31	96	4	0	1.7	79	13	8
1.0	13	12	9.4	77	14	9	33	90	10	0

The effect on perchlorate and acetate on the photoinduced reactions of bisporphyrin is depicted in Figure 4.24. The ionic strength adjustors have opposite effect on the equilibrial concentration of bisporphyrins and this effect is also valid for the quantum yield of the primary photoinduced reactions, mainly for the transformation of the cerium(III) bisporphyrin to monoporphyrins.

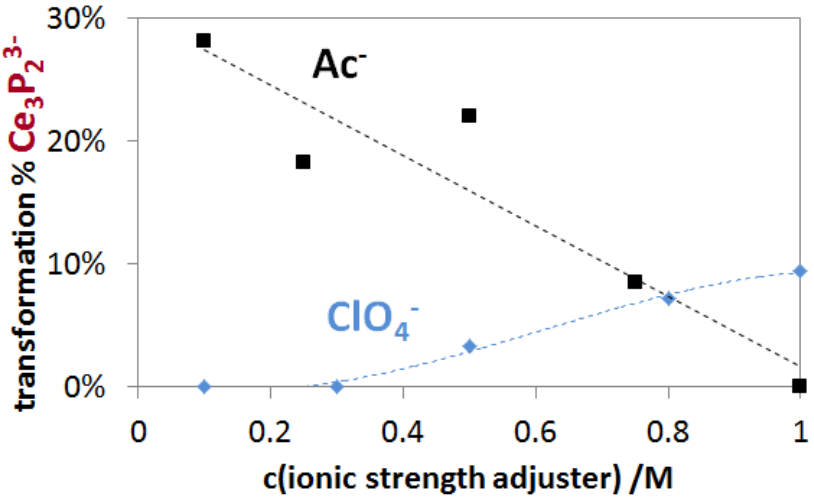

Figure 4.24. The effect on perchlorate and acetate on the percentage of photoinduced transformation

3.2. Trends in photochemical properties of lanthanide(III) porphyrins

The quantum yield values calculated by different methods for investigated lanthanide(III) porphyrins complexes in the presence of perchlorate are summarized in Table 4.10.

Table 4.10 The quantum yield values calculated by different methods for investigated lanthanide(III) porphyrins complexes, $NaClO_4$ = 0.01 M, c (Ln^{3+}) = 1.0×10^{-3} M and c (H_2P^{4-}) = 1.0×10^{-6} M

Ln(III)	ionic radius M^{3+}	Φ(initial slope)/ 10^{-4}	Φ(integral fitting)/ 10^{-4}	Φ (LnP)/ 10^{-4}	redox %	diss. %	transf. %	Φ (Ln_3P_2) 10^{-4}	redox %	diss. %	transf. %
La	116	6.9	5.0	7.6	86	10	4	15.1	78	12	10
Ce	114.3	15.5	13.7	12.8	82	0	18	11.2	74	11	15
Nd	110.9	3.5	3.2	8.1	88	12	0	22.5	86	12	2
Sm	107.9	6.8	3.4	5.2	83	12	5	16.4	76	12	12
Eu	106.6	13.8	7.2	5.0	90	3	7	6.9	90	5	5
Gd	105.3	15.8	13.5	5.9	72	15	13	5.6	99	1	0
Dy	102.7	10.5	9.9	7.5	68	13	19	2.9	100	0	0
Er	100.4	4.8	4.4	8.2	86	10	4	2.7	78	12	10
Yb	98.5	6.9	7.2	5.1	82	0	18	2.6	74	11	15

As a consequence of lanthanide contraction, the out-of-plane distance in lanthanide porphyrin decreases, which results in the decrease of photochemical quantum yield values (after a small increase) because of the less effective photoinduced charge separation after the ligand-to-metal charge transfer as depicted in Figure 4.25.

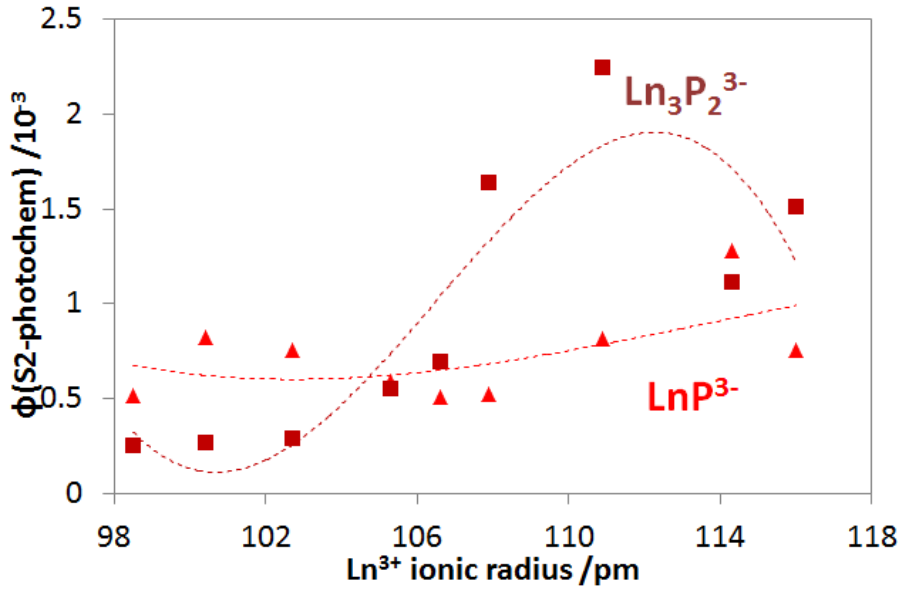

Figure 4.25. Trends in primary photochemistry of lanthanide(III) porphyrins

3.3. Applicability of lanthanide(III) porphyrin systems

The advantageous coordination, redox and photoinduced properties of out-of-plane metalloporphyrins can also be exploited in photcatalytic procedures. In out-of-plane metalloporphyrins the sensibilization of metal ions are direct and more efficient. In water-soluble lanthanide(III) porphyrin systems the out-of-plane position of the lanthanide(III) metal ion in the porphyrin molecule displays distinctive photochemistry. They undergo efficient ligand-to-metal charge-transfer processes following absorption of visible light. This photoactivity allows their utilization as a catalyst in the cyclic process for the synthesis of compounds storing solar energy and photochemical water-splitting for renewable energy technology and green chemistry.

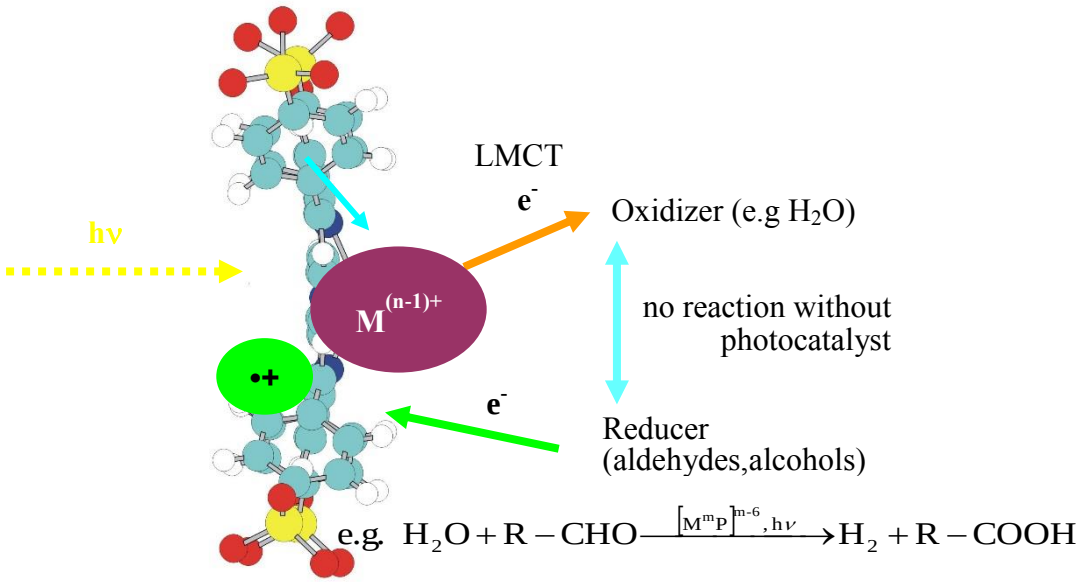

Figure 4.26. Photcatalytic cycle of OOP metalloporphyrins.

The out-of-plane position of the lanthanide(III) ion in the porphyrin cavity can under two types of photoinduced chemical reactions first is the photoinduced dissociation of the metal ion from the cavity of the ligand without charge transfer due to the lability of the complex and secondly the photoredox degradation of the macrocycle initialized by an irreversible ligand-to-metal charge transfer resulting in oxidation of the ligand and reduction of the metal center. The charge of the metal center decreases, and its size increases, thus its charge density falls down, hence the coordinative bonds can easily split. The reduced metal ion can step out from the cavity mainly in polar solvent, and can induce further redox reactions, depending on its stability in the given medium. The reduced metal ion react with weak oxidizer like water and results in the generation of hydrogen. The oxidized and metal-free porphyrin (cat)ionic radical is a very strong base: it gets immediately protons, forms the free-base radical, which is long-lived and a relatively strong oxidizer, mainly in oxygen-free solution ($\tau_{1/2}$>>1 ms, $E_{1/2}$>1 V). But it would oxidize water to oxygen only at higher pH, therefore a slightly stronger reducer, for example water-soluble alcohols or aldehydes, are required, from which useful byproducts can be formed in photcatalytic hydrogen production. In the absence of reducer (without regeneration, cyclization), the primary photochemical processes take place: in an overall four-electron oxidation, ring-opening reaction, a dioxo-tetrapyrrole derivative (bilindione) can form [144].

Indigenously designed experimental setup is used for carrying the hydrogen generation experiments from lanthanide(III) metalloporphyrins under the continuous irradiation in Soret- and Q-range as well as under whole visible light.

Summary

Despite the important roles of metalloporphyrins in coordination, photochemistry and numerous biochemical processes, slight is known about the consequences of the out-of- plane (OOP) or sitting-atop (SAT) position of the coordinated metal ion. If it is not able to fit coplanarly into the cavity of the ligand because of its size and/or coordinative features, it is located outside the plane of the porphyrin. This special coordination makes the charge separation more efficient in an irreversible photoinduced charge transfer from ligand to metal (LMCT).

Lanthanide(III) ions, due to their large ionic radius and contraction upon increasing the atomic number, proved to be suitable for the fine tuning of the out-of-plane (OOP) distance of the metal center. Their water-soluble complexes with porphyrins are of special interest because the very strong reducing power of the Ln^{2+} ions formed in the photoinduced LMCT process may offer a good chance to produce hydrogen in aqueous solution. Hence, in this work, equilibrium, photophysical and photochemical behaviour of anionic lanthanide(III) porphyrins were studied in order to gain useful pieces of information for the development of their future application in photocatalytic solar energy conversion and storage.

Insertion of a metal ion into the porphyrin cavity could be spectrophotometrically followed due to the redshifts of UV-Vis, intraligand $\pi\pi^*$ absorption bands, compared to those of the corresponding free base. Besides, a considerable decrease of the S_1-fluorescence intensity accompanied this process. Depending on the potential axial ligands, different porphyrin complexes were formed between 5,10,15,20-tetrakis(4-sulfonato-phenyl)porphyrin (H_2TSPP^{4-}) and Ln(III) ions. In the presence of acetate ions, which are efficiently coordinated to these metal ions, mainly the lanthanide(III) monoporphyrin species appeared. The much weaker coordinating perchlorate ions, however, did not hinder dimerization, allowing the formation of bisporphyrins (3:2 = metal ion : porphyrin) too. The photophysical properties of the latter species (only a moderate change of their absorption spectra and fluorescence data compared to those of the corresponding mononuclear complexes) indicated a weak interaction between the monomers. Hences, a tail-to-tail structure was suggested for the bisporphyrins, in which the monomers are bound through the peripheral sulfonato groups by a metal-ion bridge. The stability constants for both types of complexes increased with the atomic number, which could be attributed to the shorter OOP distance resulting in a stronger metal-ligand interaction, due to the lanthanide contraction.

Irradiation of the Ln(III) porphyrins at Soret- and Q-band maxima led to three types of photoinduced reactions, namely redox degradation, i.e. ring-opening, dissociation to free-base porphyrin and metal ion, and transformation between the lanthanide(III) mono- and bisporphyrins. Besides, depending on the excitation wavelength, two types of photoproducts have been detected for the fi

rst time with lanthanide(III) porphyrins, along with the determination of their molar absorption spectra. Soret-band irradiation produced a short-lived intermediate appearing at 450 nm, while Q-band excitation generated a stable end-product absorbing at 590 nm. The latter one was suggested to be lanthanide(III) complex with a ring-opened tetrapyrrolic ligand.

The individual quantum yields of all the posssible photochemical reactions were determined by the concentration distribution method for each lanthanide(III) porphyrin studied. For both the mono- and the bisporphyrins, the overall quantum yields, in which the efficiency of the redox degradation is predominant, display a decreasing trend (following a small increase) as a function of the atomic number of the metal center, as the consequence of the diminution of the out-of-plane distance and, thus, the chance for the charge separation following the photoinduced LMCT process.

Thesis points

1. The formation of sitting-atop (SAT) complexes of a water-soluble anionic porphyrin with lanthanide(III) ions (Ce^{3+}, Nd^{3+}, Sm^{3+}, Eu^{3+}, Gd^{3+}, Dy^{3+}, Er^{3+}, Yb^{3+}) were investigated in the presence of acetate and perchlorate ions. Their stability constants and structural information were spectrophotometrically determined.
   I) I confirmed the insertion of lanthanide(III) ions into the porphyrin cavity and the formation of typical out-of-plane complexes, owing to their large ionic radius, due to the redshifts of UV-Vis intraligand ππ* absorption bands.
   II) I verified that in the presence of acetate mainly the lanthanide(III) monoporphyrin (LnP^{3-}) species are formed, while in the case of perchlorate also bisporphyrins ($Ln_3P_2^{3-}$), on the basis of the further redshift and broadening of absorption bands. The axially stronger coordinating acetate ions hinder this process.
   III) Analyzing the UV-Vis spectra of free-base, Ln(III) mono- and bisporphyrins as well as the stability constant values for both Ln(III) porphyrins determined separately in the presence of acetate and perchlorate, I observed an increasing trend in the stability constants of the investigated lanthanide(III) mono- and bisporphyrins as a funnction of the atomic number in the lanthanide series, and explained by the lanthanide contraction resulting in the decrease of the out-of-plane distance, therefore the strengthening of the coordinative bonds.
2. I elucidated the structure and mode of coordination in lanthanide(III) mono- and bisporphyrins from S_1-flourescence quantum yields, lifetime, radiative and non-radiative decay rates and other photophysical parameters.
   I) I justified the out-of-plane coordination of the metal ion into the cavity of porphyrin ligand from the hypsochromic effect in the singlet-1 fluorescence and a decrease of the fluorescence quantum yield of lanthanide(III) monoporphyrins as compared to that of free-base porphyrins, as the consequence of dome distortion. Only a small further decrease of fluorescence quantum yield takes place during the formation of lanthanide(III) bisporphyrins, as a result of weak π-π interactions between the macrocycles. On the basis of these phenomena, I supposed the tail-to-tail (or head-to-tail) dimerization of monoporphyrin complexes through a metal-ion bridge

between (or to) the sulfonate groups which results in a moderate decrease of fluorescence.

II) I established that the fluorescence quantum yield of the lanthanide porphyrins studied as a function of the atomic number of the metal center displays a maximum, due to contradictory electronic and steric factors. More unpaired electrons result in strong interaction with π-electron system, degreasing the fluorescence quantum yield. Lanthanide contraction, however, results in shorter out-of-plane distance and, thus, lower dome distortion, hence, increasing the quantum yields.

III) I noticed that the lifetimes for singlet-1 fluorescence and non-radiative rate constant for mono- and bisporphyrins are comparable, while the radiative rate constant of monoporphyrin is higher as compared to bisporphyrins, which is due to the formation of head-to-tail oligomerization.

IV) I summarized the photophysical results for all the investigated Ln(III) porphyrins and observed that an increase in the radiative rate values cause an increase in the quantum yield values, while the non-radiative rate and life times are almost similar.

3) To elucidate the photoinduced reactions, I photolyzed all the Ln(III) porphyrins studied at Soret- and Q-range in open air and deoxygenated form and observed that the Ln(III) porphyrins mainly undergo three types of photoinduced reactions which are redox degradation i.e. ring opening, dissociation to the free-base porphyrin and transformation between the mono- and bisporphyrins.

I) I observed a monotonous decrease of the absorption in the Soret-range during the irradiation of the complexes studied, attributed to the cleavage of the porphyrin ring which is initialized by an irreversible LMCT reaction.

II) I identified two types of photoproduct depending on the irradiation wavelength. At Soret-band irradiation an unstable radical type intermediate appeared at 450 nm, similarly to the case of other OOP porphyrin complexes with post-transition metal center, while at Q-band excitation a stable end-product appeared at 590 nm. These photoproducts were observed for the first time with lanthanide(III) porphyrins, along with the determination of their molar absorption spectra.

III) I also established that the out-of-plane position of the metal center is favorable for the photoinduced dissociation of the metal center from the ligand cavity as a consequence of the lability of these complexes.

IV) Determining the individual and overall quantum yields for all the possible photochemical reactions by initial slope, integral fitting and concentration distribution methods for the lanthanide(III) porphyrin complexes studied, I observed a decreasing trend following small increase of the quantum yield as a function of the atomic number of the metal center. This phenomenon has been attributed the to the lanthanide contraction decreasing the lower out-of-plane distance and, thus, hindering the charge separation after the photoinduced LMCT process.

References

1. B. Minaev, H. Agren. *Chem. Phys.* 315 **(2005)** 215.
2. P. E. McGovern and R. H. Michel, *Acc. Chem. Res.* 23 **(1990)** 152.
3. M. Counterman, The porphyrin, D. Dolphin (Ed), Academic, New York, Vol III, Part A, Physical Chemistry, **1978**
4. L. R. Milgrom, *The Colours of life*: An Introduction to the Chemistry of Porphyrins and Related Compounds, Oxford University Press, Oxford, **1997**
5. M. Gouterman, in *The Porphyrins*, Vol. 3, Ed. By D.Dolphin (Academic Press, New York, **1978**, pp. 1-165.
6. T. Eicher, S. Hauptmann, The Chemistry of Heterocycles, WILEY-VCH, Weinheim, **2003**
7. M. Stepien, L. Latos-Grazynski, in Topics in Heterocyclic Chemistry, vol. 19, ed. by R.R. Gupta, Springer, Heidelberg, **2000**, pp. 83-153.
8. W. Kaim, B. Schwederski, Bioanorganische Chemie, 4th edn. B. G Teubner, Wiesbaden, **2005**
9. J. L. Hoard, *Science*, 174 **(1971)** 1295.
10. W. R. Scheidt, *Acc. Chem. Res.* 10 **(1977)**, 339.

11. H. Fischer and H. Orth, Die Chemie des pyrrols, Vol III, Akad. Verlag, Leipzig **(1940)**
12. G. P. Moss, *Pure Appl. Chem.* 59 **(1987)** 779.
13. N. Kobayashi, Theoretical interpretation of spectroscopic data, *J. Porphyrins Phthalocyanines* 4 **(2000)** 377.
14. T. Hashimoto, Y-K. Choe, H. Nakano, K. Hirao. *J. Phys. Chem. A* 103 **(1999)** 1894.
15. M. Gouterman, *J. Chem. Phys.*, 30 **(1959)** 1139.
16. L. J. Boucher. *Coord. Chem. Rev*. 7 **(1972)** 289.
17. Z. Valicsek, O. Horváth, *Microchem. J*., 107 **(2013)** 47.
18. R. Giovannetti. The Use of Spectrophotometry UV-vis for the study of Porphyrin, in Dr. Jamal Uddin (ed.) Micro to Nano Spectroscopy, (ISBN: 978-953-51-0664-7), **2012**
19. J. J. Weaver: *Corroles*, PhD Thesis, California Institute of Technology, **2005**
20. M. Gouterman, *J. Mol. Spectrosc* 6 **(1961)** 138.
21. K. Kalyanasundaram: Photochemistry of Polypyridin and Porphyrin Complexes Academic Press: New York: **1992**.
22. A. J. Lawaetz, Fluorescence Spectroscopy and Chemometrics -Applied in Cancer Diagnostics and Metabonomics, PhD thesis, University of Copenhagen **(2011).**
23. Peter TO So, C. Y. Dong, Fluorescence Spectrophotometry, Massachusetts Institute of Technology, **(2002)** Macmillan Publishers Ltd, Nature Publishing Group
24. B. Valeur. Molecular Fluorescence: Principles and Applications, Wiley-VCH, 200
25. M. Kasha, Characterization of Electronic Transitions in Complex Molecules. Discussions of the Faraday Society **(1950)** 14-9
26. J. R. Lakowicz, Principles of Fluorescence Spectroscopy, Springer **(2006).**
27. G. Stochel, M. Brindell, W. Macyk, Z. Stasicka, K. Szacilowski, Bioinorganic Photochemistry, ISBN: 978-1-405-16172-5 **(2009)**
28. Izhar Ron, Functional Optical Imaging of Tissue based on Fluorescence Lifetime Measurement, Master's thesis, Tel Aviv University, **(2004).**
29. P. Seybold, M. Gouterman, *J. Mol. Spectrosc*., 31 **(1969)** 1.
30. Z. Valicsek, G. Eller, O. Horváth, *Daltons Trans.*, 41 **(2012)** 13120.
31. Z. Valicsek, G. Lendvey, O. Horváth, *J. Phys. Chem. B* 112 **(2008)** 14509.

32. K. M. Kadish, K. M. Smith, R. Guilard, The Porphyrin Handbook, vol. I (Academic Press, San Diego, **2000**
33. D. Dolphin (ed.), The Porphyrins, Academic Press, New York **(1978)**, Vol. I.
34. R. F. Labbe and G. Nishida, *Biochim. Biophy. Act*. 26, **(1957)** 437.
35. H. Fisher, *Org. Synth*. 3 **(1955)** 442.
36. J. E. Falk, Porphyrins and Metalloporphyrins, Elsevier, Amsterdam, **1964**.
37. M. Grinstein, J. Biol. Chem. 167 **(1947)** 515.
38. J. L. W. Thudichum, *Rep. Med. Off. Privy Counc*. 10, Appendix 7, **(1867)** 152.
39. H. Fischer and F. Lindner, Hoppe-Sey1er's *Z. Physiol. Chem.* 168, **(1927)** 152.
40. H. Fischer and R. Müller, Hoppe-Seyler's *Z. Physiol. Chem.* 142, **(1925)** 120 and 155.
41. S. Schwartz, M. H. Berg, I. Bossenmaier, and H. Dinsmore, *Methods Biochem. Anal*.8, **(1960)** 221
42. W. S. Caughey, J. O. Alben, W. Y. Fujimoto, and J. L. York, *J Org. Chem*. 31 **(1966)**.31
43. G. Y. Kennedy, A. H. Jackson, G. W. Kenner, and C. J. Suckling, *FEBS Lett.* 6, **(1970)**; 9. 7, **(1970)** 205.
44. S. Sano, T. Shingu, J. M. French, and E. Thonger, *Biochem. J.* 97, **(1965)** 250.
45. J. M. French, M. T. England, J. Lines, and E. Thonger, *Arch. Biochem. Biophys.*107, **(1964)** 404.
46. H. Fischer and H. Orth, "Die chemie des Pyrrols," Vol. 2, Part 1, p. 512. Verlagsges, Leipzig, 1937 (reprinted by Johnson Reprint Corporation, New York (**1968**).
47. G. H. Elder, C. H. Gray, and D. C. Nicholson, *J. Clin. Pathol*. 25, **(1972)** 1013.
48. T. C. Chu and E. J. H. Chu, *Clin. Chem*. 13, **(1967)** 371.
49. R. Willstatter and A. Stoll, "Investigations on Chlorophyll" Printing Press, Lancaster, Pennsylvania, **1928**
50. H. Fischer and A. Stern, "Die Chemie des Pyrroles," Vol. 2, Part 2, Akad. Verlagsges. Leipzig, 1940 (reprinted by Johnson Reprint Corp. New York (**1968**)
51. S. J. Schwartz and J. H. Vonelbe, *J. Food Sci.*, 48 **(1983)** 1303.
52. A. Ina, K. Hayashi, H. Nozaki, Y. Kamei, *Int. J. Dev. Neurosci.*, 25 **(2007)** 63.
53. R. E. Nelson and M.G. Ferruzzi, *J. Food Sci*., 73 **(2008)** 86.
54. H. Fischer and W. Gleim, *Justus Liebigs Ann. Chem*., 157 **(1935)** 521.

55. P. Rothemund. *J. Am. Chem. Soc*. 58, **(1936)** 625.
56. P. Rothemund. *J. Am. Chem. Soc*. 57, **(1935)** 2010.
57. P. Hambright, *Coord. Chem. Rev*., 6 **(1971)** 247.
58. J. W. Buchler. Synthesis and properties of metalloporphyrins, in Porphyrins, Vol. 1 (D. Dolphin, ed.), Academic Press, New York. (**1978**) p. 389.
59. J.W. Buchler, Porphyrin and Metalloporphyrins, K. M. Smith (Ed.), Elsevier **(1975)**
60. B. F. Burnham, J. J. Zuckerman, *J. Am. Chem. Soc*., 6, 92 **(1970)** 1547.
61. O. A. Golubchikov and B. D. Berezin, *Russian Chem. Rev*., 55, 8 **(1986)** 768.
62. K.S. Suslick, C. T. Chen, G.R. Meredith and L. T. Cheng, *J. Am. Chem. Soc*., 114 **(1992)** 6928.
63. G. Harrach, Z. Valicsek, O. Horváth, *Inorg. Chem. Comm*., 14 **(2011)** 1756.
64. A. L. Lehninger, "Biochemistry", Kalyani Publishers, New Delhi **(1978)**
65. H.H. Seliger, W.D. McElory, Light; Physical and Biological Action, Academic Press, New York, 1965.
66. S. L. Miller and L.E. Orgel, The Origins of Life on Earth, Prentice-Hall, New Jersey **(1974)** p.33
67. K. Saner, *Annu. Rev. Phy. Chem*., 30, **(1979)**, 155
68. J.E. Huheey, E.A. Keiter and R.L. Keiter, Inorganic Chemistry-Principles of Structure and Reactivity (4^{th} Edition), Harper Collins College Publishers, New York, **1993**
69. M. N. Hughes, The Inorganic Chemistry of Biological Processes, (2^{nd} Edition), John Wiley and Sons, New York, **1988**
70. M.S. Perutz, G. Fermi, B. Luisi, B. Shaanan and R. C. Liddington, *Acc. Chem. Res.*, 20, **(1987)** 309.
71. M. S. Perutz, *Nature*, 228 **(1970)** 726.
72. T. Sjistrand, *Nature* (London), 168 **(1951)** 729 and T. Sjistrand, *Ann. N. Acad. Sci*, 174 **(1970)** 5.
73. H. Kayser, *J. Insect. Physiol*., 20 **(1974)** 89.
74. R. Tenhunen, H. S. Marver, N. R. Pimstone, W. R. Trager, D. Y. Cooper, and R. Schmid, *Biochemistry*, 11 **(1972)** 1716.
75. E. L. Smith, R. L. Hill, I. R. Lehman, R. J. Lef Kowitz, P. Handler and A. White, Principles of Bio-Chemistry-General Aspects (7^{th} Edition), McGraw-Hill Inc., Singapore, **1983**

76. S. Scheller, M. Goenrich, R. K. Thauer and B. Jaun, *J. Am. Chem. Soc*. 135 **(2013)** 1475.
77. U. Ermler, W. Grabarse, S. Shima, M. Goubeaud, R. K .Thauer, *Science*, 278 **(1997)** 1457.
78. E. C. Duin, M. L. McKee, *J. Phys. Chem. B*, 112 **(2008)** 2466.
79. A. Eschenmoser, Ann. N. Y.Acad. Sci., 471 **(1986)**, 108 and reference therein.
80. J. Shelnutt, X-Zhi Song, Jian-Guo Ma, Song-Ling Jia, W. Jentzen and C. J. Medforth. *Chem. Soc. Rev*.27 **(1998)** 31.
81. R. J. Quann and R. A. Ware, Advances in chemical engineering, volume 14 p. 97 (ISBN 0-12-008514-3) Academic Press, INC. San Diego, California 92101.
82. E. B. Fleischer, J. H. Wang, *J.Am.Chem.Soc.*82 **(1960)**3498–3502.
83. J. Michael Gottfried, Surface Science Reports, 70 **(2015)** 260-379
84. E. Raux, H. L. Schubert, J. M. Roper, K. S. Wilson, M. J. Warren, *Bioorganic Chem.*, 27 **(1999)** 100-118
85. E. B. Fleischer, *Accts. Chem. Res*., 3 **(1970)** 105.
86. J. Zaleskie, *J. Physiol. Chem.*, 37 **(1902)** 54.
87. O. Horváth, R. Huszank, Z. Valicsek, G. Lendvay, *Coor. Chem. Rev*. 250 **(2006)** 1792.
88. R. Huszank, O. Horváth, *J. Chem. Soc., Chem. Commun*. **(2005)** 224..
89. Z. Valicsek, O. Horváth, *J. Photochem. Photobiol., A* 186 **(2007**) 1.
90. O. Horváth, Z. Valicsek, G. Harrach, G. Lendvay, M. A. Fodor, *Coord. Chem. Rev.* 256 **(2012)** 1531.
91. W. Jentzen, J. G. Ma, J. A. Shelnutt, *Biophys. J.* 74 **(1998)** 753.
92. R. Harada, Y. Matsuda, H. Okawa, R. Miyamoto, S.Yamauchi, T. Kojima, *Inor. Chim. Acta*, 458 **(2005)** 2489.
93. S. Al-Karadaghi, R. Franco, M. Hansson, J. A. Shelnutt, G. Isaya, G. C. Ferreira, *Trends in Biochem. Sci.*, 31 **(2005)** 135.
94. W. A.Kaplan, K. S. Suslick, R. A. Scott, *J. Am. Chem. Soc.* 113 **(1991)** 9824.
95. C. Bruckner, M. A. Hyland, E. D. Strenberg, J. K. MacAlpine, S. J. Rettig, B. O. Patrick, D. Dolphin, *Inorg. Chim. Acta*, 358 **(2005)** 2943.
96. L. Galich, H. Huckstadt, H. Homborg, *J. Porphyrin Phthalocyanines*, 2 **(1998)** 79.
97. P.N. Dwyer, L. Puppe, J. W. Buchler, W. R. Scheidt, *Inorg. Chem*., 14 **(1975)** 1782.

98. C. M. Drain, C. Kirmaier, C. J. Medforth, D. J. Nurco, K. M. Smith, D. Holten, J. Phys. Chem. 100 **(1996)** 11984-11993.
99. T. L. Harning, E. Fujita; J. J. Fajer, *Am. Chem Soc.* 108 (**1986**) 323
100. W. Jentzen, M. C. Simpson, J. D. Hobbs, X. Song, T. Ema, N. Y. Nelson, C. J. Medforth, K. M. Smith, M. Veyrat, M. Mazzanti, R. Ramasseul, J. C. Marchon, T. Takeuchi, W. A. Goddard, J. A. Shelnutt, *J. Am. Chem. Soc*., 117 **(1995)** 11085-11097
101. K. M. Barkigia, M. D. Berber, J. Fajer, C. J. Medforth, M. W. Renner, K. M. Smith, *J. Am. Chem. Soc.*, 112 **(1990)** 8851-8857.
102. P. Bohm, H. Groger, *ChemCatChem*., 7 **(2015)** 22-28.
103. M. Natali, A. Luisa, E. Lengo, F. Scandola, *Chem. Commun.*, 50 **(2014)** 1842.
104. V.V.Vasil'ev, A. A. Lobanovskaya, *Russ. J. Appl. Chem*., 88 **(2015)** 283-288.
105. A. Treibs, *Liebigs Ann. Chem*., 115 **(1969)** 728
106. R. J. Abraham, G. E. Hawkes, M. F. Hundson, K. M. Smith, *J. Chem. Soc., Perkin Trans. 2* **(1975)** 205
107. E. Hove, W. D. Horrocks, *J. Am. Chem. Soc*., 100 **(1978)** 4386
108. K. M. Barkigia, J. Fajer, A. D. Adler, G. J. Williams, *Inorg. Chem.,* 19 **(1980)** 2057-2061.
109. H. J. Callot, B. Chevrier, R. J. Weiss, *J. Am. Chem. Soc.*, 101 **(1979)** 7729.
110. J. Barens, G. Dorough, *J. Am. Chem. Soc.*, 72 **(1950)** 4045.
111. M. Tabata, M. Tanka, *Chem. Comm*. **(1985)** 42.
112. K. Kalyanasundaram, M. N. Spallart, *J. Phys. Chem*., 86 **(1982)** 5163.
113. N. A. Kuznetsova, V. V. Okunchikov, V. M. Derkacheva, O. L. Kaliya, E. A. Lukyanets, *J. Porphyrins Phthalocyanines*, 9 **(2005)** 393.
114. A. Ogunsipe, T. Nyokong, *J. Porphyrins Phthalocyanines*, 9 **(2005)** 121.
115. M. K. Smith, J. J. Lai, *Tetrahedron Lett.*, 21 **(1980)** 433.
116. Z. Valicsek, G. Lendvay, O. Horváth, *J. Porph. Phthalocyanines*, 13 **(2009)** 910.
117. 198
118. B. Evans, K. M. Smith, J. A. S. Cavaleiro, *J. Chem. Soc. Perkin Trans*. 1 **(1978)** 768.
119. J.-J. Lai, S. Khademi, F. E. Meyer, L. D. Cullen, M. K. Smith, *J. Porphyrins Phthalocyanines,* 5 **(2001)** 621.
120. M. Tabata, M. Tanaka, *J. Chem. Soc. Dalton Trans*, **(1983)** 1955.
121. D. P. Arnold, J. Blok, *Coor. Chem. Rev*., 248 **(2004)** 299-319.

122. S. J. Simpson, H. W. Turner, R. A, Andersen, *J. Am. Chem. Soc.*, 101 **(1979)** 7729-7730.

123. O. Horváth, Z. Valicsek, A. Vogler, *Inorg. Chem. Commun*., 7 **(2004)** 854.

124. Z. Valicsek, O. Horváth, K. Patonay, *J. Photochem. Photobiol. , A.* 226 **(2011)** 23.

125. G. A. Taylor, M. Tsutsui, *J Chem. Educ*. 52 **(1975)** 715.

126. J. W. Buchler, K. Rohbock, *Inorg. Nucl. Chem. Lett*., 8 **(1972)** 1073.

127. P. Hambright, *J. Inorg, Nucl. Chem.*, 32 **(1970)** 2449.

128. M. Tsutsui, C. P. Hrung, *Chem. Lett.*, 941 **(1973).**

129. M. F. Hudson, K. M. Smith, *J, C. S., Chem. Commun*., 15 **(1973)** 515.

130. G. Ricciardi, A. Rosa, E.J. Baerends, S.A.J. van Gisbergen, *J. Am. Chem. Soc*. 124 **(2002)** 12319-12334.

131. D. L. Akin, H. R. Zhu, C. J. Guo, *J. Phys. Chem*., 98 **(1994)** 3612.

132. D. L. Akin, S. Ozcelik, H. R. Zhu, C. Guo, *J. Phys. Chem*. 100 **(1996)** 14390.

133. M. S. Liao, J. D. Watts, and M. J. Huang, *J. Phys. Chem. A* 110 **(2006)** 13089.

134. W. K. Wong, X. Zhua and W. Y. Wong, *Coord. Chem. Rev.,* 251 **(2007)** 2386-2399.

135. J.W. Buchler, A. Decian, J. Fischer, M. Kihnbotulinski, H. Paulus, R. Weiss, *J. Am. Chem. Soc.* 108 **(1986)** 3652.

136. X. Sun, Y. Bian, M. Bai, C. Ma. N. Kobayashi, J. Jiang, *Dyes and Pigments,* 65 **(2005)** 145-150

137. H. He, *Coord. Chem. Rev*., 273-274 **(2014)** 87.

138. A. F. Mironov, *Russ. Chem. Rev*., 82 **(2013)** 333.

139. C. P. Wong, R. F. Venteicher, W. D. Horrocks, *J. Am. Chem. Soc*., 96 **(1974)** 7149.

140. W. D. Horrocks, C. P. Wong, *J. Am. Chem. Soc*., 98 **(1976)** 7157.

141. F. W. Oliver, C. Thomas, E. Hoffman, D. Hill, T. P.G. Sutter, P. Hambright, S. Haye, A. N. Thrope, N. Quoc, A. Harriman, P. Neta and S. Mosseri, *Inorg. Chim. Acta,* 186 **(1991)** 119.

142. W. D. Horrocks, E. G. Hove, *J. Am. Chem. Soc.* 13 **(1978)** 4386.

143. Y. Miao, G. Chen, G. Liu, *J. Phys. Chem. of sold*, 68 **(2007)** 541-548

144. M. P. Tsvirko, K. N. Solovyov, T. F. Kachura, A. S. Piskarskas, *Chem. Phys.*, 106 **(1986)** 467-476

145. T. J. Foley, B. S. Harrison, A. S. Knefely, K. A. Abboud, J. R. Reynolds, K. S. Schanze, J. M. Boncella, *Inorg. Chem.,* 42 **(2003)** 5023-5032.

146. J. G. Bunzli, *Chem. Rev.*, 110 **(2010)** 2729-2755.

147. R. Wiglusz, J. Legendziewicz, A. Graczyk, S. Radzki, P. Gawryszewska, J. Sokolnicki, *Journal of Alloys and Compounds,* 380 **(2004)** 396-404.

148. G. E. Khalil, E. K. Thompson, M. Gouterman, J. B. Callis, L. R. Dalton, N. J. Turro, S. Jockusch, *Chem. Phys. Letts.*, 435 **(2007)** 45-49.

149. B. K. M. Tsvirko, *Chem. Phys. Letts.* **(2015)** DOI: 10.1016/j.cplett.2015.06.013

150. V. Bulach, F. Sguerra and M. W. Hosseini, *Coord. Chem. Rev*., 256 **(2012)** 1468.

151. J. Jiang, K. Machida, G. Adachi, *Journal of Alloys and Compounds*, 192 **(1993)** 296-299.

152. L. L. Witter, D. Holten, *J. Phys. Chem.*, 100 **(1996)** 860-868.

153. S. Lipstman, S. Muniappan, S. George and I. Goldberg, *Dalton Trans,* **(2007)** 3273.

154. S. Radzki, C. Giannotti, *Act. Phy. Pol., A* 90 **(1996)** 385-391.

155. C. H. Huang, Rare Earth Coordination Chemistry: Fundamentals and Applications, John Wiley & Sons (Asia) Pte. Ltd **(2010)**

156. T. Moeller: *The Chemistry of the Lanthanides*; Reinhold Publishing Corporation: New York, **(1965)**

157. N. Kaltsoyannis, P. Scott, *The f-Elements.*; Oxford University Press: London, **(1999)**

158. J. C. G .Buenzli, G. R. Choppin, Editors, *Lanthanide Probes in Life, Chemical and Earth Sciences: Theory and Practice*. **(1989)**

159. S. Cotton: *Lanthanide and Actinide Chemistry*, John Wiley & Sons, Ltd: West Sussex **(2006)**

160. A. C. Behrle, The Study of Lanthanides for Organometallic and Separation Chemistry, PhD thesis, The University of Toledo, December **2012**.

161. R. D. Shannon, *Acta Crystallogr.* Sect. A: Found. Crystallogr. 32 **(1976)** 751-767.

162. J. W. O'Laughlin, In *Handbook on the Physics and Chemistry of Rare Earths.* Karl A. Gschneidner, Jr., E. LeRoy, Eds.; Elsevier: **(1979)** Vol. 4

163. Jian Zhang, Synthesis and Near Infrared Luminescent Properties of Lanthanide Complexes, M.Sc thesis, University of Pittsburgh, **2006**.

164. De Bettencourt-Dias, A.; Barber, P. S.; Bauer, *J. Am. Chem. Soc.* 134 **(2012)** 6987.

165. D. F. Evans, *J. Chem. Soc.* **1959**, 2003.

166. S. I.Weissman, *Journal of Chemical Physics* 10, (**1942)** 214-17.

167. S. Faulkner, J. L. Matthews, *Comprehensive Coordination Chemistry II (***2004)** 9, 913-944.

168. A. Beeby, S. W, Botchway, I. M. Clarkson, S. Faulkner, A. W. Parker, D. Parker, J. A. G. Williams, *Journal of Photochemistry and Photobiology, B: Biology,* 57(**2000)** 83.

169. G. Mathis, *Journal of Biomolecular Screening.* 4 (**1999)** 309.

170. M. Imran, C. Szentgyorgyi, G. Eller, Z. Valicsek, O. Horváth, *Inorg. Chem. Commun.* 52 **(2015)** 60.

171. T. Akaska, Z. BianChan, K. W.; Chen, Z.; Gao, S.; Hu, H.; Huang, C.; Jiang, J.; Jiang, S.; Li, F.; Lu, X.; Lu, Y.; Nagase, S.; Shen, Q.; Wang, B.; Wand, E.; Wang, K.; Wang, R.; Wang, X.; Wong, W.; Xu, H.; Yang, H.; Yao, Y.; Zhang, X.; Zheng, Z. *Rare Earth Metal Coordination Chemistry. Fundamentals and Applications.* John Wiley & Sons: Singapore, (**2010**) 6.

172. J. H. Chou, M. E. Kosal, H. S. Nalwa, N. A. Rakow, K. S. Suslick, The Porphyrin Handbook, K. M. Kadish, K. M. Smith, R. Guillard (Eds.) Vol. 3, Academic Press, New York **(2000).**

173. K. S. Suslick, N. A. Rakow, M. E. Kosal and J. H. Chou, *J. Porphyrin Phthalocyanines,* 4 **(2000)** 407.

174. S. Nakagaki, G. K. B. Ferreira, G. M. Ucoski, K. A. D. de Freitas Castro, *Molecules* 18 **(2013)** 7279.

175. T. Aida, S. Inoue, *Acc. Chem. Res.,* 29 **(1996)** 39.

176. B. B. Wayland, S. Mukerjee, G. Posmik, D. C.Woska, L. Basickes, A. A. M. Gridnev, S. D. Ittel, ACS Sympo. Ser. 686 **(1998).**

177. R. Chouikrat. A. Champion, R. Vanderesse, C. Frochot, A. Moussaron, *J. Porphyrin Phthalocyanines,* 19 **(2015)** 595.

178. K. Ladomenou, M. Natali, E. Lengo, G. Charalampidis, F. Scandola, A. G. Coutsolelos, *Coord. Chem. Rev*., (**2014**) (DOI number 10.1016/j.ccr.2014.10.001)

179. J. Davila, A. Harriman, M.C. Richoux, L. R. Milgrom, *J. Chem. Soc. Chem. Commun.,* **(1987)** 25.

180. R. F. Pasternack, P. R. Huber, P. Boyd, G. Engasser, L. Francesconi, E. Gibbs, P. Fascella, G. C. Ventura and L. de C. Hinds, *J. Am. Chem. Soc*., 94 **(1972)** 4511.

181. A. Shamin, P. Hambright, *Inorg. Chem.*, 19 **(1980)** 564.

182. K. Kalyanasundaram, *Inorg. Chem.* 23 **(1984)** 2453.

183. R. F. Pasternack, *Ann. N. Y. Acad. Sci.* 206 **(1973)** 614.

184. W.I. White, "The Porphyrins", D. Dolphin (Ed.), Academic Press, New York, Vo1.5, Chapter 7 **(1978)**.

185. W.S. Caughey, H.E. Spacher, W.H. Fuchsman, S. McCoy, J.O. Alben, *Ann. N.Y. Acad. Sci.*, 153 **(1969)** 72.

186. M. Krishnamurthy, J.R. Sutter, P. Hambright, *J. Chem. Soc. Chem. Commun.*, 13 **(1975).**

187. R. F. Pasternack, L. Francesconi, D. Raff, E. Spiro, *Inorg. Chem.*, 12, 11, **(1973)** 2606.

188. E.B. Fleischer, J.M. Palmer, T.S. Srivastava, A. Chatterjee, *J. Am. Chem. Soc.*, 93 **(1971)** 3162.

189. N. Schaefle and R. Sharp, *J. Phys. Chem. A* 109, 15 **(2005)** 3267.

190. J. E. Bradshaw, K. A. Gillogly, L. J. Wilson, K. Kumar, X. Wan, M. F. Tweedle, G. Hernandez, R. G. Bryant, *Inorg. Chim. Acta*, 275-276 **(1998)** 106.

191. D. Parker, R. S. Dickins, H. Puschmann, C. Crossland and J. A. K. Howard, *Chem. Rev.* 102 **(2002)** 1977.

192. P. Caravan, J. J. Ellison, T. J. McMurray, R. B. Lauffer, *Chem. Rev*. 99 **(1999)** 2293

193. D. L. Pavia, G. M. Lampman, G. S. Kriz, **(1997).** *Introduction to spectroscopy* (Saunders Golden Sunburst Series): 2nd edition.

194. M. Tabata, K. Ozutsumi, *Bull. Chem. Soc. Jpn.*, 65 **(1992)** 1438.

195. D. C. Harris, M. C. Bertolucci: Symmetry and spectroscopy; An introduction to vibrational and electronic spectroscopy; Dover Publications, Inc., New York, 1989. (copyright: Oxford University Press, 1978)

196. H. H. Perkampus, UV-VIS spectroscopy and its applications, Springer-Verlag, ISBN-13: 978-3-642-74479-9 **(1992)**

197. R. S. Mullikan, *J. Chem. Phys*. 7 **(1939)** 14.

198. W. Arthur, Adamson, Paul D. Fleischauer: Concepts of inorganic photochemistry; A Wiley-Interscience Publication, John Wiley & Sons, Inc., **(1975).**

199. J. F. Rabek, Experimental Methods in Photochemistry and Photophysics, Wiley-Interscience Publication, New York, 1983.
200. A. D. Kirk, C. Namasivayam, *Anal. Chem*., 55 **(1983)** 2428.
201. S. L. Murov, Handbook of photochemistry, Marcel Dekker: New York, 1973.
202. J. Jiang, M. Bao, L. Rintoul, D.P. Arnold, *Coord. Chem. Rev*. 250 **(2006)** 424.
203. H. Kunkely, A. Vogler, *Inorg. Chem. Commun*. 10 **(2007)** 479.
204. J. Y. Tung, J.-H. Chen, *Inorg. Chem*. 39 **(2000)** 2120.
205. M.P. Kiss, M. Imran, C. Szentgyörgyi, Z. Valicsek, O. Horváth, *Inorg. Chem. Commun.* 48 **(2014)** 22.
206. Z. Valicsek, O. Horváth, G. Lendvay, I. Kikas, I. Skoric, *J. Photochem. Photobiol. A: Chemistry*. 218 **(2011)** 143.
207. J. R. Platt, *J. Opt. Soc. Am*. 43 **(1953)** 252.
208. J. R. Sommer, Synthesis and photophysical characterization of π-extended platinum porphyrins for application in high efficiency near-IR light emitting diodes, PhD thesis, University of Florida, **2010**.
209. M. A. Duncan, Advances in metal and semiconductor clusters, volume-5, Elsevier, 2001.
210. M. P. Tsvirko, G. F. Stelmakh, V. E. Pyatosin. *Chem. Phys. Lett.,* 73 **(1980)** 80.
211. J. M. Stanley, B. J. Holliday, *Coor. Chem. Rev*., 256 **(2012)** 1520.
212. M. D. Lim, I. M. Lorkovic and P. C. Ford, *J. Inorg. Biochem*., 99 **(2005)** 151.
213. Z. Valicsek, O. Horváth, K. L. Stevenson, *Photochem. Photobiol. Sci*. 3 **(2004)** 669.
214. X. Yan, D. Holten, *J. Phys. Chem.,* 92 **(1988)** 409.
215. J. R. Darwent, P. Douglas, A. Harriman, G. Porter, M. C, Richoux, *Coord. Chem. Rev.*, 44 **(1982)** 83
216. J. S. Baskin, H. Z. Yu. A. H. Zewail, *J. Phys. Chem*., 106 **(2002)** 9837.
217. A. Harriman, *J. Chem. Soc. Faraday Trans,* 76 **(1980)** 1978.
218. E. I. Rabinowitch, "Photosynthesis," Vol. I. Wiley (Interscience), New York, 1945; Vol. II, Part 1 (1951); Part 2 (1956).
219. D. Holten, D.F. Bocian, J.S. Lindsey, *Acc. Chem. Res.* 35 **(2002)** 57.
220. F. D'Souza, O. Ito, *Coord. Chem. Rev*. 249 **(2005)** 1410.
221. M.V. Martínez-Díaz, G. de la Torre, T. Torres, *Chem. Commun*. 46 **(2010)** 7090.
222. S. Fukuzumi, in: T.J.J. Müller, U.H.F. Bunz (Eds.), Functional Organic Materials, Wiley-VCH, 2007, p. 465.

223. S. Fukuzumi, T. Honda, T. Kojima, *Coord. Chem. Rev*., 256 **(2012)** 2488.

224. D. G. Whitten, Photochemistry of porphyrins and their metal complexes in solution and organized media, Verlag Chemie International, Inc., 1978,

225. K. M. Smith, S. B. Brown, R. F. Troxler and J. J. Lai, *Tetrahedron Lett*. 21 **(1980)** 433.

226. K. M. Smith, S. B. Brown, R. F. Troxler and J. J. Lai, *Tetrahedron Lett*. 21 **(1980)** 2763.

227. P. Neta, M. C. Pichoux, A. Harriman, L. R. Milgrom, *J. Chem. Soc. Faraday Trans*. II 82 **(1986)** 209.

228. R. Huszank, G. Lendvay, O. Horváth, *J. Biol. Inorg. Chem*., 12 **(2007)** 681.

229. J. D. Spikes, *Photochem. Photobiol.* 5 **(1992)** 797

Appendix

List of figures

List of tables

Publications and presentations related to the dissertation

Publications:

Melitta Patrícia Kiss, **Muhammad Imran**, Csanád Szentgyörgyi, Zsolt Valicsek*, Ottó Horváth
"Peculiarities of the reactions between early lanthanide(III) ions and an anionic porphyrin"
Inorg. Chem. Commun. **2014**, *48*, 22–25. http://dx.doi.org/10.1016/j.inoche.2014.08.001
I.F: 1.777

Muhammad Imran, Csanád Szentgyörgyi, Gábor Eller, Zsolt Valicsek, Ottó Horváth
"Peculiar photoinduced properties of water-soluble, early lanthanide(III) porphyrins"
Inorg. Chem. Commun. **2015**, *52*, 60-63. http://dx.doi.org/10.1016/j.inoche.2014.12.016
I.F: 1.777

Ottó Horváth, Zsolt Valicsek, Melinda A. Fodor, Máté M. Major, **Muhammad Imran**, Günter Grampp, Alexander Wankmüller
"Visible light-driven photophysics and photochemistry of water-soluble metalloporphyrins"
Coord. Chem. Rev. **2016** (in press) http://dx.doi.org/10.1016/j.ccr.2015.12.011
I.F.: 13.174 (5-Year Impact Factor)

2 further papers are under preparation:
M. Imran, C. Szentgyörgyi, Z. Valicsek, O. Horváth, RSC Advances
M. Imran, Z. Valicsek, O. Horváth, RSC Advances

Presentations

O. Horváth, Z. Valicsek, M. A. Fodor, **M. Imran**, L. Fodor, G.r Grampp, K. Rasmussen, I. Habuš
"Photocatalytic properties of water-soluble metalloporphyrins in homogeneous and microheterogeneous systems" (p)
3rd European Symposium on Photocatalysis , Portorož, Slovenia, September 25-27, 2013 (Abst. P1-3)

O. Horváth, Z. Valicsek, M.A. Fodor, **M. Imran**, L. Fodor, G. Grampp, A. Wankmüller, I. Habuš
„Photoinduced behavior of water-soluble metalloporphyrins in homogeneous and microheterogeneous systems " (t)
Central European Conference on Photochemistry 2014, Bad Hofgastein, Austria, February 9-13, 2014 (Abst. O16, p. 32)

M. Imran, Z. Valicsek, O. Horváth
„Photophysical and photochemical investigation of water-soluble, anionic cerium(III) porphyrins" (p)
Central European Conference on Photochemistry 2014, Bad Hofgastein, Austria, February 9-13, 2014 (Abst. P28, p. 71)

M. Imran, Zs. Valicsek, O. Horváth
„Photophysical and photochemical investigation of water-soluble, anionic neodymium(III) porphyrins" (t)
Session of the Hungarian Academy of Sciences Reaction Kinetics and Photochemistry Working Committee, Siófok, May 26-27, 2014.

Z. Valicsek, M.P. Kiss, **M. Imran**, O. Horváth
"Peculiar formation reactions and photoinduced properties of water-soluble lanthanide porphyrins" (p)
8th International Conference on Porphyrins and Phthalocyanines, Istanbul, Turkey, June 22-27, 2014 (Abst. S03-006, p. 738)

O. Horváth, Z. Valicsek, M.A. Fodor, **M. Imran**, M. M. Major, G. Grampp, A. Wankmüller
*"*In-plane and out-of-plane water-soluble metalloporphyrins as photocatalysts for utilization of visible light" (t)
20th International Conference on Photochemical Conversion of Solar Energy (IPS-20), July 27 – August 1 2014, Berlin, Germany (Abst. E3-4, p. 65)

O. Horváth, **M. Imran**, Z. Valicsek
„Photophysical and photochemical investigation of water-soluble, anionic neodymium(III) porphyrins" (p)
20th International Conference on Photochemical Conversion of Solar Energy (IPS-20), July 27 – August 1 2014, Berlin, Germany (Abst. PoT 75, p. 157)

O. Horváth, Z. Valicsek, M. A. Fodor, M. M. Major, **M. Imran**, G. Grampp, A.r Wankmüller
"Water-soluble metalloporphyrins as photocatalysts for utilization of visible light" (t)
12th Pannonian Symposium on Catalysis, September 16-20 2014, Třešť, Czech Republic (Abst. O38)

M. Imran, Z. Valicsek, O. Horváth
"Photophysical and photochemical investigation of water-soluble, anionic gadolinium(III) porphyrins" (p)
12th Pannonian Symposium on Catalysis, September 16-20 2014, Třešť, Czech Republik (Abst. P34)

M. Imran, Zs. Valicsek, O. Horváth
"Photophysical and photochemical investigation of water-soluble porphyrin complexes of early lanthanide(III) ions" (p)
16th Blue Danube Symposium on Heterocyclic Chemistry, Balatonalmádi, Hungary, June 14-17, 2015 (Abst. P26, p. 82)

Z. Valicsek, M.P. Kiss, **M. Imran**, O. Horváth
"Peculiarities of the reactions between early lanthanide(III) ions and an anionic porphyrin" (t)
9th International Conference on Chemical Kinetics, Ghent, Belgium, June 28 – July 2, 2015 (Abst. O79, p. 281)

O. Horváth, Z. Valicsek, M.A. Fodor, M.M. Major, **M. Imran**, G. Grampp, A. Wankmüller
"Utilization of water-soluble metalloporphyrins in visible light-driven photochemical systems" (t)
21st International Symposium on the Photochemistry and Photophysics of Coordination Compounds, Krakow, Poland, July 5-9, 2015 (Abst. KL10, p. 47)

M. Imran, Zs. Valicsek, O. Horváth
"Photophysical and photochemical investigation of water-soluble, anionic dysprosium(III) porphyrins" (p)
21st International Symposium on the Photochemistry and Photophysics of Coordination Compounds, Krakow, Poland, July 5-9, 2015 (Abst. PP41, p. 132)